

43388



National Library of Canada

Bibliothèque nationale du Canada

Canadian Theses Division / Division des thèses canadiennes

Ottawa, Canada K1A 0N4

PERMISSION TO MICROFILM — AUTORISATION DE MICROFILMER

Please print or type — Écrire en lettres moulées ou dactylographier

Full Name of Author — Nom complet de l'auteur

J. LONZO, COEN STANLEY

Date of Birth — Date de naissance

04 JUNE 1951

Country of Birth — Lieu de naissance

CANADA

Permanent Address — Résidence fixe

711 WEST 17TH STREET EDMONTON ALBERTA T6G 1K7

Title of Thesis — Titre de la thèse

A NUMERICAL STUDY OF THE BEHAVIOR OF AN OPEN CHANNEL
UNDER A PROBABLE CONDUCTIVE MODEL

University — Université

UNIVERSITY OF ALBERTA

Degree for which thesis was presented — Grade pour lequel cette thèse fut présentée

MASTER OF SCIENCE

Year this degree conferred — Année d'obtention de ce grade

1979

Name of Supervisor — Nom du directeur de thèse

DR. K. D. HAGE

Permission is hereby granted to the NATIONAL LIBRARY OF CANADA to microfilm this thesis and to lend or sell copies of the film

L'autorisation est, par la présente, accordée à la BIBLIOTHÈQUE NATIONALE DU CANADA de microfilmer cette thèse et de prêter ou de vendre des exemplaires du film.

The author reserves other publication rights, and neither the thesis nor extensive extracts from it may be printed or otherwise reproduced without the author's written permission.

L'auteur se réserve les autres droits de publication; ni la thèse ni de longs extraits de celle-ci ne doivent être imprimés ou autrement reproduits sans l'autorisation écrite de l'auteur.

Date

16 OCTOBER 1979

Signature

[Handwritten signature]



National Library of Canada

Cataloguing Branch
Canadian Theses Division

Ottawa, Canada
K1A 0N4

Bibliothèque nationale du Canada

Direction du catalogage
Division des thèses canadiennes

NOTICE

The quality of this microfiche is heavily dependent upon the quality of the original thesis submitted for microfilming. Every effort has been made to ensure the highest quality of reproduction possible.

If pages are missing, contact the university which granted the degree.

Some pages may have indistinct print especially if the original pages were typed with a poor typewriter ribbon or if the university sent us a poor photocopy.

Previously copyrighted materials (journal articles, published tests, etc.) are not filmed.

Reproduction in full or in part of this film is governed by the Canadian Copyright Act, R.S.C. 1970, c. C-30. Please read the authorization forms which accompany this thesis.

**THIS DISSERTATION
HAS BEEN MICROFILMED
EXACTLY AS RECEIVED**

AVIS

La qualité de cette microfiche dépend grandement de la qualité de la thèse soumise au microfilmage. Nous avons tout fait pour assurer une qualité supérieure de reproduction.

Si il manque des pages, veuillez communiquer avec l'université qui a conféré le grade.

La qualité d'impression de certaines pages peut laisser à désirer, surtout si les pages originales ont été dactylographiées à l'aide d'un ruban usé ou si l'université nous a fait parvenir une photocopie de mauvaise qualité.

Les documents qui font déjà l'objet d'un droit d'auteur (articles de revue, examens publiés, etc.) ne sont pas microfilmés.

La reproduction, même partielle, de ce microfilm est soumise à la Loi canadienne sur le droit d'auteur, SRC 1970, c. C-30. Veuillez prendre connaissance des formules d'autorisation qui accompagnent cette thèse.

**LA THÈSE A ÉTÉ
MICROFILMÉE TELLE QUE
NOUS L'AVONS REÇUE**

THE UNIVERSITY OF ALBERTA
A NUMERICAL STUDY OF TEMPERATURE
IN AN URBAN VALLEY
USING A RADIATIVE-CONDUCTIVE MODEL

by

C

COLIN STANLEY di CENZO

A THESIS
SUBMITTED TO THE FACULTY OF GRADUATE STUDIES AND RESEARCH
IN PARTIAL PULFILMENT OF THE REQUIREMENTS FOR THE DEGREE OF
MASTER OF SCIENCE
IN
METEOROLOGY

DEPARTMENT OF GEOGRAPHY

EDMONTON, ALBERTA

FALL, 1979

THE UNIVERSITY OF ALBERTA
FACULTY OF GRADUATE STUDIES AND RESEARCH

The undersigned certify that they have read, and recommend to the Faculty of Graduate Studies and Research, for acceptance, a thesis entitled "A Numerical Study of Temperature in an Urban Valley Using a Radiative-Conductive Model", submitted by Colin Stanley di Cenzo in partial fulfilment of the requirements for the degree of Master of Science in Meteorology.

Kurt H. Day
.....

Supervisor

Robert C. Hartman
.....

Arnold G. Dole
.....

Date *OCTOBER 16* 1979

DEDICATION

To My Parents

whose encouragement, support, and understanding
have made this work possible

ABSTRACT

A simple radiative-conductive model is developed to investigate the thermal characteristics of a small urban valley. The behaviour of the model is studied by varying parameters such as friction velocity, slope inclination, and soil diffusivity.

The non-linear flat-plane boundary-layer equations are applied to the valley, and integrated numerically. Since wind is not predicted by the model, measurements made in the lowest 5 meters are used. Stability effects on thermal diffusivity are accounted for with similarity theory. The flat-plane equations are modified for use over a gently inclined surface. In the domain of the slope wind, a neutral wind profile is superimposed onto the plane-wind profile.

It is found that the inclusion of the neutral slope layer explains 4 of the 5 C° observed slope-rim temperature difference. This compares to a 2 C° difference predicted using the unmodified plane theory. The effect of decreasing the friction velocity is to decrease evening cooling at the 1 meter level by as much as 2 C° while simultaneously increasing the inversion intensity between the 1 meter level and the surface. Decreased soil diffusivities lead to an almost 1 C° increase. Evening temperatures nearly 3 C° lower result from more steeply inclined slopes.

ACKNOWLEDGEMENTS

Foremost, I thank Dr. K.D. Hage. His adept guidance, constant encouragement, and expeditious advice with the draft revisions were invaluable to the completion of this thesis. I also thank Dr. R.B. Charlton and Professor U.M. Maydell for serving with Dr. Hage on the examining committee; as well as Dr. E.P. Lozowski for several helpful discussions.

In addition, thanks are extended to Mr. R.P. Weatherburn for his technical assistance, and the preparation of some of the figures; and to the Cartography and Photographic Services of the Department of Geography for the use of their facilities.

Financial support for the experimental aspects of this project was provided by the Research Secretariat of Alberta Environment.

This study was conducted while on Educational Leave from the Atmospheric Environment Service, Environment Canada.

TABLE OF CONTENTS

	Page
DEDICATION	iv
ABSTRACT	v
ACKNOWLEDGEMENTS	vi
TABLE OF CONTENTS	vii
LIST OF TABLES	xi
LIST OF FIGURES	xiv
LIST OF SYMBOLS	xv

CHAPTER

1	INTRODUCTION	
	1.1 General	1
	1.2 Edsonton's River Valley	2
	1.3 The Dawson Bridge Site	4
	1.4 Instrumentation	6
	1.5 Micrometeorological Characteristics of the Valley	9
2	THE THEORETICAL MODEL	
	2.1 General	13
	2.2 The Prediction Equations	15
	2.3 Simplification of the Prediction Equations	18
	2.4 The Heat Balance Equation	20
	2.5 The Eddy Diffusivities	22
	2.6 The Stable and Unstable Regimes ...	26
	2.7 Method of Solution	27

CHAPTER		Page
3	THE COMPUTER MODEL	
	3.1 General	29
	3.2 The Grid	30
	3.3 The Finite-Difference Equations ...	32
	3.4 Calculation of the Eddy Diffusivities	34
	3.5 Calculation of the Monin-Obukhov Profile Functions	37
	3.6 Calculation of the Surface Temperature	40
	3.7 Prediction Procedure for the Temperature Profiles	41
	3.8 Inclusion of a Neutral Slope Layer	43
4	INITIALIZATION PROCEDURE	
	4.1 General	45
	4.2 The Atmospheric Temperature Profile	46
	4.3 The Soil Temperature Profile	49
5	RESULTS	
	5.1 General	53
	5.2 The Results for Experiment 8	54
	5.2.1 General	54
	5.2.2 The Observations	54

CHAPTER		Page
	5.2.3 The Model Parameters	59
	5.2.4 The Model Predictions	59
	5.3 Model Sensitivity to Slope	77
	5.4 Model Sensitivity to the Soil	
	Diffusivity	81
	5.5 Model Sensitivity to the Friction	
	Velocity	83
	5.6 Comparison between Urban and Rural	
	Cooling	85
	5.7 The Results for Experiment 9	88
	5.7.1 General	88
	5.7.2 The Observations	89
	5.7.3 The Model Parameters	89
	5.7.4 The Model Predictions	97
	5.8 The Results for Experiment 11	101
	5.8.1 General	101
	5.8.2 The Observations	102
	5.8.3 The Model Parameters	102
	5.8.4 The Model Predictions	102
6	SUMMARY AND CONCLUSIONS	
	6.1 Summary	114
	6.2 Conclusions	115
	6.3 Scope for Future Work	117

REFERENCES	Page 119
-------------------------	--------------------

APPENDIX

A	Graphical Integration of the Atmosphere	
	Long-wave Flux Density	122
B	The Solar Flux Density	128
C	Gaussian Elimination of a Tri-diagonal	
	Matrix	132
D	The Model Grid	134
E	Model Parameters	136
F	The Computer Programme	138

LIST OF TABLES

TABLE		Page
1.1	Meteorological Instrumentation	8
1.2	Instrumentation Height	8
4.1	The Interpolation Table for the Initial Atmospheric Temperature Profile	48
4.2	The Interpolation Table for the Initial Soil Temperature Profile	51
5.1	The Temperatures and Winds from the Local Airports on 27 June 1978	55
5.2	The Valley Winds on 27 June 1978	56
5.3	The Slope (Drainage) Wind at Station 11 on 27 June 1978	57
5.4	The Calibrated Valley Temperatures on 27 June 1978	58
5.5	The Model Parameters for Experiment 8 ...	60
5.6	The Initial Air Temperature Profile for Experiment 8	61
5.7	The Initial Soil Temperature Profile for Experiment 8	61
5.8	The Model Winds for Experiment 8	62
5.9	The Temperatures and Winds from the Local Airports on 04 July 1978	90
5.10	The Valley Winds on 04 July 1978	91
5.11	The Slope (Drainage) Wind at Station 11 on 04 July 1978	92

TABLE		Page
5.12	The Calibrated Valley Temperatures on 08 July 1978	93
5.13	The Model Parameters for Experiment 9 ...	94
5.14	The Initial Air Temperature Profile for Experiment 9	95
5.15	The Initial Soil Temperature Profile for Experiment 9	95
5.16	The Model Winds for Experiment 9	96
5.17	The Temperatures and Winds from the Local Airports on 28 August 1978	103
5.18	The Valley Winds on 28 August 1978	104
5.19	The Slope (Drainage) Wind at Station 11 on 28 August 1978	105
5.20	The Calibrated Valley Temperatures on 27 August 1978	106
5.21	The Model Parameters for Experiment 11 ...	107
5.22	The Initial Air Temperature Profile for Experiment 11	108
5.23	The Initial Soil Temperature Profile for Experiment 11	108
5.24	The Model Winds for Experiment 11	109
A.1	The Atmospheric Sounding for Experiment 8	126
A.2	The Atmospheric Sounding for Experiment 9	126

TABLE		Page
A.3	The Atmospheric Sounding	
	for Experiment 11	127
D.1	The Grid Point Values within the	
	Boundary Layer	134
D.2	The Grid Point Values within the	
	Soil Layer	135
E.1	The Common Model Parameters	136

LIST OF FIGURES

FIGURE		Page
1.1	Edmonton Topography	3
1.2	The Dawson Bridge Site	5
1.3	North Saskatchewan River Valley	
	Cross-section	7
3.1	The Model Grid	31
3.2	Finite-Differences on an Irregularly-	
	Spaced Grid	33
4.1	The Interpolation Curve for the Initial	
	Atmospheric Temperature Profile	47
4.2	The Interpolation Curve for the Initial	
	Soil Temperature Profile	50
5.1	The Assessment of the Model-Predicted Solar	
	Flux Density for Experiment 8	65
5.2	The Assessment of the Model-Predicted Net	
	Flux Density for Experiment 8	66
5.3	The Model-Predicted Heat Flux Density	
	to the Atmosphere for Experiment 8 ...	67
5.4	The Model-Predicted Heat Flux Density	
	to the Soil for Experiment 8	68
5.5	The Model-Predicted Temperature Field	
	at the Rim for Experiment 8	70
5.6	The Model-Predicted Temperature Field	
	over the Slope with the Inclusion	
	of the Neutral Surface Layer for	
	Experiment 8	71

FIGURE**Page**

5.7	Progression of the 1 meter Temperature with Time for Experiment 8	72
5.8	The Vertical Temperature Profiles over the Slope for Experiment 8	74
5.9	The Soil Temperatures for Experiment 8 ...	76
5.10	The Double Structure Inversion for Experiment 8	78
5.11	The Model Sensitivity to Slope	80
5.12	The Model Sensitivity to the Soil Diffusivity	82
5.13	The Model Sensitivity to the Friction Velocity	84
5.14	Comparison between Urban and Rural Cooling	87
5.15	The Model-Predicted Temperature Field at the Rim for Experiment 9	98
5.16	The Model-Predicted Temperature Field over the Slope with the Inclusion of the Neutral Surface Layer for Experiment 9	99
5.17	Progression of the 1 meter Temperature with Time for Experiment 9	100
5.18	The Model-Predicted Temperature Field at the Rim for Experiment 11	111

FIGURE

Page

5.19	The Model-Predicted Temperature Field over the Slope with the Inclusion of the Neutral Surface Layer for Experiment 11	112
5.20	Progression of the 1 meter Temperature with Time for Experiment 11	113
A.1	The Elsasser Diagram	124
B.1	The Celestial Dome	129

LIST OF SYMBOLS

SYMBOL

c_p	specific heat of air at constant pressure
c_s	soil heat capacity
\vec{e}	$\equiv (\hat{e}_1, \hat{e}_2, \hat{e}_3)$, \hat{e}_1 is the unit vector in the 1^{th} direction
E	emissivity due to water vapour
f	coriolis parameter
F_{CO_2}	long-wave flux density due to carbon dioxide
F_{LH}	latent heat flux density
F_{LW}	terrestrial long-wave flux density
F_N	net flux density
F_{SH}	sensible heat flux density
F_{SHS}	soil heat flux density
F_{SW}	short-wave flux density
F_{WV}	long-wave flux density due to water vapour
g	acceleration due to gravity
h	Shir's boundary layer height
HAN	hour angle of surface normal
HAS	hour angle of sun
I	water vapour flux density from phase changes
k	von Karman's constant
\vec{K}_h	thermal diffusivity
K_h	vertical thermal diffusivity
\vec{K}_m	momentum diffusivity (eddy viscosity)
K_m	vertical momentum diffusivity

SYMBOL

K_N	vertical momentum diffusivity under neutral conditions
\bar{k}_q	specific humidity diffusivity
K_s	soil diffusivity
\log	base e logarithmic function
\log_{10}	base ten logarithmic function
L	Obukhov characteristic length
P	atmospheric pressure
q	specific humidity
R	gas constant for dry air
R_i	Richardson number
S	total heat sources and sinks
S_0	solar constant
t	time
T	atmospheric temperature; occasionally used as surface temperature
T_s	soil temperature
u	wind speed
u^*	friction velocity
\vec{V}	wind velocity
\vec{V}_g	geostrophic wind
w	optical depth due to water vapour; also earth's angular rotation
z_0	roughness length
z_{SB}	soil depth
z_T	boundary layer height

SYMBOL

α	inclination of slope
β	orientation of slope
γ	angle of incidence between solar flux and slope
δ	declination of sun
δ_{ij}	Kronecker delta
ζ	dimensionless height
θ	potential temperature
λ	free atmosphere eddy mixing length
Λ	latitude
μ	albedo-turbidity-diffuse solar radiation factor
ϵ	angle between celestial pole and slope normal
ρ	air density
ρ_s	soil density
σ	Stephan-Boltzmann constant
τ	surface stress
ϕ	earth's geopotential
ϕ_h	dimensionless mean temperature gradient
ϕ_m	dimensionless mean wind shear
ω_e	earth's angular velocity

CHAPTER 1

INTRODUCTION

1.1 General

Many cities are situated in a river valley. The valley is often the heart of the city, containing the focus for heavy industrial, commercial, and recreational activities. The air quality in such an urban valley will, among other considerations, depend on its micrometeorology. In cities where the valley is used for parkland and as a main transit corridor, there is mounting public concern over the continued compatibility of these diverse uses. In this respect, it is most important to identify the meteorological factors affecting both the dispersal and entrapment of vehicle pollutants in a valley environment.

Under normal conditions, the concentration of pollutants is not greatly influenced by the presence of these valleys, mainly because of their small physical extent. Perhaps this is why so few studies have been completed on small urban valleys. However, the formation of

an inversion in the valley acts to suppress/atmospheric turbulence and thermal mixing, reducing both the wind speed and its variation. This process allows the concentration of pollutants in the valley. Thus one major consideration in determining the pollution potential of an urban valley is the evolution of its temperature field. This thesis develops a simple radiative-conductive model, and uses it to study temperature in Edmonton's river valley.

1.2 Edmonton's River Valley

The City of Edmonton is located at latitude $53^{\circ}33'N$, longitude $113^{\circ}30'W$ on the banks of the North Saskatchewan River in central Alberta. The Edmonton location is ideal for conducting a study of an urban valley. The valley itself is steep sided and well defined with an average depth of 50 meters and a width varying between 1000 meters and 1500 meters. It is cut into a fairly level uniform plain that slopes gently from the southwest to the northeast (Figure 1.1). Further, it is removed from the influence of rough terrain and large water bodies. The valley is generally comprised of parkland, roadways, and residential areas. Little industrialization is present. These particular geographical characteristics favour the identification of the true valley micrometeorology.

To date, thirteen field experiments have been carried out by Hage (1979) in Edmonton's river valley. Two

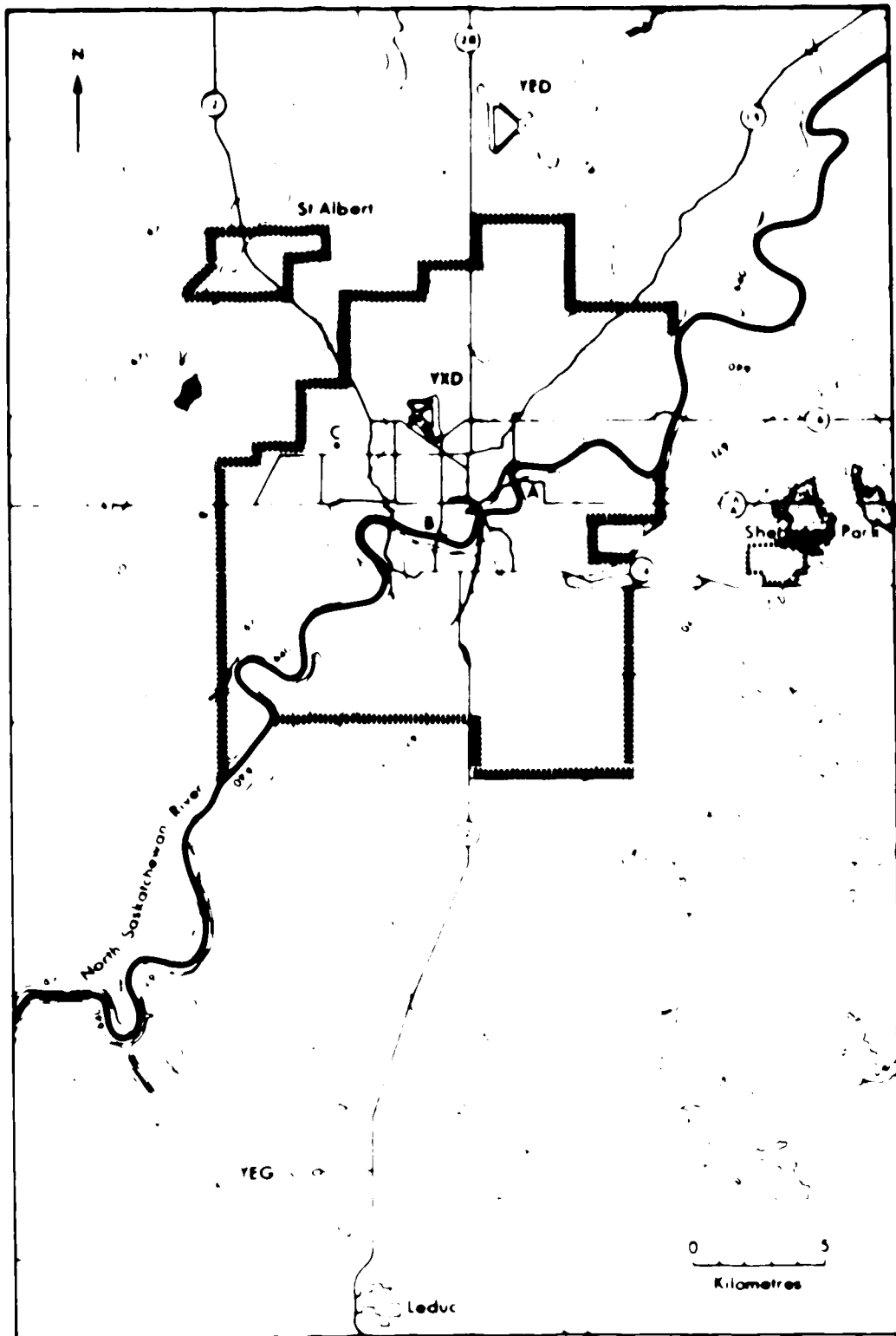


Figure 1.1 Edmonton Topography

principal sites have been used to collect the data: a north-south river section near Dawson Bridge, indicated as (A), Figure 1.1, and an east-west river section near the High Level Bridge, indicated as (B), Figure 1.1. In addition certain data from Edmonton City Tower, Nampa Airport, Municipal Airport, and International Airport, indicated as (C), (YED), (YXD), and (YEG), respectively, in Figure 1.1, are available to augment the experimental data. In this thesis, attention will be focussed on the three experiments carried out in the vicinity of Dawson Bridge during the summer of 1978. To ensure that the microclimatology of the valley would dominate the observations, it was attempted to conduct these experiments on days with clear skies and light winds. Under these conditions the boundary layer is sufficiently decoupled from the synoptic flow aloft.

1.3 The Dawson Bridge Site

The locations of the experimental observation stations at the Dawson Bridge site are indicated in Figure 1.2. Station 8 was situated atop the east river bank on an exposed short grass location away from any obstruction. Slope station 9 was located in approximately 1 meter high grass of the more steeply inclined west-facing slope. Slope station 11 was situated across the river in an almost level interruption of the east-facing slope. Upslope of the

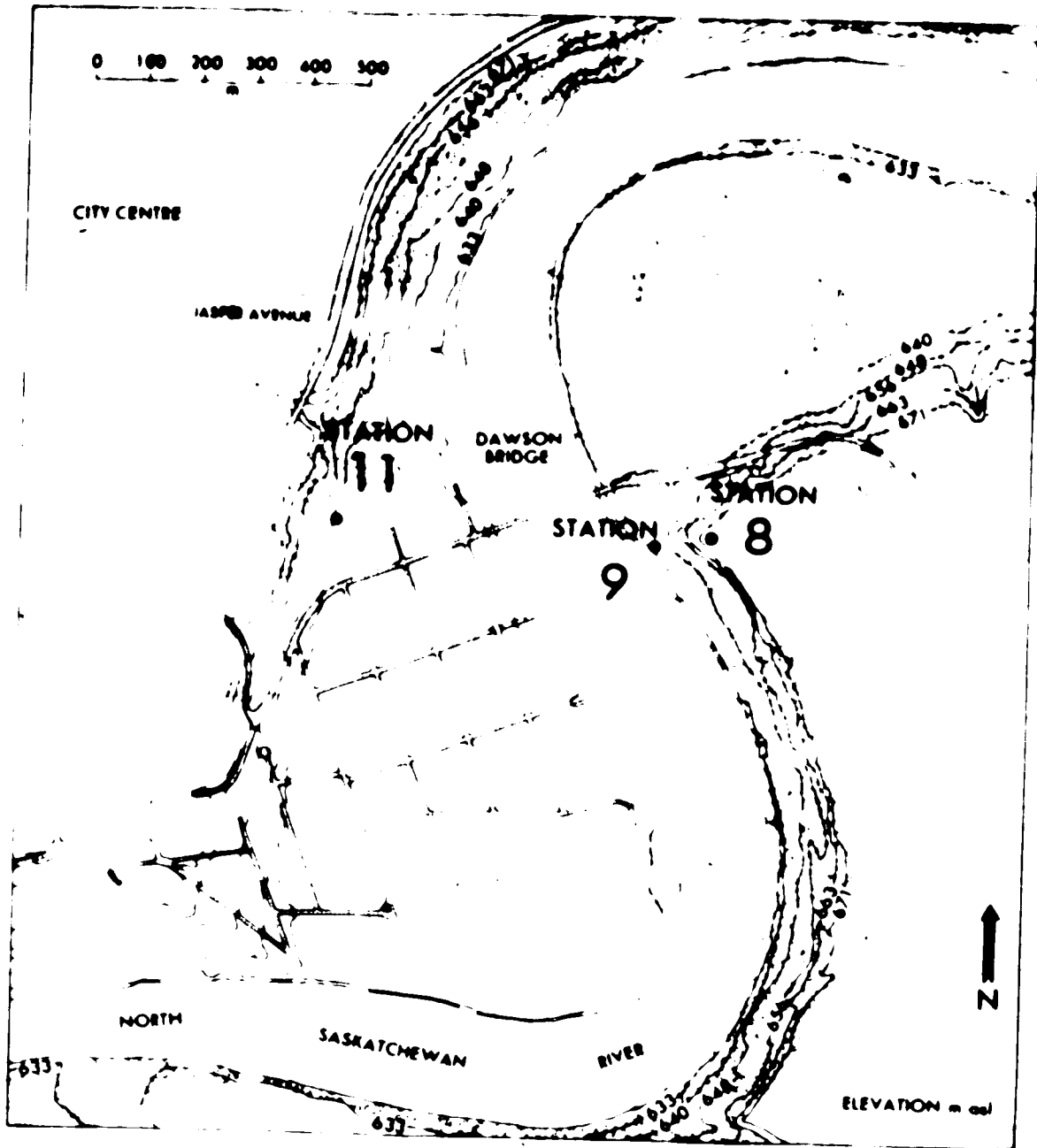


Figure 1.2 The Dawson Bridge Site

station was lightly forested, and further downslope was a small residential area. Station 11 was located 150 meters downslope from the rim at a depth of approximately 30 meters below plain level (Figure 1.3). The average slope at the station was determined to be 16°. The orientation of the valley at this point was estimated to be 13° east of North.

1.4 Instrumentation

The instrumentation at each station is given in Table 1.1. The height of the instrumentation above ground is shown in Table 1.2. The thermographs were always housed in a Stevenson screen, and were either of the Casella¹ or Thies² type. The temperature profiles were measured with chromel constantan thermocouples of 0.013 millimeters diameter³. Winds were measured with Rincos CS180⁴ cup anemometers and Gill⁵ propeller anemometers. Mechanical impulse counters⁶ were used with the cup anemometers, and Rustrak chart recorders⁷ with the propeller anemometers. Comprehensive description regarding the electronics,

¹Casella model F9150/9154

²Thies model 2.0602.00.20

³Omega 0.013 millimeter diameter chromel constantan (type E) thermocouple

⁴Rinco Commonwealth Scientific and Industrial Research Organization model ASI

⁵Gill Propeller Anemometer models 27103 and 27004

⁶German Post Office message counter 12 Volt 6 Ampere Type E16.11

⁷Rustrak Instrument Company model number 214C

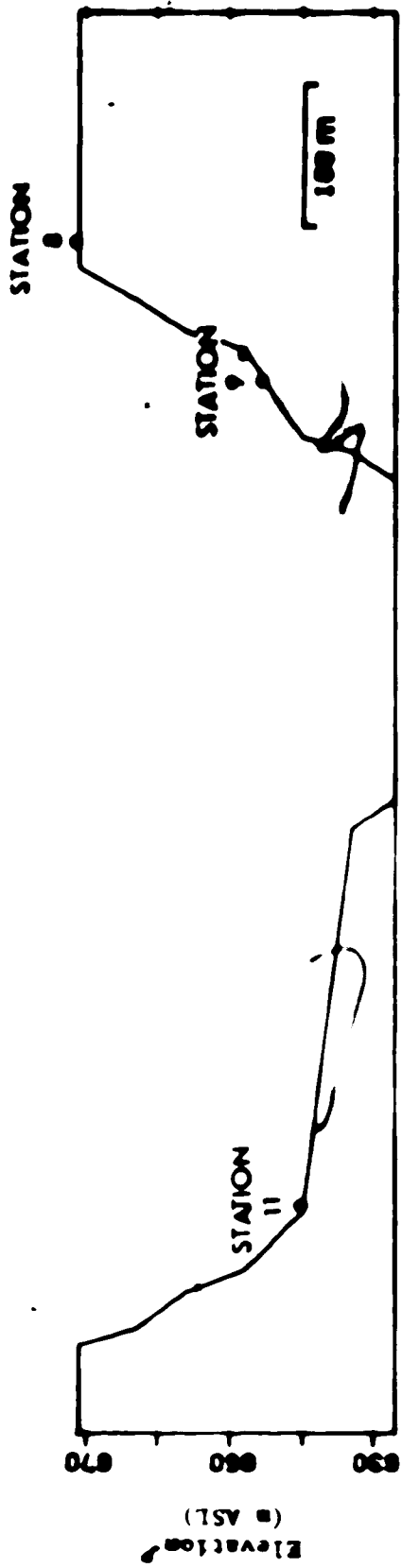


Figure 1.3 North Saskatchewan River Valley Cross-section at the Lawson Bridge Site

Table 1.1 Meteorological Instrumentation

Station	Parameter	Instrumentation
8	wind speed and direction screen temperature	cup and vane anemometer thermograph
9	slope wind screen temperature	propeller anemometer thermograph
11	wind speed profile slope wind valley wind temperature profile screen temperature	cup anemometers propeller anemometer propeller anemometer thermocouples thermograph

Table 1.2 Instrumentation Height

Instrumentation	Station	Experiment	Height (meters)
thermograph	8, 9, 11	8, 9, 11	1.2
cup anemometers	9 11	8, 9, 11 8, 9, 11	2.64 1.70, 3.84, 5.84
propeller anemometers	9, 11	8, 9, 11	0.8
thermocouples	11	8 9 11	0.34, 2.60, 5.06, 7.10, 9.45 2.44, 4.82, 7.10, 9.45 0.12, 3.72, 6.89, 14.73

calibration, and characteristics of these instruments has been detailed previously (Paterson, 1978), and will not be included here.

1.5 Micrometeorological Characteristics of the Valley

Under conditions of light winds and clear skies, observations from different field experiments conducted in Edmonton's river valley showed remarkably consistent results. This section describes the general characteristics of the valley micrometeorology deduced from these observations.

Throughout the afternoon lapse conditions prevailed. Air was well mixed, both mechanically, and thermally. Edmonton City Tower data indicated that superadiabatic lapse rates (typically 2 or 3 times the dry adiabatic lapse rate) extended to at least a height of 90 meters (the top of the tower). Temperatures over both of the valley slopes were generally higher than those along the rim. Winds within the valley were consistently weaker than those observed on the rim. This was likely due to the sheltering and aspect characteristics of the valley. These lighter winds would be responsible for weaker mechanical mixing and less efficient transport of heat out of the lowest levels of the boundary layer. Hence the higher slope temperatures that were recorded. Maximum temperatures were recorded in the late afternoon or early evening.

A one-to-one relationship, with considerable scatter, existed between the wind speed at the rim stations and that observed at the Municipal Airport. Wind speed normally peaked in the mid-afternoon and then decreased towards sunset. Wind direction was not necessarily that of the prevailing flow. This was due to the presence of channel effects and compensating flows (Paterson, 1978).

By early evening, the effects of decreased insolation became apparent and the screen temperatures began declining within one to two hours before sunset. The air in the valley generally became isothermal prior to the air above the plain. Similarly, after sunset, the formation of an inversion in the valley preceded that over the plain. Further, the inversion was observed to be stronger on the north- and east-facing slopes. On some occasions the inversion was observed only on these slopes. Valley temperatures were often comparable to the rural temperatures reported at the International Airport, while rim temperatures compared favourably with the Municipal Airport observations (Hage, 1972). The earlier onset of cooling over the slope is presumed to be caused by the difference in solar radiation extinction between the slope and the plain. After the sun has completely set, the continued maintenance of the slope-rim temperature difference is believed to be due to the presence of the slope wind which is responsible for both the drainage of cooler air down the slope, and the presence of a shallow neutral layer just above the slope. A

neutral layer has a greater thermal diffusivity than a stable layer.

Slope winds were observed on both walls of the valley. The slope wind began on the bank shaded first (the north- and east-facing slopes) at or near the time of slope sunset. Speeds of up to 0.9 m/s were recorded for these winds. There appears to be a weak 15 to 20 minute periodicity associated with oscillations in the recorded speed (Paterson, 1978). Further, it is possible that the wind speed periodicities are correlated to those recorded for temperature. This gives rise to the interesting possibility that there exists a brake on the slope wind due to competition between radiational cooling, advection, and mixing. However, the resolution of the temperature data is such that further investigation is precluded. The slope wind is measured at the 0.8 meter level, hence its vertical extent is at least this value. Paterson (1978) has established that the vertical extent can reach at least 3 meters at a location half way up the slope, and at least 15 meters over the flood plain.

There is some evidence for the existence of a downvalley wind. Thus there is the possibility of a helical double vortex circulation below rim levels. If this is in fact true, the potential for pollutant concentration within the valley under inversion conditions is enhanced.

In addition to the valley inversion forming prior to the urban inversion, it was found that the valley inversion

was usually more intense. Inversion gradients up to 18°C/100 m have been recorded over the slope. It has also been postulated by Paterson and Hage (1979) that the urban inversion can 'drift' over the valley giving rise to a double structure inversion. The exact influence of the urban environment on the micrometeorology of the valley has yet to be ascertained.

CHAPTER 2

THE THEORETICAL MODEL

2.1 General

In this chapter the governing equations for the prediction of temperature by a mathematical valley model are presented. This set of equations was solved numerically by employing a finite-difference scheme on an appropriate mesh of grid points.

The presence of strong vertical gradients in the lower levels of both the wind and temperature profiles is a problem when finite differences are used. There are two approaches available to overcome this difficulty.

The first, due to Estoque (1963), is to introduce a constant-flux layer into the first 50 meters of the boundary layer and to interpolate the temperature and wind profiles below this height. Interpolation is accomplished by using the 'minus one-third power law' (Lumley and Panofsky, 1964), or by using the flux-profile relationships of Businger, et al. (1971), or by some other appropriate technique.

The second approach, adopted by Zdunkowski (1971) and others, is to employ a denser network of grid points close to the ground thereby more properly accounting for the changes occurring near the surface.

The nature of the observations from the river valley dictated that predictions at points below 50 meters would be required. Further, model performance in the lower levels was of greater interest than in the upper levels. Hence the use of Estoque's constant-flux layer technique with interpolation in the region of interest was less desirable. Some authors, for example Sellers (1965), maintain that it is only permissible to assume a constant-flux layer in the lowest meter, and even then only under certain conditions. Thus the second approach was adopted. In the first 100 meters, a logarithmic spacing was used. Logarithmic spacing was employed so as to be compatible with the logarithmic nature of the temperature and wind profiles.

The top of the boundary layer was chosen to be 2000 meters. This is similar to the value of 2050 meters chosen by Estoque (1963). Other investigators have chosen different values. For example Zdunkowski (1971) chose 3000 meters, and Thorpe and Guymer (1977) chose heights ranging between 600 and 1200 meters. According to Shir (1973), a grid 2000 meters high should exceed the top of the real boundary layer on most occasions. More specifically, for a station with Edmonton's latitude, the grid will be adequate for friction velocities less than 0.5 m/s. In any case, it

was assumed that the height of the top of the boundary layer chosen would not be crucial since interest is mainly confined to the lowest 100 meters. The grid spacing between the 100 meter level and the top of the model is constant and equal to 100 meters.

2.2 The Prediction Equations

For present purposes the planetary boundary layer can be described using the Navier-Stokes Equation, the thermodynamic energy or heat equation, the specific-humidity equation, and the continuity-of-mass equation, in conjunction with the equation of state and Poisson's equation. These equations can be written, respectively, as

$$\begin{aligned} \frac{\partial \vec{V}}{\partial t} + (\vec{V} \cdot \vec{\nabla}) \vec{V} = & - \frac{1}{\rho} \vec{\nabla} p - \vec{\nabla} \phi - 2\vec{\Omega} \cdot \vec{V} \\ & + \delta_{ij} \frac{\partial}{\partial x_j} \left(\hat{e}_i \cdot \vec{K}_m \frac{\partial \vec{V}}{\partial x_i} \right) \end{aligned} \quad (2.2.1)$$

$$\begin{aligned} \frac{\partial \theta}{\partial t} + \vec{V} \cdot \vec{\nabla} \theta = & \delta_{ij} \frac{\partial}{\partial x_j} \left(\hat{e}_i \cdot \vec{K}_h \frac{\partial \theta}{\partial x_i} \right) - \frac{1}{\rho c_p} \left(\frac{p_\Omega}{p} \right)^{R/c_p} \frac{\partial E_N}{\partial z} \\ & - \frac{1}{\rho c_p} \left(\frac{p_\Omega}{p} \right)^{R/c_p} I + S \end{aligned} \quad (2.2.2)$$

$$\frac{\partial q}{\partial t} + \vec{V} \cdot \vec{\nabla} q = \delta_{ij} \frac{\partial}{\partial x_j} \left(\hat{e}_i \cdot \vec{K}_q \frac{\partial q}{\partial x_i} \right) \quad (2.2.3)$$

$$\vec{\nabla} \cdot \vec{V} = 0 \quad (2.2.4)$$

$$p = \rho RT \quad (2.2.5)$$

$$\theta = \Gamma \left\{ \frac{p_{\Omega}}{p} \right\}^{R/c_p} \quad (2.2.6)$$

where, after Zdankowski et al. (1976),

\vec{K}_1 is the parameterized microturbulent diffusivity for either momentum, temperature, or specific humidity,

F_N is the net flux density of short- and long-wave radiation,

I is the water vapour flux density due to phase changes, and,

S is the sum of heat sources or sinks.

The remaining symbols have their usual meanings. It is understood that a repeated Latin index implies a summation with respect to that index, and that the indices take on the values 1, 2, and 3 corresponding to the familiar x-, y-, and z-directions in space.

The necessary kinematic boundary conditions are

$$\vec{V}(z_0) = 0 \quad (2.2.7)$$

$$\vec{V}(z_T) = \vec{V}_g \quad (2.2.8)$$

where z_0 is the roughness height and z_T is the height to the top of the boundary layer.

There are two methods of introducing the surface temperature into the model. The simpler method is to use a prescribed function for the surface temperature. This approach has been used, for example, by Fisher (1961). The second method, which has the advantage of being more

realistic, is to compute the surface temperature from given profiles of the air temperature, θ , and the soil temperature, T_s , in conjunction with the heat balance equation. The heat balance equation is a statement regarding the flux densities through the air-soil interface. This method requires the addition of a soil layer to the model wherein the soil temperature equation is given by

$$\frac{\partial T_s}{\partial t} = K_s \frac{\partial^2 T_s}{\partial z^2} \quad (2.2.9)$$

The heat balance approach has been used, among others, by Estoque (1963), and Krishna (1968), and Sasarori (1970).

The heat balance equation is a consequence of an application of the law of heat conservation applied to a column of soil. The column is bounded at the top by the air-soil interface. The lower boundary is taken to be that surface below which vertical heat exchange is negligible. For soil it can be assumed (Sellers, 1965) that the net horizontal transport of heat through the column is zero. Thus the net rate of change of heat in the soil column will be equal to the sum of the vertical flux densities across the air-soil interface. This amounts to the insistence of continuity in heat flow between the soil and air. The system is closed by requiring

$$T_s(z_0) = \theta(z_0) \quad (2.2.10)$$

The boundary conditions imposed at the top and bottom

of the system are

$$\theta(z_T) = \text{const} \quad (2.2.11)$$

$$T_m(z_{SB}) = \text{const} \quad (2.2.12)$$

where z_{SB} , the depth to the soil bottom, is the level below which vertical heat exchange is small.

2.3 Simplification of the Prediction Equations

The primary aim of the model is to describe the evolution of the temperature field at and near the surface. This model would then be gloved with a second model (Stovel, 1979) to yield a time-dependent model capable of predicting both the valley wind and temperature fields. Thus the prime concern of the present study was temperature prediction. Therefore, it was decided to input observed winds into the model and remove the momentum and continuity equations from the prediction set.

The potential temperature equation was simplified with the following assumptions:

1. no advection,
2. no flux divergence near the ground,
3. no changes of water phase,
4. no heat sources or sinks, and,
5. no horizontal diffusion of temperature.

Therefore the potential temperature equation becomes

$$\frac{\partial \theta}{\partial t} = \frac{\partial}{\partial z} \left(K_h \frac{\partial \theta}{\partial z} \right) \quad (2.3.1)$$

The model is mostly concerned with dry summer days. Thus, after Sellers (1965), the latent heat flux density was parameterized in terms of the sensible heat flux density, and the specific humidity equation removed from the set of prediction equations.

Therefore the set of equations of direct concern to the model is

$$\frac{\partial \theta}{\partial t} = \frac{\partial}{\partial z} \left(K_h \frac{\partial \theta}{\partial z} \right) \quad (2.3.2)$$

$$\frac{\partial T_s}{\partial t} = K_s \frac{\partial^2 T_s}{\partial z^2} \quad (2.3.3)$$

with the boundary conditions

$$T_s(z_0) = T_a(z_0) \quad (2.3.4)$$

$$\theta(z_T) = \text{const} \quad (2.3.5)$$

$$T_s(z_{SB}) = \text{const} \quad (2.3.5)$$

and the imposition of the heat balance equation to guarantee continuity of heat flow.

A further simplification was made to the continuity of temperature and heat flow across the air-soil interface. After Zdunkowski (1976), the height of the air-soil interface was taken as $z=0$ rather than $z=z_0$.

2.4 The Heat Balance Equation

Recalling the previous simplifications, the heat balance equation takes the form

$$F_{SW} + F_{CO_2} + F_{WV} - F_{SH} - F_{LH} - F_{SHS} - F_{LW} = 0 \quad (2.4.1)$$

where F_{SW} is the short-wave radiation to the ground,

F_{CO_2} is the long-wave radiation to the ground due to carbon dioxide,

F_{WV} is the long-wave radiation to the ground due to water vapour,

F_{SH} is the sensible heat flux density to the atmosphere,

F_{LH} is the latent heat flux density to the atmosphere,

F_{SHS} is the heat flux density to the soil, and,

F_{LW} is the long wave radiation from the ground.

The carbon dioxide flux density can be expressed as a known fraction of the terrestrial long-wave radiation (Hess, 1959) and, for temperature values near 20°C, this fraction is approximately 0.18. Thus

$$F_{CO_2} = F_{LW} = 0.18 F_{LW} \quad (2.4.2)$$

where T is the surface temperature.

The atmospheric long-wave radiation due to water vapor can be evaluated as

$$F_{LW} = \int_0^{\infty} \sigma T^4 \left(\frac{\partial E}{\partial w} \right) \frac{\partial w}{\partial z} dz \quad (2.4.3)$$

where E is the emissivity due to water vapour, and, w is the optical depth due to water vapour. For the model purposes,

the atmospheric long-wave radiation was assumed constant over the forecast period, and integrated graphically using the Blasser chart published by the U.S. Weather Bureau. After Kondratyev (1969), the atmospheric long-wave radiation intercepted by the slope as a fraction of the hemispheric long-wave radiation is

$$\cos^2(\alpha/2)$$

where α is the inclination of the slope. The graphical integration is described in Appendix A.

The short-wave flux density is a function of the solar constant, the solar hour angle, the solar declination, the latitude, orientation, and inclination of the slope, and a combined albedo, turbidity, and diffuse solar radiation factor. The precise expression used is

$$F_{SW} = S_0(1-\rho) \left[\sin(\delta) \cos(\epsilon) \cos(\beta) \sin(\epsilon) \cos(HAN - \omega t - HATD) \right] \quad (2.4.4)$$

This expression is derived in Appendix B. Values of 1353 W/m^2 (Paltridge and Platt, 1976) and 0.39 (Houghton, 1954) were used, respectively, for the solar constant and for the combined albedo-turbidity-diffuse solar radiation factor for clear sky radiation.

The expressions for the sensible heat flux and the soil heat flux densities are given by

$$F_{SH} = \rho_c c_p K_h \left. \frac{\partial \theta}{\partial z} \right|_{z=0} \quad (2.4.5)$$

$$F_{SHS} = \rho_s c_s K_s \left. \frac{\partial T_s}{\partial z} \right|_{z=0} \quad (2.4.6)$$

2.5 The Eddy Diffusivities

When the atmosphere is completely at rest, the transfer of physical properties such as heat and momentum is accomplished at the molecular level. The transfer process takes place according to such familiar concepts of molecular theory as molecular mean free path and kinematic viscosity. The major hypothesis in molecular transport is that the mean flux of a quantity is directly proportional to its gradient. The proportionality in the case of momentum transfer is the kinematic viscosity, and in the case of heat transfer is the thermometric conductivity. However the atmosphere is rarely completely at rest, even under extremely stable conditions. When the atmosphere is turbulent, transport is accomplished by turbulent transfer processes. The simplest turbulent transfer theory is a quasi-analogy to the molecular transfer process. The turbulent flow is said to possess a granular structure in which small chunks of fluid or eddies can break away from the mean flow and act as vehicles for heat and momentum transfer in a manner similar to molecules in the molecular case. The hypothesis is that the eddy flux of a quantity is proportional to its gradient. This theory is known as the Flux-Gradient Hypothesis, and the constant of proportionality as either the eddy diffusivity or the eddy exchange co-efficient. The eddy diffusivity for momentum, also called the eddy viscosity, is the analogue of kinematic viscosity. Similarly, the eddy diffusivity for heat, also called the eddy conductivity, is the analogue of

thermometric conductivity. The turbulent analogue of the molecular mean free path is the characteristic eddy length scale or mixing length. This quantity can be interpreted as the distance over which the significant eddies will maintain their identity. The mixing length, and other eddy parameters, are not solely properties of the fluid but also of the flow. In other words, although it is characteristic of the local turbulent mixing, the length scale is also a function of its position in the flow, the mean velocity of the flow, and the history of the flow's turbulent structure. These characteristics demonstrate the prime weakness of the Flux-Gradient Hypothesis: turbulence cannot be properly treated as a property of the fluid. - However, according to Plate (1971), the theory is adequate if the local turbulence structure develops in the same manner as the mean flow. The model proceeds on this basis.

The diffusivities are generally complicated and unknown functions. The usual approach is to determine the diffusivity for momentum under neutral atmospheric conditions and then transform it into any diffusivity under any stability condition using the corresponding universal profile function. Monin and Obukhov (1954) have postulated the existence of such universal profile functions, and several experimental determinations of these functions have been published by various authors, for example Webb (1970), Paulson (1970), Businger, et al. (1971), and Carl (1973).

Several specifications of the neutral exchange

coefficient K_N have been suggested. Ekman (1905) proposed K_N to be constant and independent of height, and derived, for the ocean surface layer, the now well known 'Ekman spiral' velocity distribution. For present purposes there exist three possibilities for the evaluation of the neutral exchange coefficient.

The first expression, due to Blackadar (1962), is

$$K_N = \left(\frac{kz}{1 + kz/\lambda} \right)^2 \left| \frac{\partial \vec{V}_g}{\partial z} \right| \quad (2.5.1)$$

where $\lambda = 2.7 \cdot 10^{-4} |\vec{V}_g| / f$ is the free atmosphere eddy mixing length, and, k is von Karman's constant. Free atmosphere mixing length refers to the characteristic size of an eddy at heights where surface friction is no longer an important consideration, ie. the eddy is free of surface constraints.

Physically, the effectiveness of turbulent transport is determined by two factors: shear and eddy size. A larger eddy will act over a greater distance, and a larger shear will make available to the eddy more turbulent energy for the transfer process. Blackadar's expression for K_N reflects these two factors if the bracketed quantity, which is dimensionally a length, is interpreted as the characteristic eddy size. The behaviour of the length scale is appropriate. Near the ground, the eddy size is of the same order of its distance from the ground; and, at greater heights, the eddy size approaches a fixed value.

The second possible formula for the eddy viscosity,

based on the KEYPS^{*} (Sellers, 1961) expression, is

$$K = kz u_* \{1 - \epsilon R_1\}^{1/2} \quad (2.5.2)$$

where u_* is the friction velocity $\equiv (\tau/\rho)^{1/2}$,

$\tau \equiv$ surface stress,

R_1 is the Richardson number $\equiv \frac{g}{\theta} \frac{(\partial\theta/\partial z)}{(\partial\bar{u}/\partial z)^2}$, and,

ϵ is a constant determined experimentally and ranging in value from 9 (Pandolfo, 1966) to 18 (Panofsky, Blackadar, and McVehil, 1960).

The KEYPS equation is really an interpolation formula for the diffusivity in both the neutral and unstable regimes. The first term is the contribution due to forced convection arising from mechanical mixing. The second term represents the contribution due to free convection arising from buoyancy.

The last parameterization is due to Shir (1973) and is given by

$$K_N = u_* \frac{kz}{2} \left\{ e^{-4z/h} + \left(1 + 16(z/h)^{1.6} \right)^{-1} \right\} \quad (2.5.3)$$

where $h = .455u_*/f$ is the height of the boundary layer. This particular parameterization arose from one of the first successful attempts to model atmospheric turbulent flow in the planetary boundary layer. The equation represents the best curve fit to the numerically computed neutral eddy

^{*}from the initial letters of the investigators who independently proposed the formula: Kazanski and Monin (1956), Ellison (1957), Yamamoto (1959), Panofsky (1961), and Sellers (1962)

diffusivity.

The present model does not predict the winds at every level but uses instead observed winds at distinct levels. Hence a choice of the least wind-sensitive parameterization for the exchange coefficient seemed the most desirable. Thus Shir's parameterization was adopted.

2.6 The Stable and Unstable Regimes

It is assumed that the diffusivities can be extended from the neutral regime by

$$K_i = K_N / \phi_i(\zeta) \quad (2.6.1)$$

where $\zeta = z/L$ is the dimensionless height,

L is the characteristic Obukhov length, and,

ϕ_i is the Monin-Obukhov profile function for either temperature or momentum.

It is further assumed that expressions determined by Businger, et al. (1971) from the Kansas data for ϕ_i are applicable

$$\phi_m(\zeta < 0) = (1 - 15\zeta)^{-1/2} \quad (2.6.2)$$

$$\phi_m(\zeta > 0) = 1 + 4.7\zeta \quad (2.6.3)$$

$$\phi_h(\zeta < 0) = .74(1 - 9\zeta)^{-1/2} \quad (2.6.4)$$

$$\phi_h(\zeta > 0) = .74 + 4.7\zeta \quad (2.6.5)$$

These relations also provide an expression for the

Richardson number; namely

$$R_1(\zeta) = \frac{.74 (1 - 15\zeta)^{1/2}}{(1 - 9\zeta)^{1/2}}, \quad R_1 < 0 \quad (2.6.6)$$

$$R_1(\zeta) = \frac{\zeta(.74 + 4.7\zeta)}{(1 + 4.7\zeta)^2}, \quad R_1 > 0 \quad (2.6.7)$$

In the model, the Richardson number is computed, and then used to determine the non-dimensional height ζ from the previous equations. The value of ζ obtained is used to calculate the Monin-Obukhov functions, and hence the diffusivities, for the appropriate stability regime.

2.7 Method of Solution

To recapitulate and clarify the general method of the model, the following steps to solution are presented:

1. using initial observed temperature profiles for the air and soil, calculate the surface temperature via the heat balance equation,
2. advance the profiles in time at all levels but the surface,
3. calculate the surface temperature at the new time from the new profiles for that time, and,
4. repeat steps 2 and 3 for desired length of forecast.

In the model, only the surface is allowed to absorb and re-emit radiation. The remainder of the boundary layer is assumed transparent to radiation.

According to Estoque (1963) the assumption of transparency is reasonable since the radiative temperature changes in the boundary layer are insignificant in comparison with the contributions to temperature change by eddy diffusion. However, if the boundary layer is polluted, Zdunkowski (1976) has shown that a less intense and less extensive inversion will result when radiative flux divergence calculations are neglected.

It is assumed that the present model atmosphere is unpolluted. Hence the assumption of transparency is applicable. The atmospheric long-wave flux density is therefore deemed to originate at the top of the model boundary layer, even though there might be some water vapour contributing to this flux density within the boundary layer thereby invalidating the assumption of transparency. Thus model heating (or cooling) due to radiation takes place only at the surface and the rest of the model atmosphere is heated by 'conduction', with the rate of mixing determined by the diffusivities as a function of stability.

CHAPTER 3

THE COMPUTER MODEL

3.1 General

In this chapter the equations of Chapter 2 are presented in their numerical form for use in computational algorithms. The model is one dimensional in the sense that profiles are generated in the vertical for a point on the surface. The model predicts two such profiles: one for the rim of the valley (plain), and one for the slope.

It is necessary to run the model in extended precision. The diurnal variation of temperature during summer at Edmonton is 10 to 15 C°/day. To be conservative, it is assumed that the smallest rate of temperature change is 100 times smaller than this rate. This corresponds to a rate of 0.0003 C° per 5 minute time step. Again, to be on the safe side, the iteration scheme assumes that a zero rate of change has been reached when the change is another order of magnitude smaller, ie. a rate of change of 0.00001 C° per 5 minute time step. Potential temperature is generally near

borne out by Lettau and Davidson (1957).

3.3 The Finite-Difference Equations

According to Smith (1965), equations of the form

$$\frac{\partial \Psi(z,t)}{\partial t} = K \frac{\partial^2 \Psi(z,t)}{\partial z^2} \quad (3.3.1)$$

are unconditionally stable and convergent in their finite-difference form

$$\begin{aligned} \psi_j^{k+1} = & \psi_j^k + \frac{a\delta t}{2\delta z^2} K \left\{ \psi_{j+1}^{k+1} - 2\psi_j^{k+1} + \psi_{j-1}^{k+1} \right\} \\ & + \frac{b\delta t}{2\delta z^2} K \left\{ \psi_{j+1}^k - 2\psi_j^k + \psi_{j-1}^k \right\} \end{aligned} \quad (3.3.2)$$

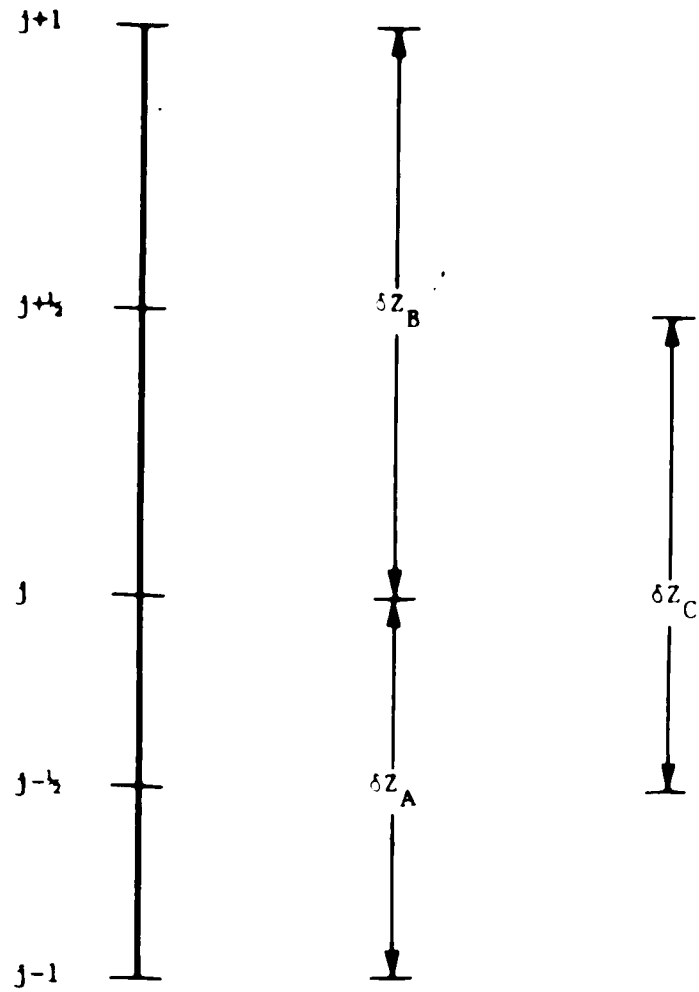
if $a + b = 1$, and $1 \leq b \leq 2$. Subscripts and superscripts are used to identify space and time increments, respectively.

Both the air and soil temperature equations are parabolic partial differential equations of the form

$$\frac{\partial \Psi(z,t)}{\partial t} = \frac{\partial}{\partial z} \left(K(z) \frac{\partial \Psi(z,t)}{\partial z} \right) \quad (3.3.3)$$

For an irregularly-spaced grid, this equation, in finite-difference form, becomes (see Figure 3.2)

$$\begin{aligned} \psi_j^{k+1} = & \psi_j^k + \frac{a\delta t}{2\delta z_c} \left\{ K_{j+\frac{1}{2}} \frac{\psi_{j+1}^{k+1} - \psi_j^{k+1}}{\delta z_b} - K_{j-\frac{1}{2}} \frac{\psi_j^{k+1} - \psi_{j-1}^{k+1}}{\delta z_a} \right\} \\ & + \frac{b\delta t}{2\delta z_c} \left\{ K_{j+\frac{1}{2}} \frac{\psi_{j+1}^k - \psi_j^k}{\delta z_b} - K_{j-\frac{1}{2}} \frac{\psi_j^k - \psi_{j-1}^k}{\delta z_a} \right\} \end{aligned} \quad (3.3.4)$$



$$\delta Z_A = z_j - z_{j-1}$$

$$\delta Z_B = z_{j+1} - z_j$$

$$\delta Z_C = z_{j+1/2} - z_{j-1/2}$$

$$z_{j+1/2} = (z_{j+1} + z_j) / 2$$

Figure 3.2 Finite-Differences on an Irregularly-Spaced Grid

It is assumed this finite-difference equation is also unconditionally stable and convergent for

$$a + b = 1, \text{ and } 1 \leq b \leq 2.$$

Zdenkowski (1976) has found this to be valid for the values $a = 1.5$ and $b = 0.5$. These numbers were adopted in this model.

3.4 Calculation of the Eddy Diffusivities

The neutral exchange coefficient K_N was calculated according to the finite-difference form of Shir's parameterization, equation (2.5.3), with the inclusion, for completeness, of the molecular viscosity. This expression is

$$K_{Nj+\frac{1}{2}} = \frac{u_*^2 k}{2} Z_{j+\frac{1}{2}} \left\{ e^{-(4/h)Z_{j+\frac{1}{2}}} + (1 + 16(Z_{j+\frac{1}{2}}/h)^{1.6})^{-1} \right\} + K_{mol} \quad (3.4.1)$$

where $h = 0.455u_* / f$, and, K_{mol} is the molecular diffusivity of air. The friction velocity, u_* , obtained from the observational data, was periodically input into the model at a predetermined time interval ' Δt '. This friction velocity was calculated from the observations using (Businger, 1973)

$$u_* = k\bar{u} / \log\left(\frac{z + z_0}{z_0}\right) \quad (3.4.2)$$

The model was started at local noon. This was usually several hours before the observed valley data were

available. The earlier model start-up was desirable for two reasons. Firstly, if necessary, the model has time to settle down prior to the comparison with the observations. Secondly, profile initialization can better be accomplished at this time.

The noon model start-up time complicated the calculation of the friction velocity for the rim, since values for the mean wind at 2.64 meter height were not yet available. To this end, it was assumed that the wind at the Municipal Airport could be taken as the rim wind at 2.64 meters. The airport wind is measured at 10 meters using a short-period average value from a slow-response anemometer. The error due to measurement at different heights is expected to be masked by the error due to both the removed location and less sensitive anemometer. Further, because experience has shown that calm conditions rarely prevail in central urban districts, and because of the relatively high threshold value of the airport anemometer, a calm reading at the airport was assigned the value of 1 m/s. Municipal Airport data were also used when it was desired to run the model past the end of the observation period. Whenever the actual rim wind observations were available they were used. Thus the friction velocity for the rim was calculated by

$$u_{*rim} = 0.4 \bar{u} / \log\left(\frac{2.64 + 0.01}{0.01}\right) \quad (3.4.3)$$

where Von Karman's constant is taken as 0.4, the surface

roughness as 0.01 meters, and, the mean wind as either the measured valley rim wind or the airport wind.

During the observation periods, comparison between the recorded 2.64 meter wind at the rim and the wind interpolated to the same height over the slope showed the slope wind to be weaker than the rim wind on the average by an amount

$$\eta = \text{ave} \{ \bar{u}_{\text{slope}} / \bar{u}_{\text{rim}} \}$$

of the rim wind. It was assumed that this fraction, η , was valid outside the observational time frame. Thus the friction velocity for the slope was calculated by

$$u_{* \text{slope}} = 0.4 \eta \bar{u}_{\text{rim}} / \log \left(\frac{2.64 + 0.25}{0.25} \right) \quad (3.4.4)$$

where the slope surface roughness is taken as 0.25 meters.

Hence

$$\frac{u_{* \text{slope}}}{u_{* \text{rim}}} = 2.28 \eta \quad (3.4.5)$$

These friction velocities, calculated at the 2.64 meter level, were used in calculating the diffusivities, $K_{N_{j+\frac{1}{2}}}$, at all model levels. In practice, the friction velocities were calculated at one-half hourly intervals and then smoothed with a three point running mean.

The kinematic viscosity used for air (Sutton, 1953) is

$$K_{\text{mol}} = 1.5 \times 10^{-5} \text{ m}^2/\text{sec} \quad (3.4.6)$$

Once the neutral eddy viscosity has been calculated, the desired diffusivities are determined by equation (2.6.1). This equation requires the evaluation of the

Monin-Obukhov profile functions.

3.5 Calculation of the Monin-Obukhov Profile Functions

The Businger relations, equations (2.6.4) and (2.6.5), are used to evaluate the Monin-Obukhov profile functions for heat. The equations require the dimensionless height which may be calculated, via equations (2.6.6) and (2.6.7), from the Richardson number. Thus the Richardson number must be computed.

The Richardson number has previously been defined as

$$R_i = \frac{g}{\theta} \left(\frac{\partial \theta}{\partial z} \right) / \left(\frac{\partial \bar{u}}{\partial z} \right)^2 \quad (3.5.1)$$

Using this form of the Richardson number poses a problem. Strictly speaking the wind shear and hence the wind must be known at every level. But wind is not predicted by the model. Further, only observed winds at one level are input into the model. To overcome this difficulty, the bulk Richardson number, in conjunction with stability relations similar to those of Golder (1972), was employed. The bulk Richardson number (Lettau and Davidson, 1957) is defined by

$$B = \frac{g}{\theta} \left(\frac{\partial \theta}{\partial z} \right) \frac{\bar{z}^2}{\bar{u}^2} \quad (3.5.2)$$

where \bar{z} is the geometric mean height between the top and bottom of the layer considered. Only one wind measurement is required to determine the bulk Richardson number. The bulk Richardson number is related to the Richardson

number by

$$\frac{R_i}{B} = \bar{u}^2 / \left(\frac{\partial \bar{u}}{\partial \log z} \right)^2 \quad (3.5.3)$$

Also the Businger profile functions for momentum may be integrated (Paulson 1970) to yield

$$\frac{k\bar{u}}{u_*} = \log(z/z_0) - \psi_m \quad (3.5.4)$$

where $\psi_m(\zeta < 0) = 2 \log\left(\frac{1 + \phi_m^{-1}}{2}\right) + \log\left(\frac{1 + \phi_m^{-2}}{2}\right) - 2 \tan^{-1}(\phi_m^{-1}) + \pi/2$

and $\psi_m(\zeta > 0) = -4.7 \zeta$

Equations (2.6.6), (2.6.7), (3.5.3), and (3.5.4) may be combined, remembering that

$$\phi_m(\zeta) \equiv \frac{kz}{u_*} \frac{\partial \bar{u}}{\partial z}$$

to give

$$1 = \frac{B \{ \log(z/z_0) - \psi_m \} (1-9\zeta)^{-1/2}}{.74\zeta}, \quad \zeta < 0 \quad (3.5.5)$$

$$1 = \frac{B \{ \log(z/z_0) - \psi_m \}^2}{\zeta (.74 + 4.7\zeta)}, \quad \zeta > 0 \quad (3.5.6)$$

These stability relations differ from those of Golder (1972) in that the ratio of the exchange co-efficients is not assumed to be unity. There is only one unknown in the above equations, and that is the dimensionless height ζ . If the bulk Richardson number is negative, ζ is solved for iteratively using Newton's Method (Conte and de Boor, 1972).

By taking the bulk Richardson number equal to the dimensionless height as a first guess, solution to within 5 per cent of ζ is usually encountered in three iterations. If the bulk Richardson number is positive, the solution for ζ is analytical. With a value for ζ now determined, the profile functions, and hence the diffusivities can be calculated.

To guard against the possibility of the diffusivities inappropriately assuming molecular values, a minimum friction velocity and hence maximum ϕ_h is determined from the observed data, and then, if a ϕ_h is computed that exceeds this maximum, it is reset to the maximum value. In the actual computations, the formula for the eddy viscosity is recast (Businger, 1973) as

$$K_m = u_*^2 / \left(\partial \bar{u} / \partial z \right) \quad (3.5.7)$$

The exact procedure to determine the maximum ϕ_h is as follows

1. determine $u_{* \min}$ via equation (2.4.2) using the minimum u observed,
2. determine $K_{m \min}$ via equation (3.5.7),
3. assume $K_N \equiv K_{m \text{ neutral}}$ is given by K_m at sunset, and determine K_m via steps 1 and 2 using observed sunset values, and,
4. using equations (2.6.1) and (2.6.3), calculate

$$\zeta_{\max} = \left(\frac{K_N}{K_{m \min}} - 1 \right) / 4.7$$

5. hence calculate $\phi_{h \max}$.

3.6 Calculation of the Surface Temperature

The method used to calculate the surface temperature follows the same procedure as Jacobs and Brown (1973). The heat balance equation is recast as

$$0 = T - \left\{ \left(F_{SW} + F_{WV} - F_{SH}(T) - F_{LH}(T) - F_{SHS}(T) \right) / .82\sigma \right\}^{-1/4} \quad (3.6.1)$$

This is an implicit equation in the surface temperature, T . Difficulties arise in solving this equation iteratively. The quantity in brackets can take on values less than zero. To overcome this problem, let T_c be the temperature at which the quantity in brackets becomes zero, and define a function

$$g(T) = \begin{cases} T - \left\{ \left(F_{SW} + F_{WV} - F_{SH}(T) - F_{LH}(T) - F_{SHS}(T) \right) / .82\sigma \right\}^{-1/4}, & T \leq T_c \\ T & , T > T_c \end{cases} \quad (3.6.2)$$

The real root of $g(T) = 0$ determines the surface temperature. For $T \leq T_c$, the root is found iteratively either by Newton's Method (Conte and de Boor, 1972) or, if the root lies in a region where $g(T)$ is not continuously differentiable, by the Secant Method (Conte and de Boor, 1972). For $T > T_c$, the Reguli Falsi Method (Conte and de Boor, 1972) is used. If T happens to be greater than T_c on the first iteration, an initial value of $T = 250$ °K is used in the Reguli Falsi method. This value is usually smaller than any Edmonton summer surface temperature. Thus bracketing of the root is accomplished.

The sensible and soil heat flux densities are of the form

$$F = -\lambda \left. \frac{\partial T}{\partial z} \right|_{z=0} \quad (3.6.3)$$

Due to the logarithmic nature of temperature near the surface, a second order Taylor Series expansion is used in the finite-difference approximation of the derivative, namely

$$\left. \frac{\partial T}{\partial z} \right|_{z=0} = \frac{z_2^2 T(z_1) - z_1^2 T(z_2) - (z_2^2 - z_1^2) T(0)}{z_1 z_2 (z_2 - z_1)} \quad (3.6.4)$$

The latent heat flux density is parameterized in terms of the sensible heat flux density (after Sellers, 1965) in the following manner

$$F_{LH} = \begin{cases} F_{SH}, & F_{SH} > 0 \\ -0.5 F_{SH}, & F_{SH} < 0 \end{cases} \quad (3.6.5)$$

3.7 Prediction Procedure for the Temperature Profiles

The atmospheric temperature profile is approximated by the temperature values at $N=NZPTS$ discrete points. It is assumed that the temperature at the top of the profile (the top of the boundary layer) is constant. Similarly, the soil temperature profile is approximated by values at $N=NZSPTS$ points, and the soil bottom temperature assumed constant. Further, the temperature at the interface is determined by the heat balance equation. Thus the temperature is only

forecast at $N-2$ points, namely 2 through $N-1$. Equation (3.3.4) can be rewritten as

$$A_j \psi_{j+1}^{k+1} + B_j \psi_j^{k+1} + C_j \psi_{j-1}^{k+1} = D_j \quad (3.7.1)$$

This set of equations forms a tridiagonal matrix for the interior points, and can be solved (see Appendix C) using Gaussian elimination, ie.

$$\psi_j^{k+1} = \frac{D_j - A_j F_{j+1}}{B_j + A_j G_{j+1}} + \frac{-C_j}{B_j + A_j G_{j+1}} \psi_{j-1}^{k+1} \quad (3.7.2)$$

$$F_j = \frac{D_j - A_j F_{j+1}}{B_j + A_j G_{j+1}} \quad (3.7.3)$$

$$G_j = \frac{-C_j}{B_j + A_j G_{j+1}} \quad (3.7.4)$$

Thus a procedure to find the profile at time $t + (k+1)\Delta t$ is

1. assume surface temperature changes little over one time step and take $T_1^{k+1} = T_1^k$,
2. solve for T_j^{k+1} , $j=2, \dots, N-1$ by equation (3.7.2),
3. using the new profile obtained in step 2, calculate a new T_1^{k+1} , and,
4. advance one time level, and repeat steps 1 to 3.

This procedure has an inherent weakness. Due to step 1, the time step must be small. However, this problem can be overcome by employing an iterative procedure. Before advancing to step 4, simply repeat steps 2 to 3 until the

surface temperature calculated at the most recent iteration differs from that obtained from the previous iteration by a predetermined small amount. As mentioned in section 3.1, 0.00001 C° is an appropriate difference, and this value was used. With this approach, time steps as large as 20 minutes have given consistent profiles. However, the settling-down time needed for the model increases with the size of time step. A time step of 5 minutes generally ensures stable results after half an hour. This can be reduced, if desired, by re-initializing the model after 2 or 3 time steps. Generally, the oscillations initially present are not severe and damp out quickly.

3.8 Inclusion of a Neutral Slope Layer

By late evening, the model consistently predicts a one meter slope temperature that lies close to the rim temperature. This is contrary to a 3 to 6 C° spread observed when there is a slope wind present. The behaviour of the model is not surprising since no provision for the increased mixing due to the slope wind has been incorporated.

In Chapter 1, it was indicated that the slope wind had an effective depth of at least 3 meters and possibly as large as 15 meters. For model purposes, the slope wind was taken to be operative up to the tenth grid point, or approximately 4.6 meters. It was then postulated that the

profiles for below the 1.2 meter screen height were then extrapolated using screen height temperatures. The initial profile between 1.2 meters and 850 millibars was determined by assuming a constant lapse rate between the temperatures at these two levels. The initial profile above the 850 millibar level was determined solely from the radiosonde data. It was assumed that the 850 mb temperature at radiosonde time would not differ greatly from its temperature at local noon.

The values for the soil thermometric and thermal conductivities used in the model were also those of the Plains data, namely $1.5 \times 10^{-7} \text{ m}^2/\text{sec}$ and $0.25 \text{ J/m}^2/\text{sec}/^\circ\text{K}$.

4.2 The Atmospheric Temperature Profile

The temperature profile from the first experiment of the Plains Field Programme is plotted, with the 0.1 meter temperature subtracted from every value, in Figure 4.1. Superimposed is a similar plot obtained from the third Plains experiment. A straight line is fitted visually to the data (given the magnitude of the assumption made, a more accurate fit was deemed unnecessary). The axis of the graph was then shifted so that a temperature difference of zero co-aligned with the screen height. Hence Table 4.1 was constructed. The last entry in the table for 0.0 meters was obtained by linearly extrapolating between 0.01 and 0.05 meters.

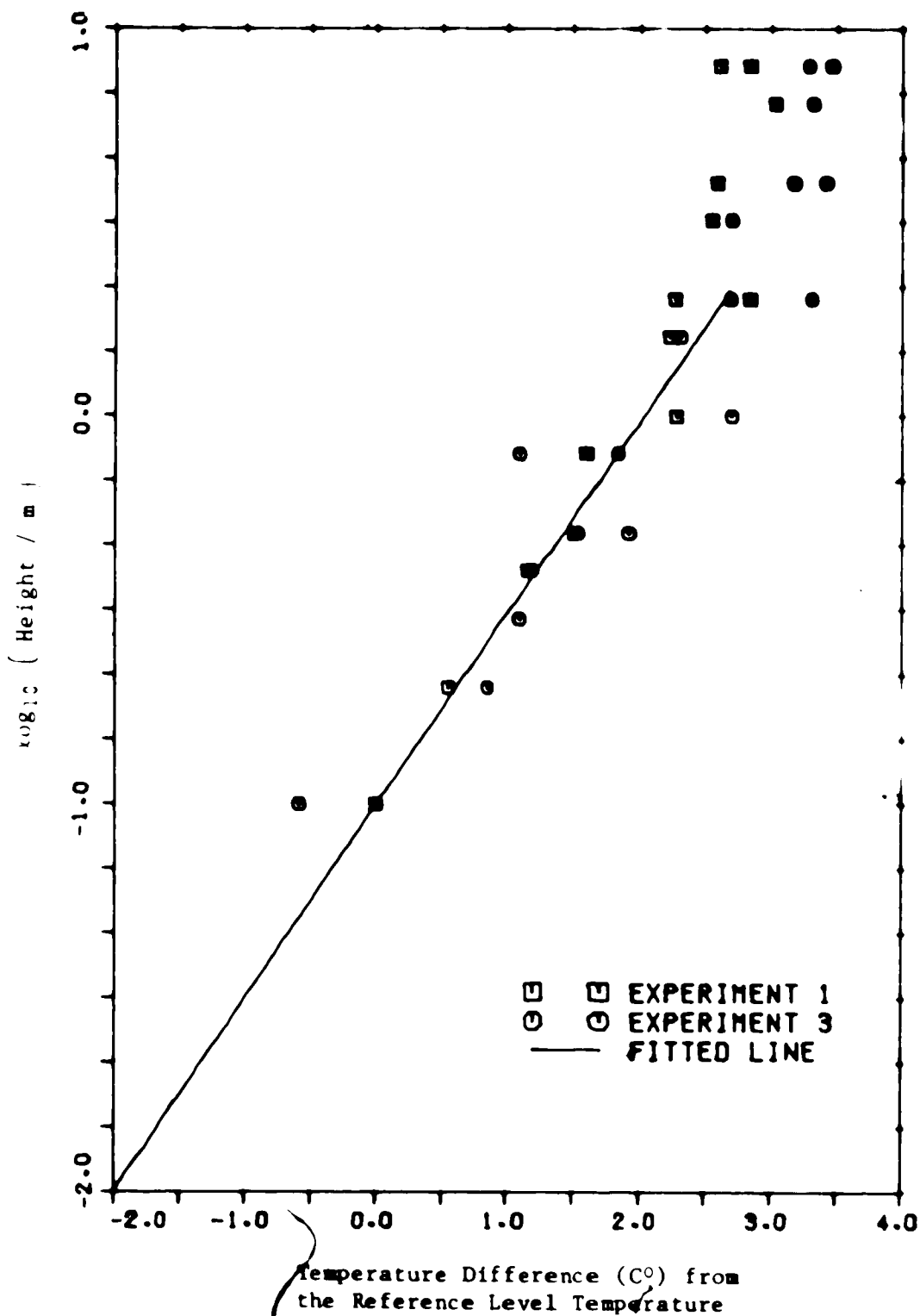


Figure 4.1 The Interpolation Curve for the Initial Atmospheric Temperature Profile

Table 4.1 The Interpolation Table for the Initial
Atmospheric Temperature Profile

Height (m)	Difference from the Screen Temperature (C°)
1.20	0.0
1.00	0.2
0.46	0.8
0.22	1.5
0.10	2.2
0.05	2.9
0.00	4.6

Thus the model initialization procedure is to take the screen temperature at local noon and using Table 4.1 arrive at a guess for the temperature profile in the lowest 1.2 meters. The discretization of the input profile need not align with the grid. The model has the capability of interpolating grid point values from the input profile. The input profile is converted to potential temperature by

$$T_j = T_1 \left(\frac{P_1}{P_j} \right)^{.286} \quad (4.2.1)$$

where

$$P_j = P_{j+1} e^{g(z_j - z_{j+1}) / (RT)} \quad (4.2.2)$$

$$\bar{T} = \frac{T_{sfc} + T_{850}}{2} \quad (4.2.3)$$

$$T_{sfc} = \frac{T_{sfc_{min}} + T_{sfc_{max}}}{2} \quad (4.2.4)$$

4.3 The Soil Temperature Profile

In a fashion similar to that of Section 4.2, the Plains data (Lettau and Davidson, 1957) were used to construct Figure 4.2 and Table 4.2 for soil. In Figure 4.2, the curve fitted to the data below 10 cm was justified on the basis that the data below this level was measured by a different observer with different instruments. The trend of the curve is still maintained.

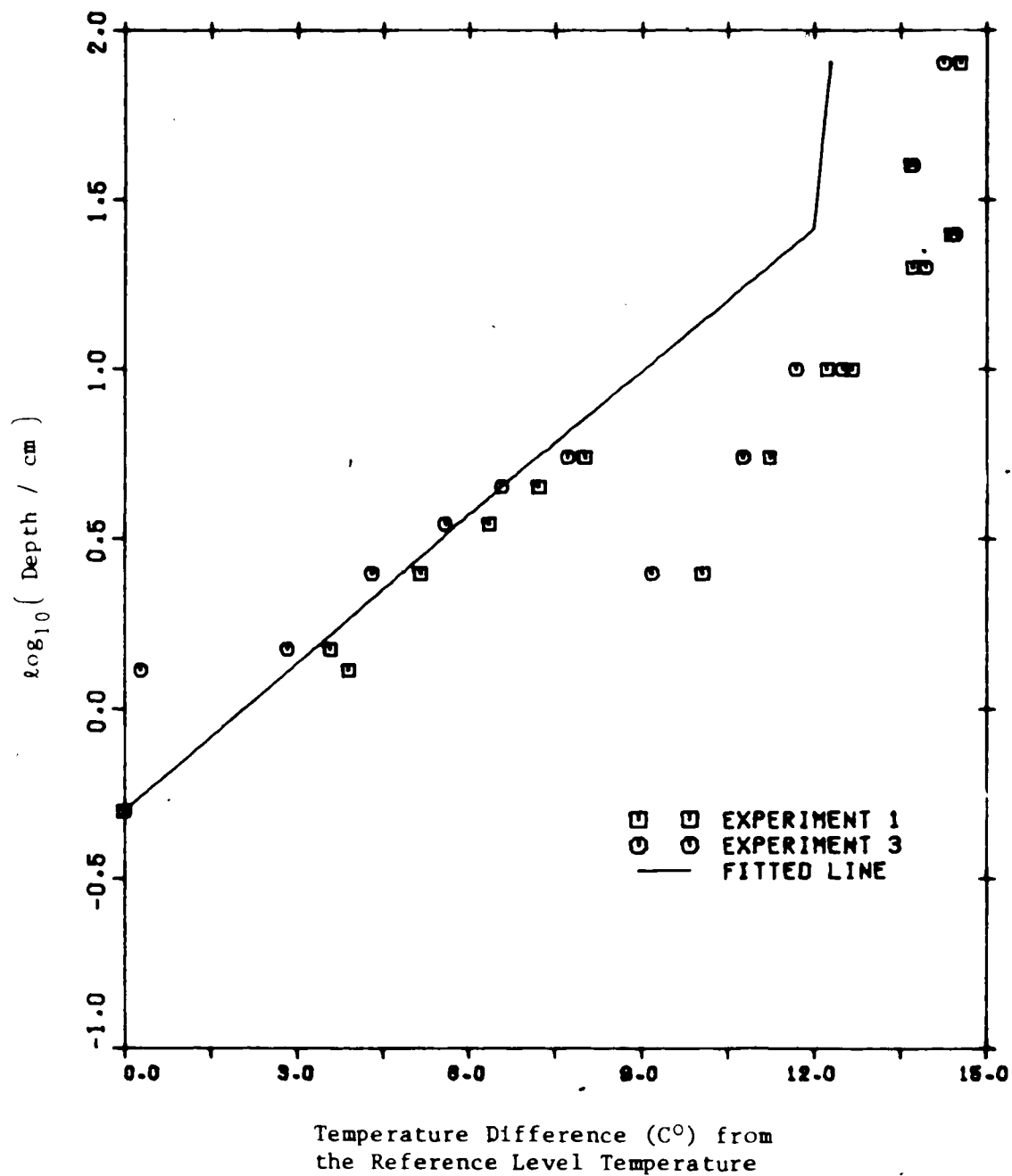


Figure 4.2 The Interpolation Curve for the Initial Soil Temperature Profile

Table 4.2 The Interpolation Table for the Initial Soil Temperature Profile

Soil Depth (cm)	Difference from the Surface Temperature (C°)
0.00	0.0
0.50	- 2.1
1.04	- 4.2
2.15	- 6.4
4.47	- 8.7
9.28	-10.9
19.30	-13.1
40.00	-14.2

The initialization procedure is to take the temperature obtained for the surface in the previous section, and use Table 4.2 to arrive at a guess for the input soil profile. As with the atmospheric input profile, the points of the input soil profile need not be co-aligned with the soil grid.

CHAPTER 5

RESULTS

5.1 General

In this chapter the results from the computer simulations of Experiments 8, 9, and 11 are presented. The results are discussed in relation to the observed data, and observations pertinent to the model are also included. Occasionally recourse is made to observations not obtained at the Dawson Bridge site. In addition, the viability of a double structure inversion in the valley is examined, and the differences between urban and rural cooling is studied. Further, sensitivity to certain model parameters is considered. In each experiment, the model was run for a period of 12 hours starting at local noon. The grid employed by the model throughout all simulations is given in Appendix D. Appendix E lists the parameters which were common to all the experiments, and Appendix F lists the programme for the model.

5.2 The Results for Experiment 8

5.2.1 General

Experiment 8 was conducted on 27 June 1978. Conditions were very favourable. No significant synoptic or mesoscale activity existed in the vicinity. Scattered fair-weather cumulus prevailed during the day, and, occasionally, scattered altocumulus occurred during the evening. The progression of wind and temperature throughout the day was almost ideal. At noon the surface winds were light. Then, as insolation incited buoyancy in the boundary layer, convective overturning mixed the stronger winds aloft downward. A mid-afternoon maximum of 6 m/s was reached. Finally, by sunset (approximately 1853 MST), with the decrease of surface heating, the winds again became light. Temperature throughout the afternoon was essentially constant although small variations, likely due to thermals, were present. A maximum of 26.5°C (at the Municipal Airport) was reached in the late afternoon, and a definite steady temperature decline began within two hours of sunset.

5.2.2 The Observations

The winds and temperatures from the local airports are given in Table 5.1. Valley winds are given Tables 5.2 and 5.3. Valley temperatures are presented in Table 5.4.

Table 5.1 The Temperatures and Winds from the Local Airports on 27 June 1978

Time (GMT)	Airport					
	Municipal		Nanao		International	
	Temp (°C)	Wind (°/ m/s)	Temp (°C)	Wind (°/ m/s)	Temp (°C)	Wind (°/ m/s)
1800	22.0	300/3.1	21.8	290/6.2	21.6	290/4.6
1900	22.7	280/2.7	22.8	280/6.2	22.4	280/2.6
2000	22.9	310/5.7	22.7	300/7.7	22.6	310/5.7
2100	23.1	280/6.2	23.7	270/6.7	23.3	270/3.1
2200	24.1	290/3.1	23.9	260/6.7	24.2	270/4.1
2300	24.4	270/2.6	24.2	310/4.6	25.1	270/4.1
2400	24.8	320/3.1	24.2	310/2.6	25.2	250/2.6
0000	24.6	320/2.6	23.9	320/4.6	25.4	270/1.0
0100	24.0	260/1.5	23.9	210/1.0	24.2	0
0200	23.5	270/1.0	23.6	280/1.0	23.1	010/2.1
0300	22.6	0	20.8	0	18.7	0
0400	21.7	0	19.4	0	16.4	0
0500	20.2	180/1.0	18.8	020/1.0	14.2	120/1.0
0600	16.3	0	17.4	0	13.6	160/1.0
0700	16.5	0	13.0	360/1.5	12.9	150/1.0
0800	15.7	0	15.4	0	12.5	310/3.6

Table 5.2 The Valley Winds (m/s) on 27 June 1978

Time (MDT)	Mean Wind Station 11				Mean Wind Station 8
	1.70	2.84	5.84	2.64	Height (m) 2.64
1530-1600					3.95
1600-1630					4.16
1630-1700					3.30
1700-1730					3.70
1730-1800	1.17	1.26	1.28	1.21	2.96
1800-1830	0.86	0.91	0.94	0.88	3.36
1830-1900	0.89	1.00	1.04	0.94	2.51
1900-1930	0.76	0.89	0.98	0.82	2.30
1930-2000	0.52	0.55	0.61	0.53	2.25
2000-2030	0.61	0.57	0.53	0.59	1.89
2030-2100	0.43	0.35	0.30	0.40	1.66
2100-2130	0.41	0.42	0.28	0.41	1.25
2130-2200	0.28	0.25	0.17	0.27	1.05
2200-2230	0.20	0.32	0.29	0.25	0.79
2230-2300	0.11	0.33	0.26	0.21	0.80
2300-2330	0.15	0.25	0.23	0.19	1.54
2330-2400	0.09	0.08	0.07	0.09	1.26
0000-0030					0.79

interpolated linearly from 1.70 m and 2.84 m winds.

Table 5.3 The Slope (Drainage) Wind at Station 11
on 27 June 1978

Time (MDT)	Mean Wind (m/s)	Time (GMT)	Mean Wind (m/s)
1915	-0.04 ¹	2145	0.64
20	-0.04 ¹	50	0.63
25	0.06	55	0.64
1930	0.06	2200	0.66
35	0.38	05	0.70
40	0.28	10	0.60
1945	0.17	2215	0.56
50	0.51	20	0.66
55	0.38	25	0.58
2000	0.15	2230	0.71
05	0.59	35	0.51
10	0.21	40	0.60
2015	0.68	2245	0.70
20	0.42	50	0.66 ²
25	0.62	55	0.62 ²
2030	0.77	2300	0.57 ²
35	0.77	05	0.53
40	0.49	10	0.49
2045	0.71	2315	0.43
50	0.70	20	0.62
55	0.54	25	0.64
2100	0.85	2330	0.45
05	0.72	35	0.53
10	0.66	40	0.58
2115	0.79	2345	0.47
20	0.80	50	0.36
25	0.71		
2130	0.86		
35	0.81		
40	0.68		

¹minus sign indicates an upslope wind.
²linearly interpolated value.

Table 5.4 The Calibrated Valley Temperatures (°C) on
28 June 1978

Time (MDT)	Station 8		Station 11				
	Height (m)	0.36	1.20	Height (m)			
				2.60	5.06	7.10	9.45
1530	26.0						
45	25.4						
1600	25.6						
15	25.9						
30	25.4						
45	25.6						
1700	26.6						
15	25.3		27.9	25.7	25.6	25.4	25.3
30	26.2		26.9	25.0	24.5	24.9	25.1
45	26.5		27.1	25.6	25.3	25.3	25.1
1800	25.8		27.0	25.6	25.6	25.5	25.3
15	25.8		26.7	25.3	25.3	25.7	25.5
30	26.0		25.9	24.6	24.5	25.3	25.2
45	26.6		25.7	25.6	25.2	25.3	25.2
1900	26.4	23.4	25.1	24.2	25.3	25.3	25.1
15	26.1	23.1	24.5	24.7	25.1	25.3	25.2
30	25.9	21.0	23.1	23.8	25.4	25.4	25.4
45	26.3	20.8	22.6	24.1	25.1	25.2	25.1
2000	25.7	19.3	21.6	22.0	25.1	24.5	24.7
15	25.4	18.7	21.5	22.6	24.7	24.6	24.3
30	25.8	18.1	20.5	22.8	23.4	24.2	25.1
45	25.3	16.7	19.6	20.6	21.7	21.7	22.8
2100	25.0	16.1	19.4	20.2	21.6	22.3	23.8
15	24.5	15.1	18.5	21.6	23.5	24.0	24.8
30	24.3	15.4	18.0	19.7	22.0	23.5	24.3
45	23.4	13.8	17.4	20.9	21.1	21.3	22.1
2200	22.9	13.4	17.0	18.2	19.8	20.8	20.7
15	22.1	11.5	16.5	19.2	19.5	19.4	20.0
30	21.7	10.8	15.9	17.8	18.8	19.6	20.2
45	21.5	10.6	15.5	17.7	18.3	18.7	19.3
2300	20.7	11.3	15.0	16.3	17.6	18.0	18.8
15	20.0	10.8	14.7	16.5	17.4	18.3	18.8
30	19.6	10.4	14.3	16.1	16.6	16.8	17.8
45	19.4	10.2	14.0	16.0	17.2	17.2	17.5
0000	19.2	10.8	13.8	16.2	16.1	16.2	16.8
15	18.8						
30	18.2						
45	17.7						

5.2.3 The Model Parameters

The parameters used in the computer simulation have been calculated according to previously detailed procedures, and are listed in Table 5.5. The start-up temperature profiles for the atmosphere and soil are specified in Tables 5.6 and 5.7. The 2.64 meter winds required by the model are given in Table 5.8. The slope friction velocity was calculated according to equation (3.4.4) using an n of 0.27 determined from Table 5.2. The drainage winds required by the model were extracted from Table 5.3. The value for a missing entry was linearly interpolated from its nearest neighbours. Further, in the interval between the termination of the experimental observations and the model termination, an average slope wind was used.

5.2.4 The Model Predictions

In this section, the model predictions for Experiment 8 are discussed. Evidence for the validity of the calculated flux density profiles is presented; the characteristics of the temperature profiles are shown; and the possibility of a double structure inversion is proffered.

Generally, the magnitudes and trends of the predicted flux densities as a function of time were consistent with the literature (see, for example, Lettau and Davidson 1957). However, proper evaluation of the flux densities produced by the numerical model was difficult since it was not possible

Table 5.5 The Model Parameters for Experiment 8

Parameter	Programme Name	Value
Declination	DEC	23° 18.8'
Equation of Time	EOT	2 min 58 sec
Sun's Hour Angle at Model Start-up	HATO	-1° 14.3'
Maximum ϕ_h	PHILIM	1.069
Slope Wind Start Time	TSLE	18.58 hrs MST
Surface Pressure	PS	922 mb
Average Layer Temperature throughout Period	TAV	293.06 °C
Atmospheric Flux Density	FLWA	265 W m^{-2}

**Table 5.6 The Initial Air Temperature Profile
for Experiment 8**

Height (m)	Temperature (°K)
2000.	278.96
708.	290.16
1.20	295.96
1.00	296.16
0.46	296.76
0.22	297.46
0.10	298.16
0.05	298.86
0.00	300.52

**Table 5.7 The Initial Soil Temperature Profile
for Experiment 8**

Depth (cm)	Temperature (°K)
0.00	300.52
0.50	298.42
1.04	296.32
2.15	294.12
4.47	291.82
9.28	289.62
19.30	287.42
40.00	286.32

Table 5.8 The Nodel Winds (m/s) for Experiment 8

Time (GMT)	Mean Wind (Municipal)	Mean Wind (Observed)	Mean Wind (Filtered ¹)	Friction Velocity (Rim)	Friction Velocity (Slope)
1800	3.09				
1900	2.06		3.60	.258	.159
30			4.12	.295	.182
2000	5.66		4.63	.332	.204
30			4.99	.358	.220
2100	6.17		5.34	.383	.236
30			4.95	.355	.219
2200		4.20	4.55	.326	.201
30			4.07	.292	.180
2300		3.28	3.58	.257	.158
30			3.35	.240	.148
0000		3.26	3.11	.223	.137
30			2.98	.214	.132
0100		2.78	2.85	.204	.126
30			2.58	.185	.114
0200		2.52	2.30	.165	.102
30			2.01	.144	.089
0300		1.61	1.72	.123	.076
30			1.42	.102	.063
0400		1.03	1.12	.080	.049
30			1.05	.075	.046
0500		0.71	0.97	.070	.043
30			0.97	.070	.043
0600		1.16	0.96	.069	.042
30			1.01	.072	.044
0700	1.00 ²		1.05	.075	.046
30			1.03	.074	.045
0800	1.00 ²		1.00	.072	.044
30			1.00	.072	.044
0900	1.00 ²		1.00	.072	.044

¹a three-point Bartlett filter was used.

²rain reading assigned a value of 1 m/s as per section 3.4.

to obtain any flux measurements in any of the river valley experiments. Nevertheless, an attempt to demonstrate that the model flux densities are reasonable was undertaken.

Measured net radiation and solar radiation data* for 1977 are available from Stony Plain, a location approximately 35 kilometers west of Edmonton. Within certain limitations, the assessment of the predicted solar flux density can be accomplished using this data. Errors arising from differences in location were presumed unimportant. Errors due to the one year time difference were more formidable. Astronomically, the solar radiation reaching a certain point at a particular time is constant from year to year. Thus any difference is due to atmospheric effects with cloud cover in particular being a major factor. Fortunately, in late June the rate of change in the sun's declination is a minimum. Thus, it can be assumed that the solar radiation is similar in a ten day period preceding and following the 27 June 1977. Further, it is assumed that the variable nature of cloud cover will ensure that each of the 24 hourly observation slots will be cloud-free at least once during the period considered. Hence a good estimation of the solar radiation can be made by taking, for each hour, the maximum value recorded. This procedure was carried out, and the results plotted in

*This data is published in the Monthly Radiation Summary, ISSN 0027-0482, by the Atmospheric Environment Service, Environment Canada.

]

Figure 5.1. The solar radiation measured at Stony Plain consisted of the total downward direct and diffuse solar flux; no measurement of reflected solar radiation was made. Thus a standard reflection of 20 per cent was adopted. The solar radiation calculated by the model is also plotted in Figure 5.1. Given the magnitude of the assumptions made, the agreement is quite reasonable. The observed maximum calculated between 1100 and 1200 local time may not be real. Significantly lower data values were recorded before and after this maximum, making its selection suspect.

A similar comparison was carried out for the net flux of radiation reaching the earth's surface. The results are shown in Figure 5.2. Since the net flux density is not necessarily symmetric, and since the computer simulation was for a 12 hour period, only twelve hours of the Stony Plain data are plotted. The results are not out of line. The net flux density calculated by the model makes no allowance for cloud cover. Thus the smaller afternoon amplitude in the calculated observed curve is likely due to procedural inability to remove completely the effect of cloud. Typically summer mornings and evenings are cloud-free, while the afternoons develop fair-weather cumulus.

The model-predicted latent plus sensible heat flux densities to the atmosphere, and soil heat flux density to the ground are given in Figures 5.3 and 5.4, respectively. Unhappily, the Stony Plain data does not include these flux measurements. However, the verification of the model solar

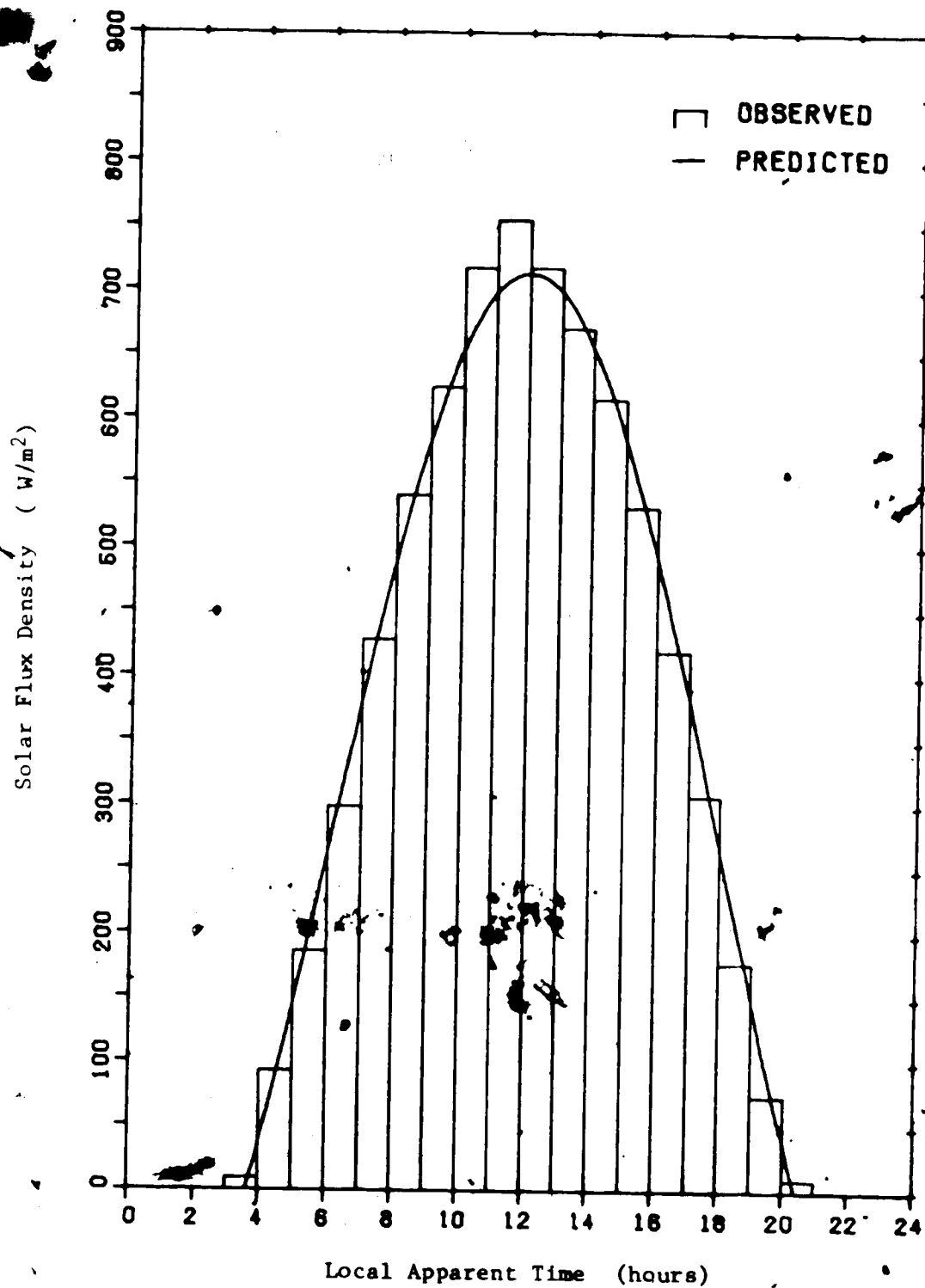


Figure 5.1 The Assessment of the Model-Predicted Solar Flux Density for Experiment 8

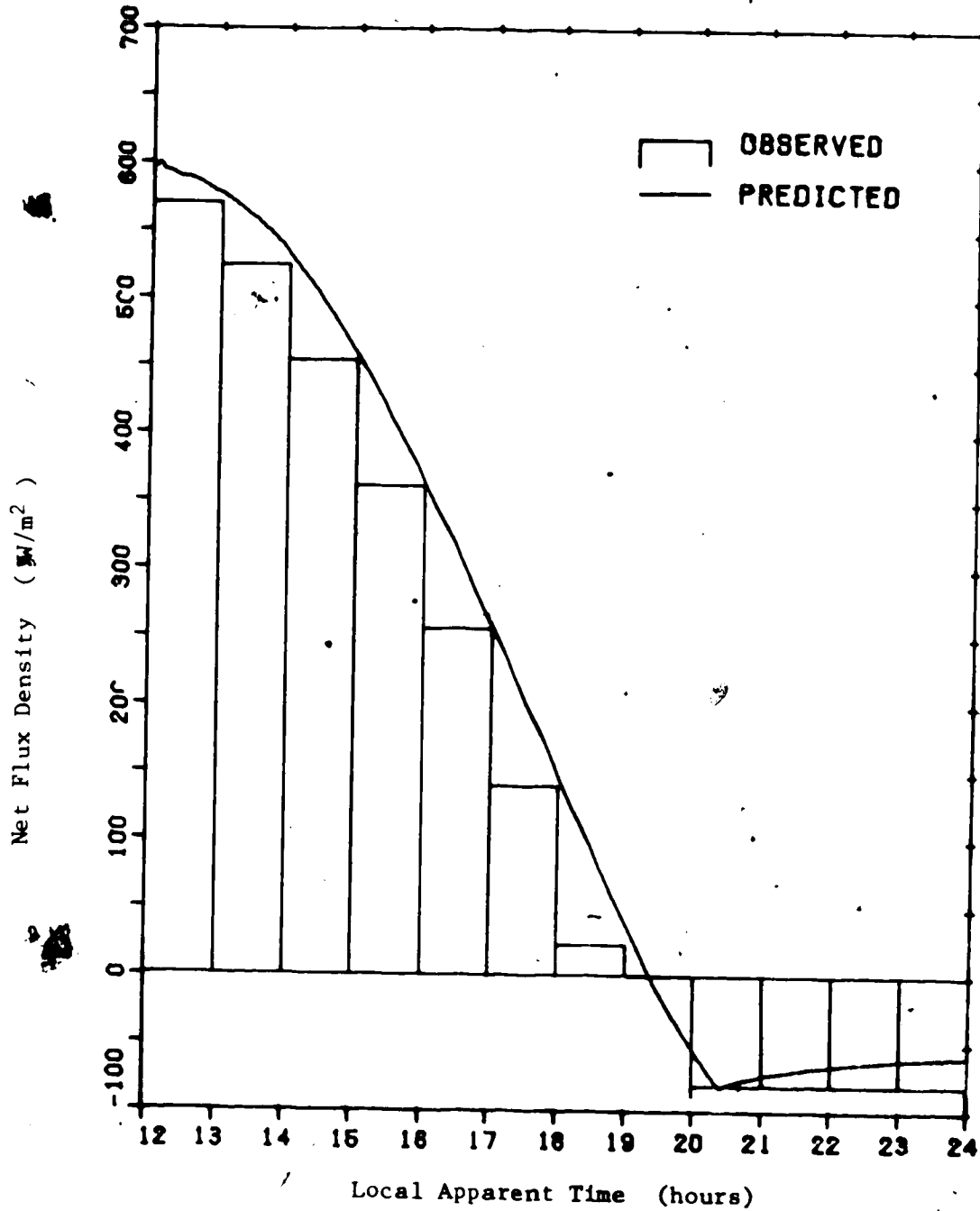


Figure 5.2 The Assessment of the Model-Predicted Net Flux Density for Experiment 8

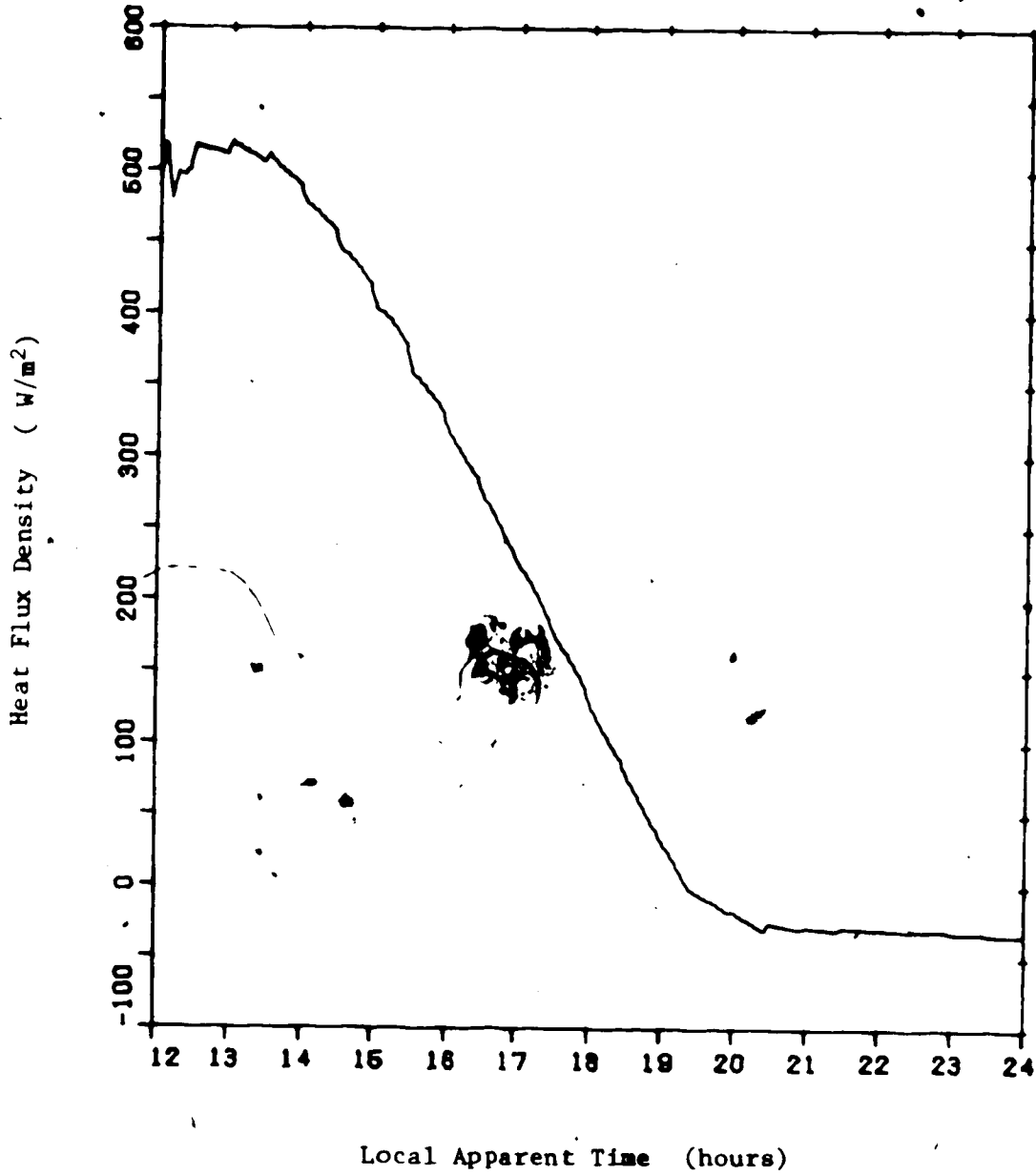


Figure 5.3 The Model-Predicted Heat Flux Density to the Atmosphere for Experiment 8 .

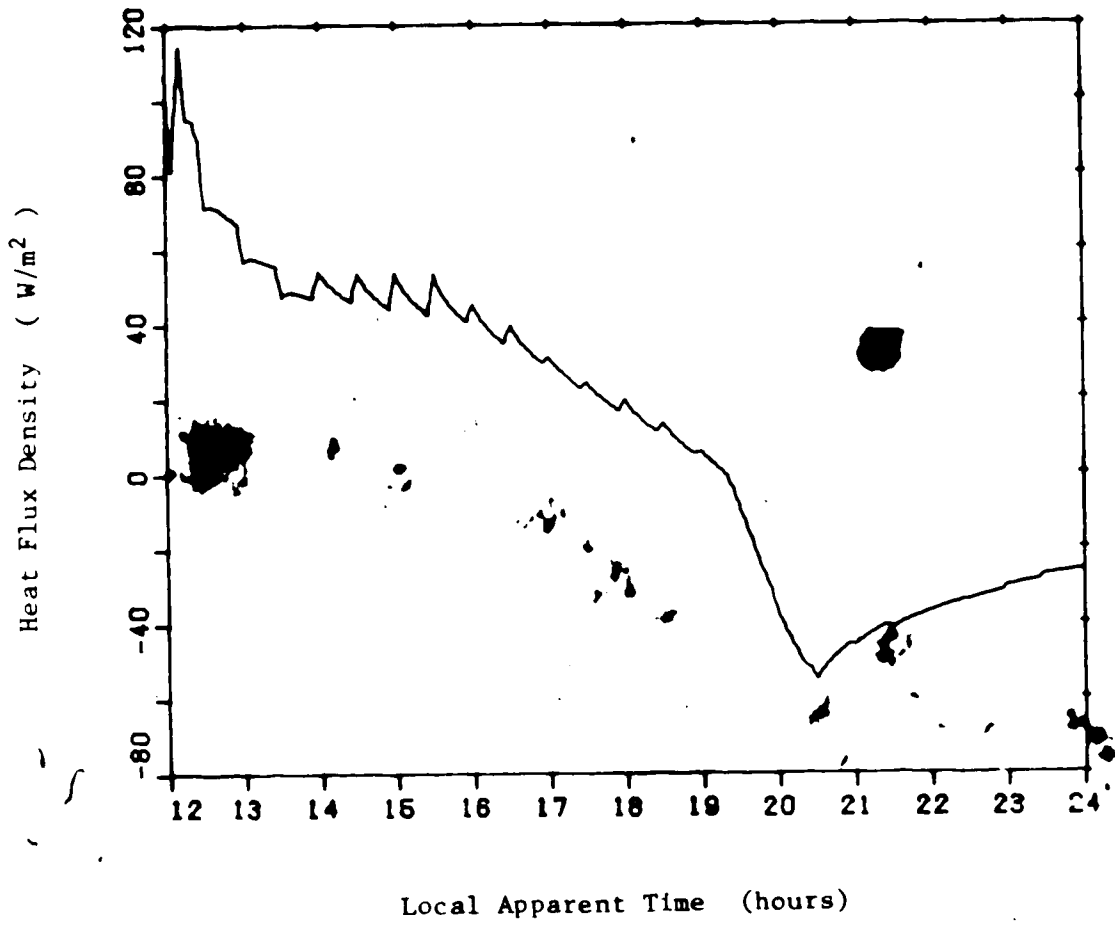


Figure 5.4 The Model-Predicted Heat Flux Density to the Soil for Experiment 8

and net radiative flux densities, and the general acceptability of the magnitude and trend in the remaining model-predicted flux densities indicate that these flux densities are sufficiently reliable.

The evolution of the model-predicted temperature fields for both the rim and slope between 1235 and 0035 MST is presented in Figures 5.5 and 5.6. In order to more closely scrutinize the results, attention will be focussed on two aspects of the output: the variation of the temperature at a particular level throughout the period; and the profile of the temperature in the vertical at a particular

The progression of predicted temperature with time for the 1 meter level over the slope is shown in Figure 5.7. The observed screen temperature curves are also plotted in the figure. The agreement between the observed and predicted rim temperatures is quite good. The predicted curve, although generally almost one degree warmer, is congruent to the observed trace, and the times of maximum temperature coincide. Only after approximately 2300 MDT does the predicted trend diverge from that observed. The slope traces do not agree to the same extent. Initially the agreement is good. However, once the slope (drainage) wind is initiated, the trend is not preserved, and by 2400 MDT, there is a 5 degree difference between the observed and predicted values. The inclusion of a neutral layer in the regime of the slope wind tended to alleviate this problem. As demonstrated in Figure 5.7, the trends of the observed

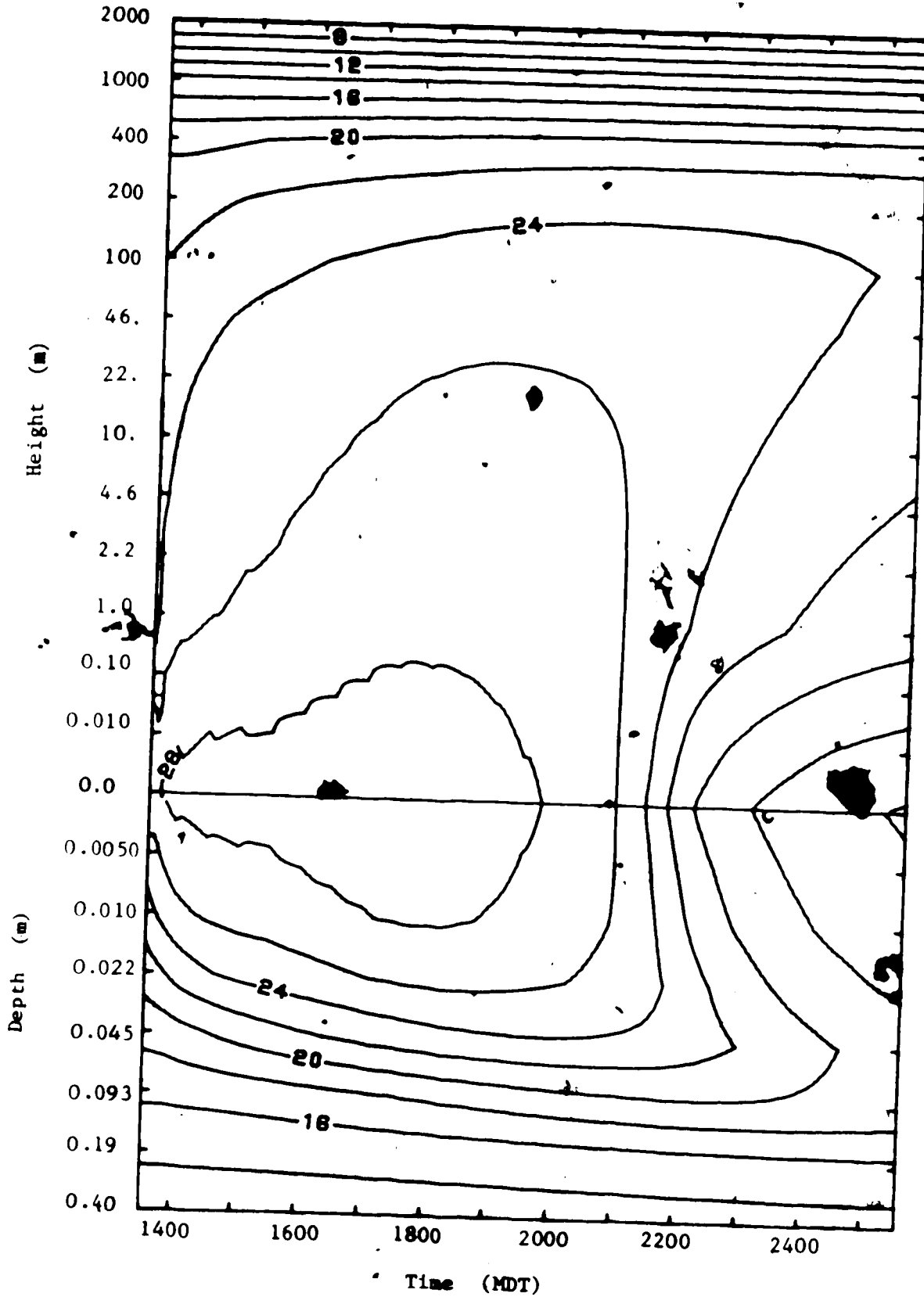


Figure 5.5. The Model-Predicted Temperature Field at the Ris for Experiment 8

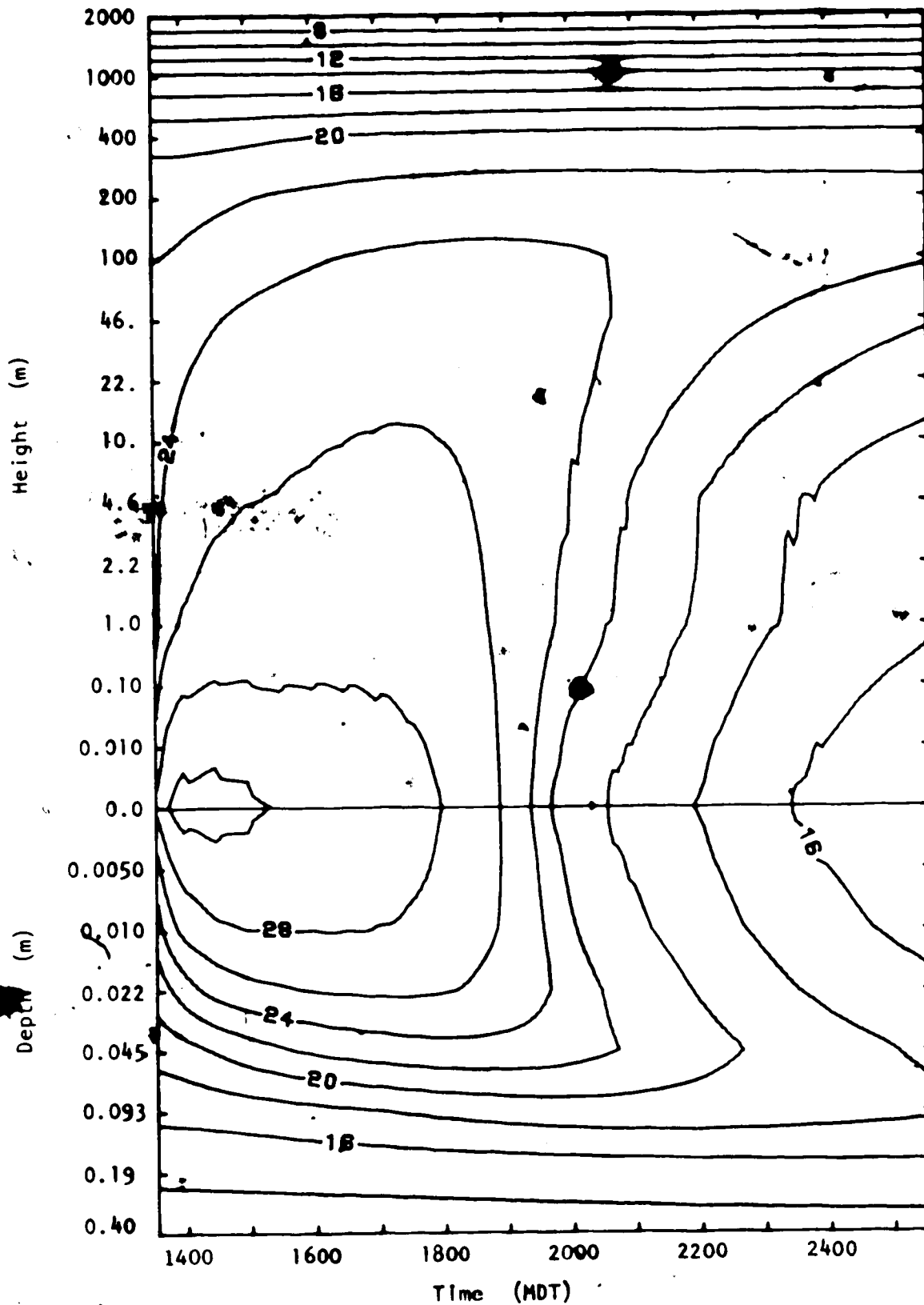


Figure 5.6 The Model-Predicted Temperature Field over the Slope with the Inclusion of the Neutral Flux Layer for Experiment 8

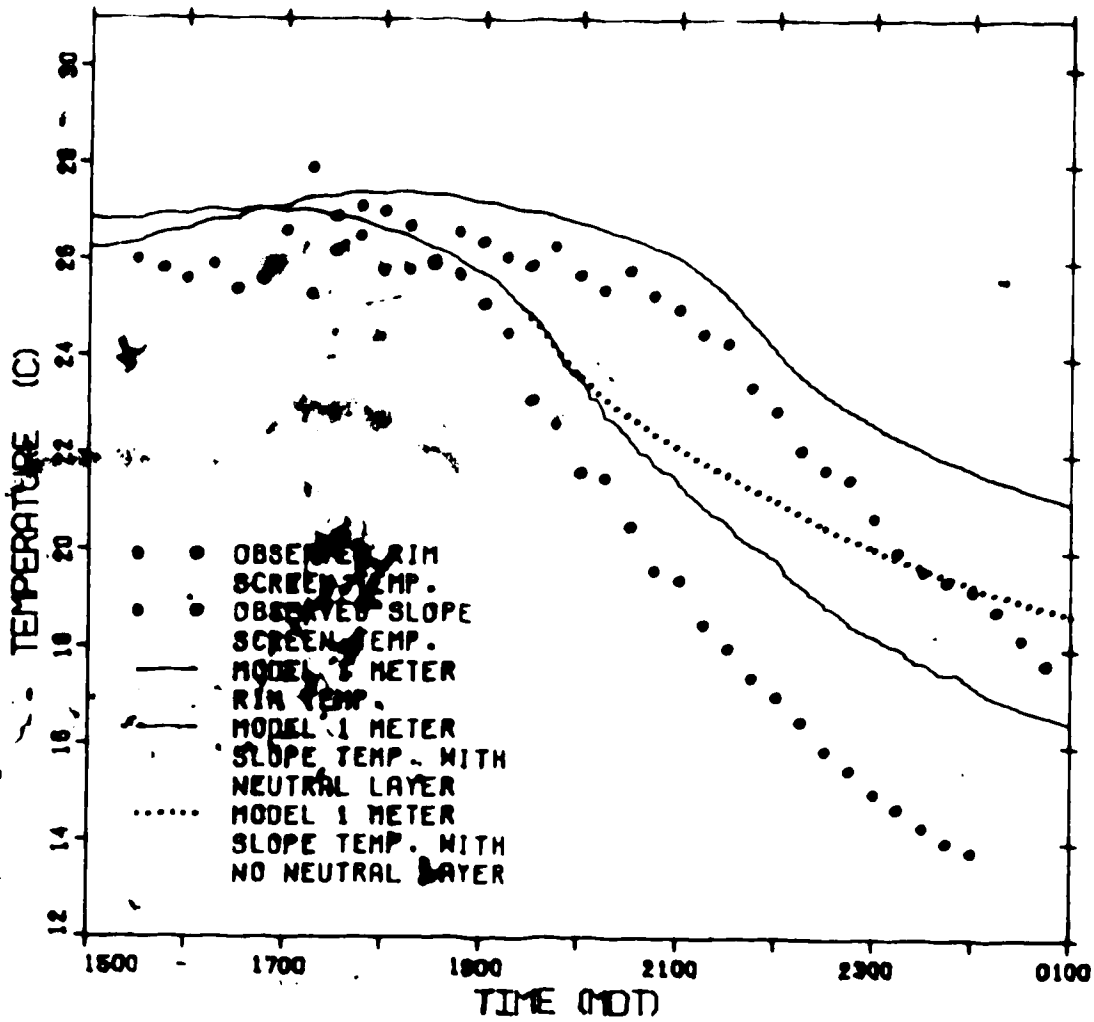


Figure 5.7 Progression of the 1 meter Temperature with Time for Experiment 8

and predicted curves are considerably closer. Although the absolute values of the predicted temperatures are discouraging, the 4.5 degree difference predicted between the rim and the slope stations is very close to the 5 degree difference observed. Presumably the remaining difference, and the actual magnitude of the temperatures, could be accounted for with the inclusion in the model of both advection and a more sophisticated mechanism of mixing by the slope wind.

The vertical temperature profiles are considered at four times: 1615, 1800, 2000, and 2200 MST. The model-produced profiles for the slope are displayed in Figure 5.8. The observed profiles below 10 metres were actually recorded. The 'observed' profiles between 10 and 90 meters were determined from the Edmonton City Tower data of 1977. The procedure was to select a day most closely resembling the day of Experiment 8 and, assuming the temperature gradients between 10 and 90 meters at the appropriate times are applicable, use them to calculate an estimation for the observed profile. Short dashes display these crude estimations in Figure 5.8.

Comparison of the computed profiles with those observed show that the match was not perfect. However, many essential features were duplicated. The trends in the 1615 MST curves were in good agreement even though the computed curve was about 1 degree too warm. Agreement between the 1800 MST profiles was poorer. Again the computed trace is

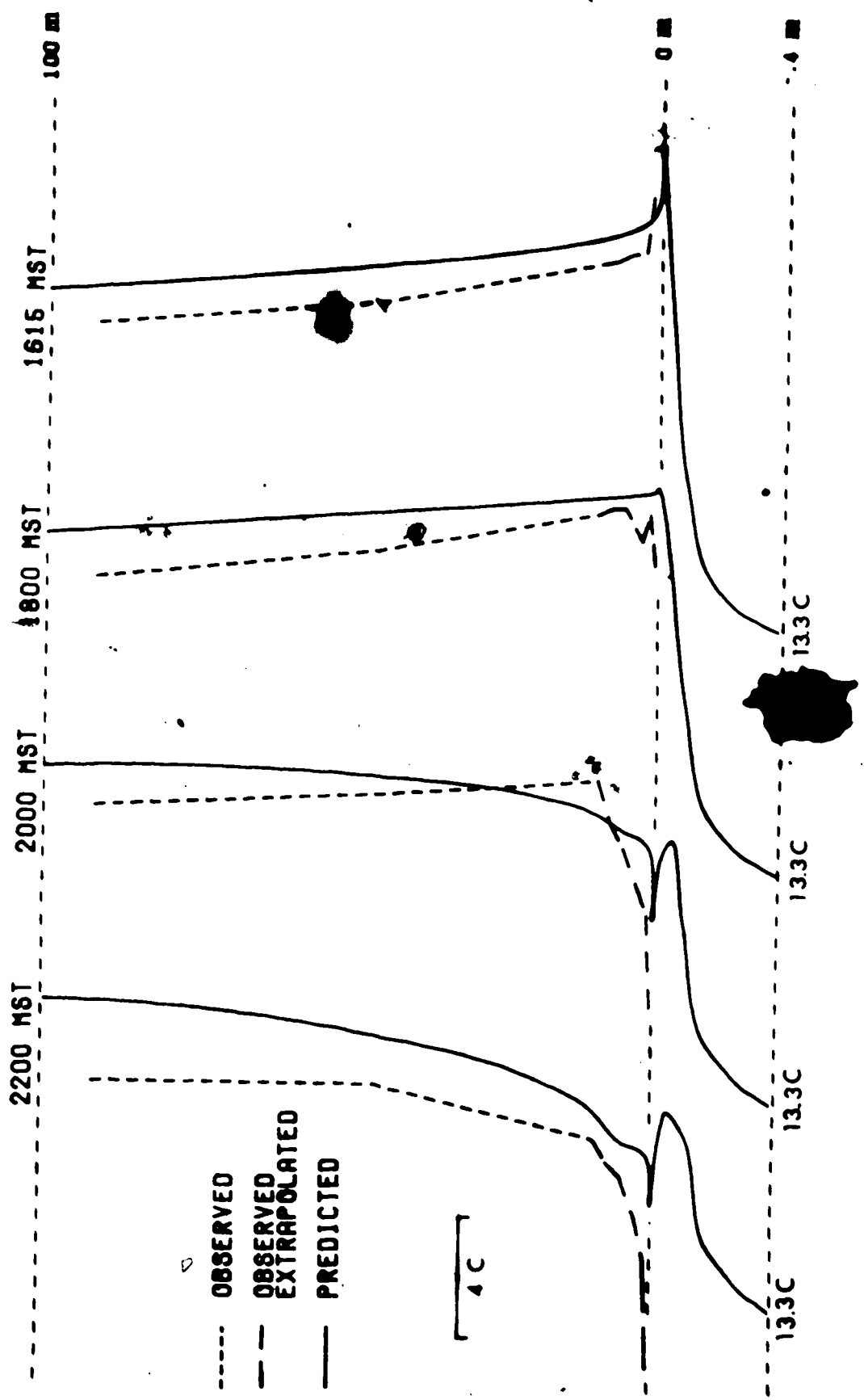


Figure 5.8 The Vertical Temperature Profiles over the Slope for Experiment 64

warmer than the observed. In the lowest 10 meters, the observed profile indicated that the formation of the inversion was well under way, whereas the computed profile was just approaching neutrality. Further, the observed curve marked a much more unstable trace between 10 and 50 meters than did the computed profile. However, this may have been a result of the extrapolation used to arrive at the observed curve in this region. Similarly, comparison of the 2000 and 2200 MST computed and observed profiles show that the trend was duplicated, at least in the lower levels, and that the computed curves continued to be warmer. It is disconcerting that the trends above 10 meters did not align more closely with observation. This is difficult to account for; and, again, the methodology of the extrapolation is offered as the explanation.

The distribution of heating and cooling in the soil layer follows a very regular course. The model results (see Figure 5.9) are exactly those expected for a soil layer with a constant thermometric conductivity (see, for example, Sellers 1965). During periods of maximum heating, the uppermost layers in the soil are the warmest. The temperature profile is essentially linear with depth. The lowest layers are at minimum values. Gradually, the surface heat wave propagates downwards through the soil. Meanwhile, the surface layers have begun to cool. By late evening the result is a zone of maximum temperature about 10 cm deep with cooler soil above and below. The temperatures in this

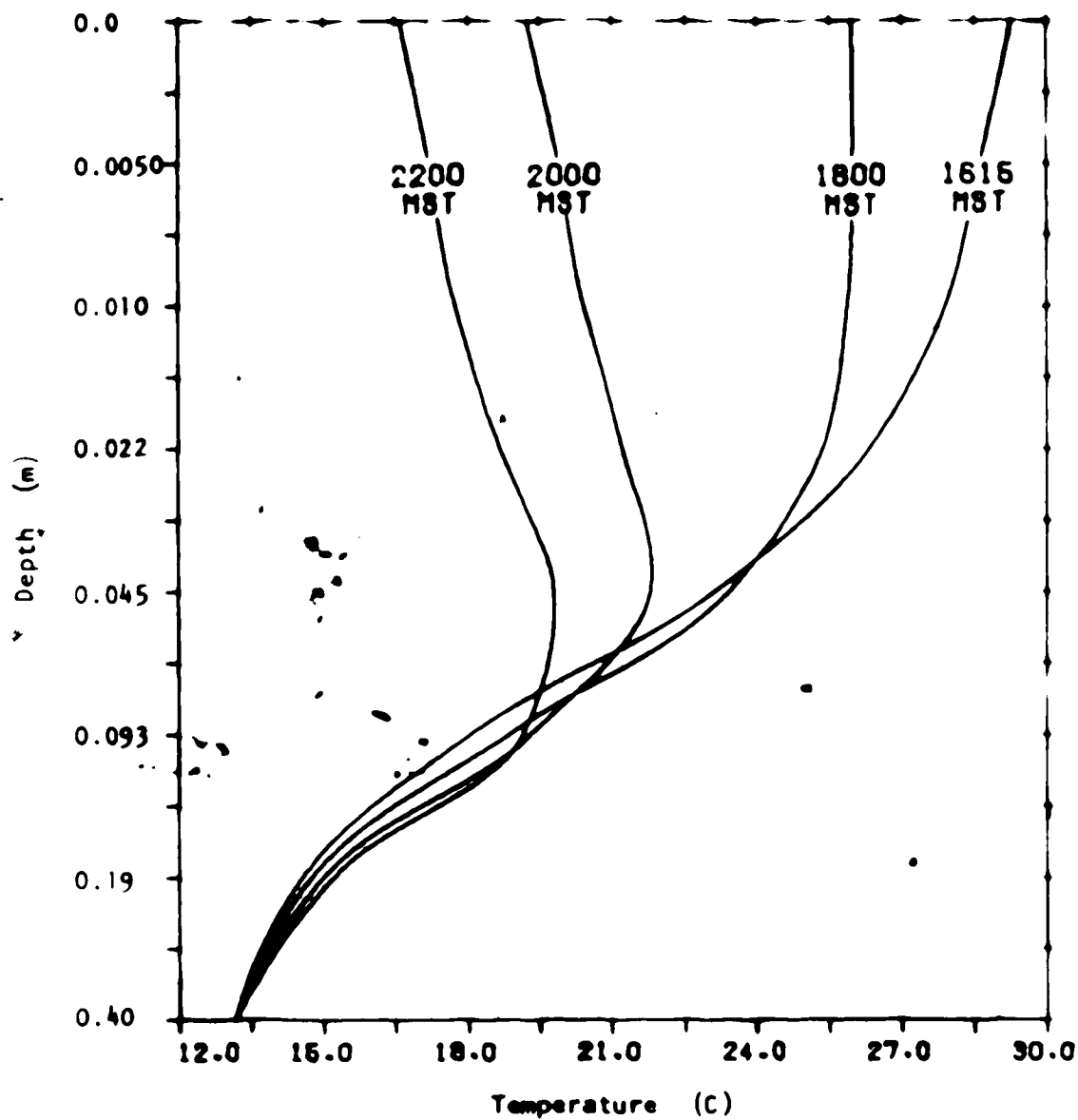


Figure 5.9 The Soil Temperatures for Experiment 8

zone are not nearly as high as the mid-afternoon maximums, for the temperature wave, as it moves downwards, dampens by conduction of heat to the cooling surface above and the cooler depths below it. Verification of the model soil predictions, other than the fact that proper behaviour of the profiles is exhibited, was not possible.

It is unrealistic to expect that the profile generated by the model for the slope would be legitimate much above rim level. Advection and mixing between the more extensive air mass over the plain, as represented by the rim profile, and the air over the valley above rim level should ensure that the slope profile would lose its identity. If the model rim and slope profiles for 2200 MST are superimposed as if the air over the rim had drifted over the valley and mixed only in a 10 meter cushion each side of the rim level, then a double structure inversion results (Figure 5.10). This structure was observed by Paterson and Hage (1979), and the results agree qualitatively.

5.3 Model Sensitivity to Slope

In Experiment 8, the model-calculated sunset time was 18:53:29 MST. This time was determined using a flat uniform slope. No account was made for terrain irregularities. The predicted temperatures near the slope surface were consistently warmer than observed. A possible explanation for this trend is that the extinction of solar radiation

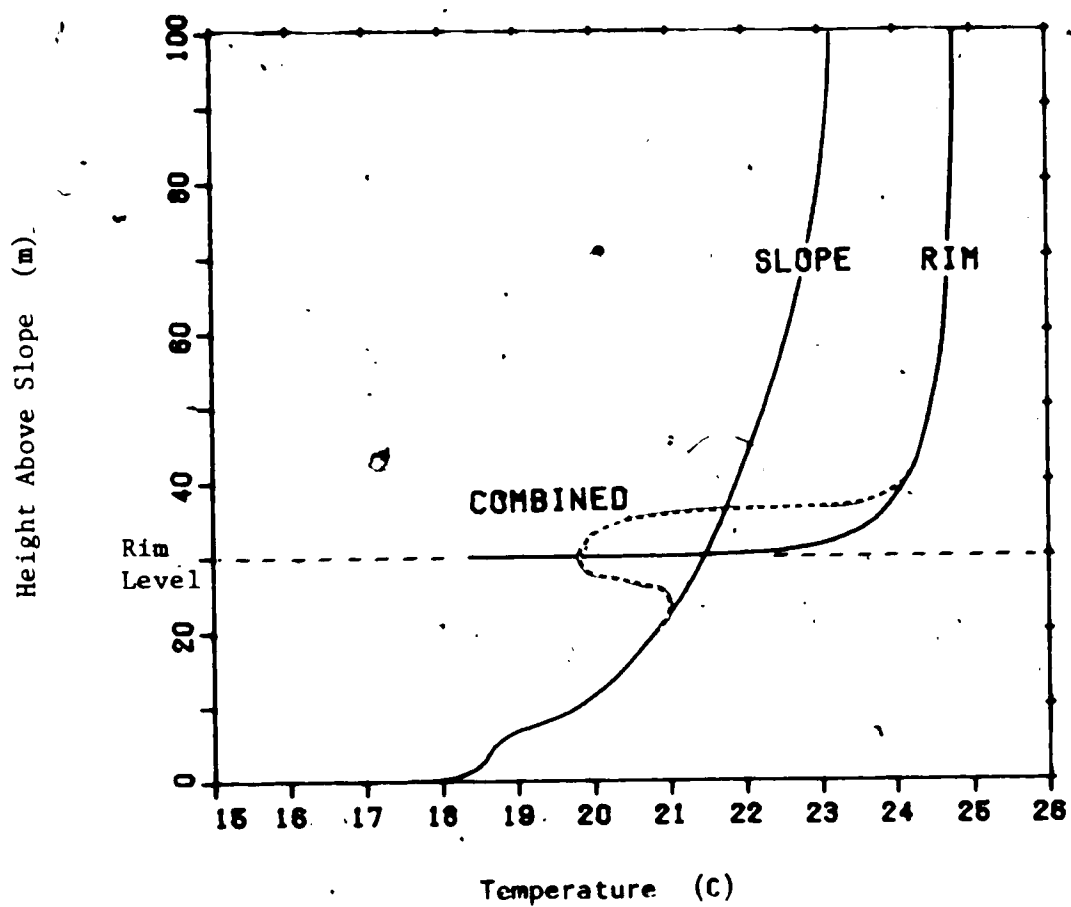


Figure 5.10 The Double-Structure Inversion for Experiment 8

actually took place earlier due to the shading from trees. Alternatively, it could be that the slope was actually steeper than that used in the model. To test the viability of these explanations, the sensitivity of the model to the value used for the inclination of the slope was examined. A run for Experiment 8 was conducted in which the slope was doubled. A comparison of the 1 meter temperature progression for both slopes is presented in Figure 5.11. The slope sunset at the doubled value was 17:09:00 MST, approximately an hour and three-quarters earlier. The figure shows that cooling for the doubled slope preceded that of the regular slope by about the same time. The slightly lower initial temperature for the doubled slope is expected in light of the decreased insolation received throughout the afternoon. With its earlier onset of cooling, the steeper slope yields a temperature more than 2.5 degrees lower by midnight. This result is not unanticipated. The trends of the two curves did not quite agree around 1800 MDT. This is due to the fact that no allowance was made to start the model slope wind at an earlier time. Other than this discrepancy, the characteristics of the two curves matched. Further, as can be seen from Figures 5.7 and 5.11, the predicted cooling rates near sunset for both slopes were essentially in agreement with those observed. Thus it is concluded that the model did not exhibit any undesired sensitivity to the value of the slope used, and that the model was only

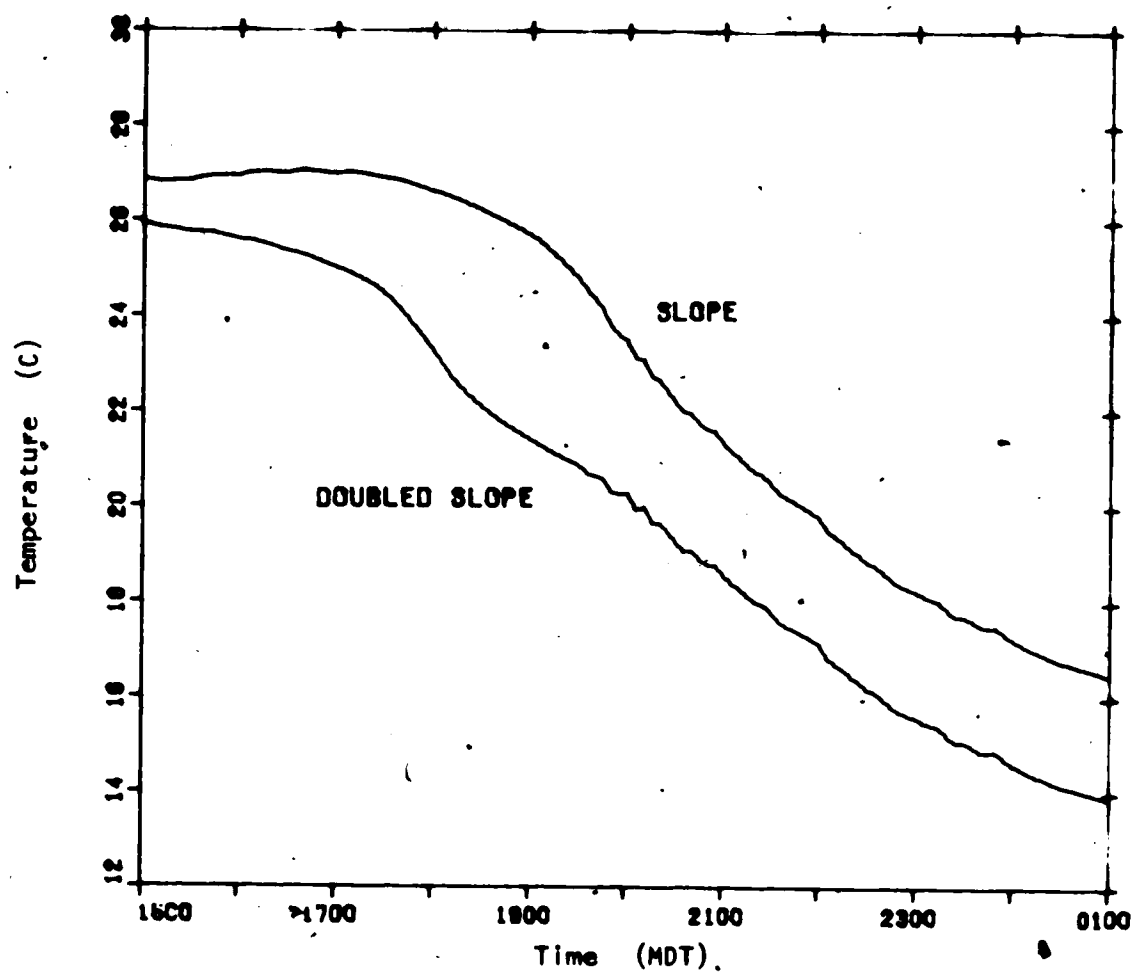


Figure 5.11 The Model Sensitivity to Slope

sensitive to slope in that it determines the time for the onset of cooling. Hence the higher predicted temperatures near the surface can indeed be due to an improper consideration of the physical aspects of the valley and to an imprecise slope value. It is also surmised that the orientation of the slope, which affects the onset time for cooling, is responsible for the lower temperatures and stronger inversions recorded over the east- and north-facing slopes.

5.4 Model Sensitivity to the Soil Diffusivity

To determine the model sensitivity to the soil diffusivity, the run for Experiment 8 was repeated using a thermal conductivity of $0.10 \text{ Wm}^{-1}\text{K}^{-1}$ in place of the previous $0.25 \text{ Wm}^{-1}\text{K}^{-1}$ value, and a corresponding thermal diffusivity of $0.6 \times 10^{-7} \text{ m}^2\text{s}^{-1}$ in lieu of $1.5 \times 10^{-7} \text{ m}^2\text{s}^{-1}$. The resulting 1 meter slope temperature curves are plotted in Figure 5.12. Figure 5.12 indicates that prior to sunset, the model experienced very little sensitivity to the soil. However, once the atmosphere became stable, and the sensible and soil heat flux densities became the dominant terms in the heat balance equation, a slight sensitivity to the soil diffusivity became apparent. By 2400 MDT, close to 0.5 C° differences in the 1 meter temperature were found with the 40 per cent lower soil diffusivity.

The lower temperatures predicted were in agreement with

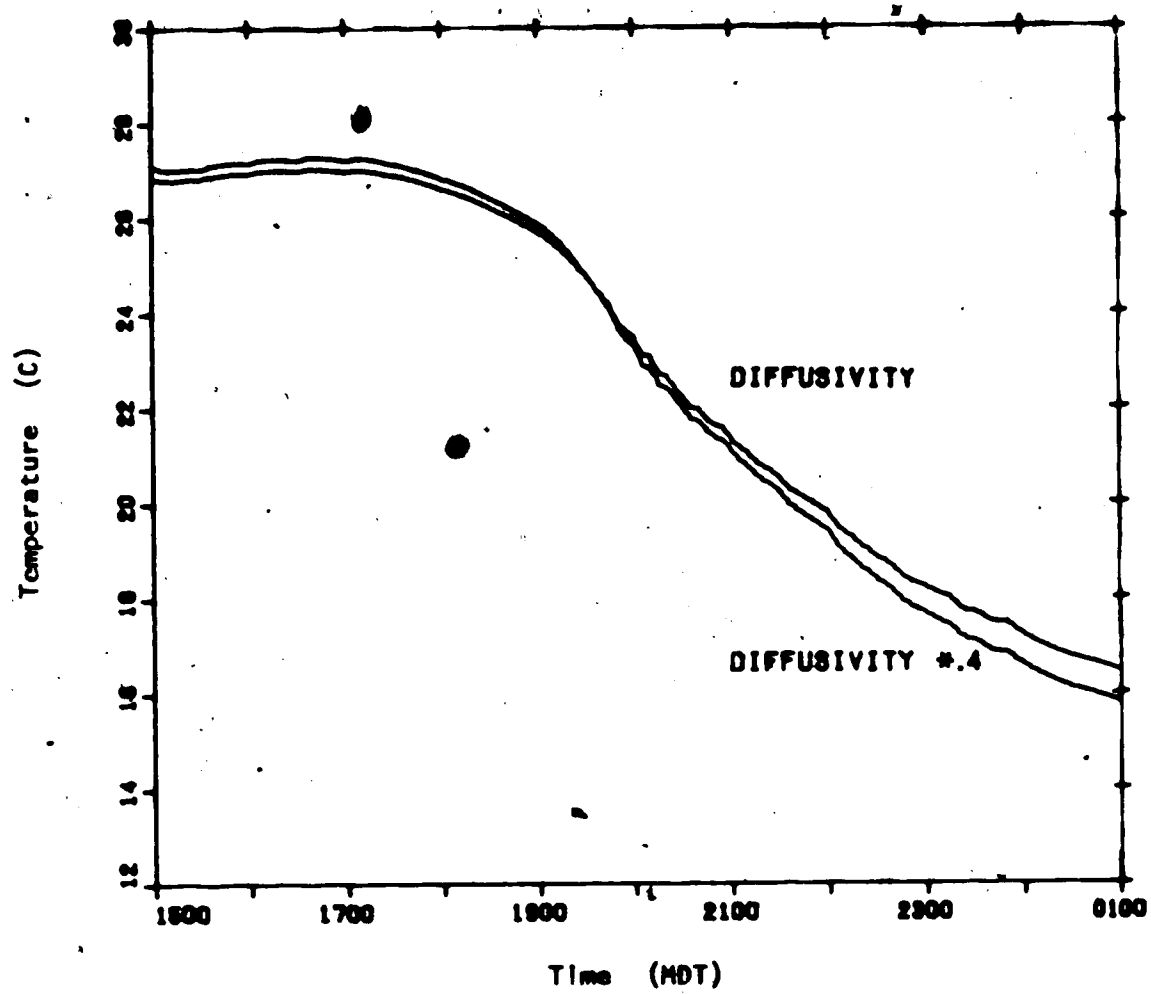


Figure 5.12 The Model Sensitivity to the Soil Diffusivity

the physics of the model. During the evening, both the sensible and soil heat flux densities are directed towards the surface. If the magnitude of the soil flux density is decreased, then the heat directed to the surface must be decreased, and the resulting surface temperature lowered. By conduction, the lower surface temperatures yields lower 1 meter temperatures.

These changes in evening temperatures indicate some model sensitivity in the stable regime to the value chosen for the soil diffusivity.

5.4 Model Sensitivity to the Friction Velocity

Figure 5.13 displays the 1 meter temperature curves for two cases: the observed friction velocity under stable conditions (about .072 m/s), and one-quarter of this friction velocity. The curves are divergent, and by midnight more than a 1.5 degree discrepancy was apparent. In addition to predicting a decreased cooling rate at the 1 meter level for the lower friction velocity, the model also predicted a 15 per cent more intense inversion between the 1 meter height and the surface. These results indicated that the model is quite sensitive to wind, and that a major source of error will be the error in the observed winds. This error is difficult to estimate given the non-linear numerical relationship between the wind and the diffusivities.

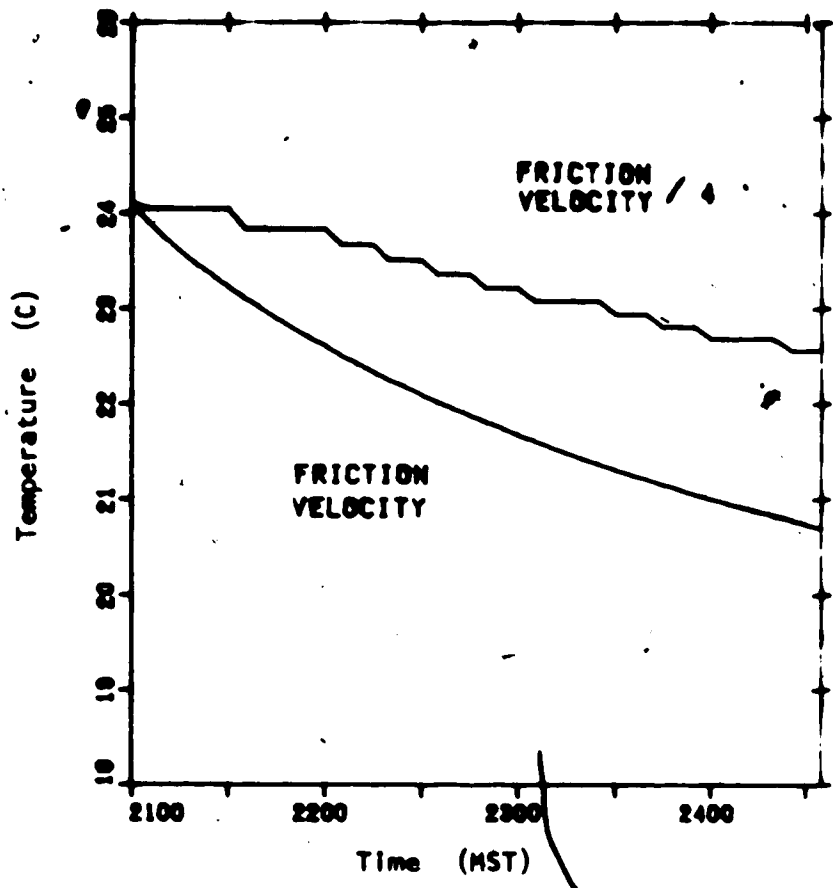


Figure 5.13 The Model Sensitivity to the Friction Velocity

Although the sensitivity to wind under stable conditions is large, it is not unexpected. In the stable case, the thermal diffusivity is very small, and it is possible that not all the heat available for mixing will get mixed. In such a situation, the magnitude of the thermal diffusivity is crucial. Since the thermal diffusivity is essentially proportional to the friction velocity, the model will be sensitive to this wind parameter. Under unstable conditions, this sensitivity does not arise. Presumably, the mixing is always sufficient so that, in the case of a change in the diffusivity, all of the available heat will be completely diffused.

5.6 Comparison between Urban and Rural Cooling

In Chapter 1, it was stated that the rural temperatures and nocturnal cooling rates were comparable to those within the valley. Yet the mechanisms involved appear quite distinct. The urban environment is generally windier, and the soil diffusivity, because of concrete, is higher. Further, on the valley slopes there are the drainage winds and earlier extinction of solar radiation. To ascertain whether the model was capable of accounting for the rural temperature decline, an evening run was made. The run used the previous values of wind and soil diffusivity for the rim station, and, at the rural station, used one-quarter of the urban wind, and one-fifth of the soil diffusivity.

Geiger (1966) indicates that the diffusivity for soil is about an order of magnitude smaller than that of concrete. The exact contribution of concrete to the effective soil diffusivity is not known, so the rural soil diffusivity was arbitrarily chosen as one-fifth the urban value. The results for the 1 meter temperatures are displayed in Figure 5.14. It is encouraging to see that the rural curve was indeed lower than the rim trace. However, the difference in the cooling rate, approximately $0.16 \text{ }^{\circ}\text{C/hr}$, was smaller by half than the average rate of $0.32 \text{ }^{\circ}\text{C/hr}$ observed for the same period (calculated from the International and Municipal Airport temperatures in Table 5.1). Further, the absolute magnitudes of the predicted temperatures were disappointing. At 2400 MDT the predicted temperature of $21.2 \text{ }^{\circ}\text{C}$ was much larger than the $17.1 \text{ }^{\circ}\text{C}$ temperature predicted for the valley. In fact it was only about $0.4 \text{ }^{\circ}\text{C}$ lower than the predicted rim temperature. Hence, it must be concluded that, to explain the rural-urban difference in a more satisfactory way, the model needs additional physics.

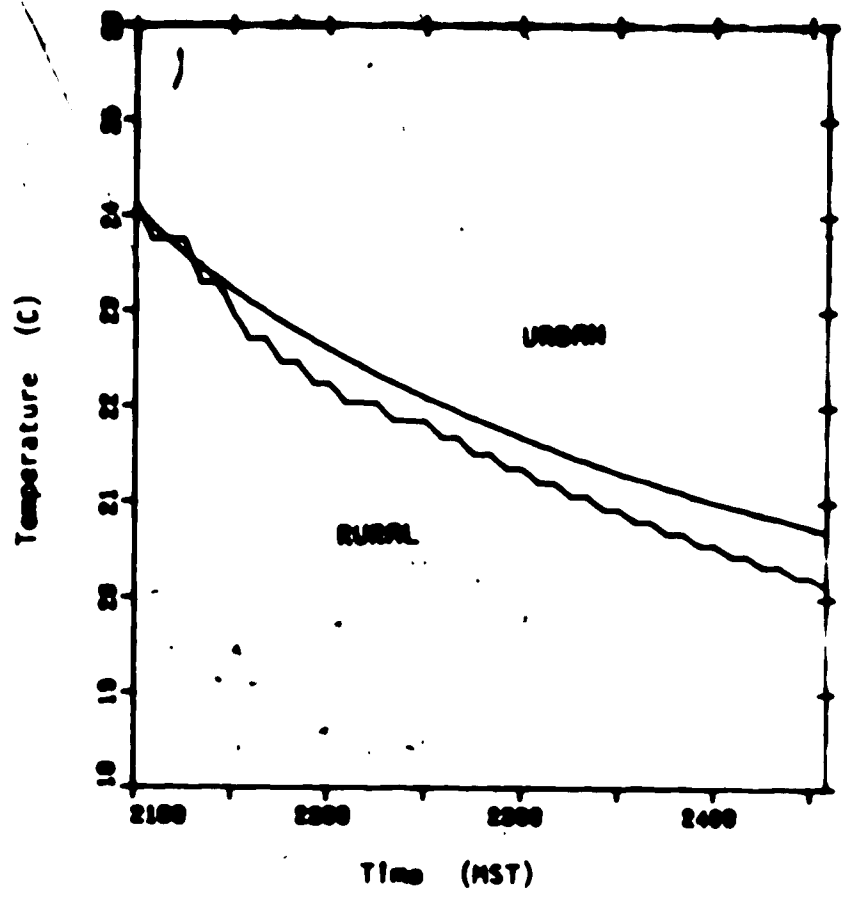


Figure 5.14 Comparison between Urban and Rural Cooling

5.7 The Results for Experiment 9

5.7.1 General

Experiment 9 was conducted on 04 July 1970. Conditions on this day were also favorable for mesoscale valley effects. Initially no significant synoptic or mesoscale activity existed in the area. Scattered fair-weather cumulus prevailed in the early afternoon and developed into scattered towering cumulus by late afternoon. In the early evening all convective activity halted, and the sky condition for the remainder of the experiment consisted of a few teaths of stratocumulus and altocumulus, with some thin cirrus. During the afternoon the winds were initially light, then increased to a mid-afternoon peak (3.4 m/s at 1600 MDT), after which they gradually decreased, becoming light just before sunset. However, at about 2200 MDT the wind began to increase again reaching an overnight maximum of 3.6 m/s. Further, after the experiment had terminated, the stratocumulus thickened up to a broken condition, and at midnight the Municipal Airport recorded a light shower. The exact nature of this mesoscale activity is not known. Thus conditions for Experiment 9 were not as ideal as for Experiment 8 for three reasons: firstly, the stronger afternoon convective activity indicated an afternoon latent heat flux density greater than the ideal case assumed by the model; secondly, the mid-evening increase in wind resulted

is a larger diffusivity; and, thirdly, the increased air-carrying cloud cover resulted in a greater than assumed atmospheric long-wave flux density.

~~5.7.2 The Observations~~

The winds and temperatures from the local airports are given in Table 5.9. Valley winds are displayed in Tables 5.10 and 5.11. Table 5.12 presents the valley temperatures. In addition to the complicating meteorological factors mentioned in the previous section, there was an observational difficulty. The rim station anemometer was periodically unreliable during the evening with a mechanical problem. Thus the valley data had to be augmented further with airport data.

5.7.3 The Model Parameters

The computer simulation for Experiment 9 used a set of parameters similar to Experiment 8. These parameters were calculated in an identical fashion, and are given in Table 5.13. The start-up profiles for the atmosphere and soil are specified in Tables 5.14 and 5.15. The 2.64 meter winds required by the model are given in Table 5.16. An n of 0.42 was determined from Table 5.10, and Table 5.11 also lists the drainage winds needed by the model. For missing values, interpolation and extrapolation procedures initiated

Table 3.9. The Temperature and Wind Speed from the Level
 2100m on 04 July 1964

Time (GMT)	Principal		Tango		International	
	Temp (°C)	Wind (°/ Kts)	Temp (°C)	Wind (°/ Kts)	Temp (°C)	Wind (°/ Kts)
1800	24.3	290/1.5	23.6	270/3.1	24.2	270/2.1
1900	25.7	280/2.1	25.2	270/2.1	25.9	230/1.5
2000	25.5	270/3.1	26.3	260/1.5	26.6	280/3.6
2100	26.6	220/2.6	24.2	270/4.1	27.9	210/2.6
2200	27.2	260/1.0	25.8	270/2.6	27.2	220/1.0
2300	26.9	260/2.0	27.7	300/4.6	26.9	300/3.1
0000	27.1	300/2.1	27.6	300/1.5	27.2	290/2.6
0100	26.0	340/1.5	27.8	300/2.6	26.8	200/1.5
0200	26.3	290/2.1	26.1	310/1.5	25.8	320/2.1
0300	26.1	330/1.0	26.9	0	25.2	330/1.0
0400	20.9	330/1.0	20.1	0	20.8	290/1.0
0500	20.2	070/1.5	18.6	030/2.1	19.1	290/1.0
0600	19.6	050/4.1	17.0	020/4.1	19.3	010/2.7
0700	17.0	020/2.0	16.6	030/5.1	18.1	020/4.1
0800	16.3	070/3.6	15.4	070/2.6	16.8	030/3.1
0900	15.5	030/2.6	14.0	020/1.5	16.1	030/2.6

Table 5.10 The Valley Winds (m/s) on 04 July 1978

Time (MDT)	Mean Wind Station 11				Mean Wind Station 8
	1.70	Height (m) 2.84 5.84		2.64 ¹	Height (m) 2.64
1500-1530					2.48
1530-1600					2.39
1600-1630					1.52
1630-1700	1.11	1.17	1.20	1.14	1.79
1700-1730	0.96	1.09	1.14	1.02	1.48
1730-1800	1.20	1.27	1.29	1.23	2.27
1800-1830	0.93	1.02	1.36	0.97	1.40
1830-1900	0.80	0.86	0.93	0.83	1.51
1900-1930	0.62	0.72	0.78	0.66	0.71
1930-2000	0.57	0.58	0.55	0.57	1.07
2000-2030	0.54	0.50	0.46	0.52	0.44
2030-2100	0.53	0.38	0.43	0.46	0.05 ²
2100-2130	0.33	0.31	0.24	0.32	0.02 ²
2130-2200	0.23	0.19	0.09	0.21	0.28
2200-2230	0.43	0.50	0.58	0.46	2.34
2230-2300					0.41

¹interpolated linearly from 1.70 m and 2.84 m winds.

²suspect; not used.

Table 5.11 The Slope (Drainage) Wind at Station 11
on 04 July 1978

Time (MDT)	Mean Wind (m/s)	Time (GMT)	Mean Wind (m/s)
1835	-0.29 ¹	2035	0.65
40	-0.56 ¹	40	0.62
1845	0.02	2045	0.58
50	-0.41 ¹	50	0.63
55	-0.15 ¹	55	0.71
1900	0.06	2100	0.68
05	0.02	05	0.74
10	0.19	10	0.68
1915	-0.04 ¹	2115	0.68
20	0.22	20	0.72
25	0.38	25	0.59
1930	0.00	2130	0.57
35	0.42	35	0.62
40	0.62	40	0.73
1945	0.79	2145	0.54
50	0.26	50	0.54
55	0.34	55	0.66
2000	0.15	2200	0.49
05	0.38	05	0.30
10	0.47	10	0.57
2015	0.32	2215	-0.11 ¹
20	0.56	20	0.19
25	0.53	25	0.45
2030	0.56		

¹minus sign indicates an upslope wind

Table 5.12 The Calibrated Valley Temperatures (°C) on
04 July 1978

Time (MDT)	Station 8		Station 11					
	Height (m)	1.20	1.20	2.44	Height (m)	4.82	7.10	9.45
1600	29.3							
15	27.9							
30	29.0	29.4	27.7	27.4	28.1	27.6		
45	28.7	29.3	28.2	28.0	28.3	28.4		
1700	29.1	29.5	28.7	28.0	28.2	27.8		
15	29.6	29.4	28.2	28.0	28.4	28.3		
30	29.2	29.4	28.2	28.1	28.6	28.2		
45	29.4	29.3	28.5	28.2	28.4	28.2		
1800	29.3	29.0	28.6	28.9	29.0	28.5		
15	29.2	29.0	28.0	28.1	28.3	28.0		
30	28.9	28.7	27.6	28.0	28.1	28.3		
45	29.1	28.1	28.2	28.3	28.6	28.2		
1900	29.2	27.4	28.4	28.2	28.2	28.1		
15	29.5	26.4	27.4	27.4	27.8	27.7		
30	28.7	25.6	26.0	26.7	27.7	27.1		
45	28.0	24.0	26.2	26.7	27.0	27.2		
2000	28.4	24.7	23.5	25.8	27.1	27.2		
15	28.0	23.2	24.9	26.6	26.6	26.8		
30	28.2	22.5	22.2	23.4	23.9	25.2		
45	27.4	21.9	23.6	25.8	25.6	26.3		
2100	26.5	22.0	22.3	25.7	25.6	26.1		
15	25.9	21.0	21.5	24.3	25.4	25.9		
30	25.1	20.1	21.2	22.6	24.1	24.9		
45	25.3	19.3	22.0	23.6	23.4	24.7		
2200	24.3	19.6	22.2	22.8	22.8	23.7		
15	22.2	20.8	22.0	22.3	22.3	22.7		
30	21.5	20.5	21.5	21.3	21.3	21.6		
45	21.3							
2300	21.1							

Table 5.13 The Model Parameters for Experiment 9

Parameter	Programme Name	Value
Declination	DEC	22° 51.3'
Equation of Time	EOT	4 min 19 sec
Sun's Hour Angle at Model Start-up	HATC	-1° 54.7'
Maximum ϕ_h	PHILIM	0.740
Slope Wind Start Time	TSLP	18.58 hrs MST
Surface Pressure	PB	922 mb
Average Layer Temperature throughout Period	TAV	295.34 °C
Atmospheric Flux Density	FLWA	260 W m^{-2}

**Table 5.14 The Initial Air Temperature Profile
for Experiment 9**

Height (m)	Temperature (°K)
2000.	279.83
702.	292.16
1.20	298.76
1.00	298.96
0.46	299.56
0.22	300.26
0.10	300.96
0.05	301.66
0.00	303.32

**Table 5.15 The Initial Soil Temperature Profile
for Experiment 9**

Depth (cm)	Temperature (°K)
0.00	303.32
0.50	301.22
1.04	299.12
2.15	296.92
4.47	294.62
9.28	292.42
19.30	290.22
40.00	289.12

Table 5.16 The Model Winds (m/s) for Experiment 9

Time (GMT)	Mean Wind (Municipal)	Mean Wind (Observed)	Mean Wind (Filtered ¹)	Friction Velocity (Rin)	Friction Velocity (Slope)
1800	1.54				
1900	2.06		2.23	.160	.153
30			2.40	.172	.165
2000	3.09		2.87	.184	.176
30			2.79	.200	.191
2100	2.57		3.00	.215	.206
30			2.78	.200	.191
2200		3.35	2.56	.184	.176
30			2.54	.183	.175
2300		1.77	2.52	.181	.173
30			2.17	.156	.149
0000		2.43	1.81	.130	.124
30			1.81	.130	.124
0100		1.22	1.80	.129	.124
30			1.57	.112	.108
0200		1.74	1.33	.095	.091
30			1.30	.093	.089
0300	1.03	0.01 ²	1.27	.091	.087
30			1.24	.089	.085
0400	1.03	0.54 ²	1.20	.086	.082
30			1.72	.123	.118
0500	1.54	0.05 ²	2.23	.160	.153
30			2.49	.178	.171
0600	4.12		2.74	.196	.188
30			3.09	.221	.212
0700	2.57		3.43	.246	.236
30			3.17	.228	.218
0800	3.60		2.91	.209	.200
30			2.83	.203	.194
0900	2.57		2.74	.196	.188

¹a three-point Bartlett filter was used.

²suspect; not used.

those of Experiment 8.

5.7.4 The Model Predictions

This section discusses the model predictions for Experiment 9. The main intention is to demonstrate that the computer model was not tuned specifically to Experiment 8. The forecast temperature fields between 1235 and 0035 MST for the rim and the slope are shown in Figures 5.15 and 5.16. It is seen that the model behaved properly: the general features were consistent with the observations. The progression of the 1 meter temperatures with time is given Figure 5.17. Again there is a reasonable correlation between the predicted and observed trends. However, the absolute values predicted were discouraging. Near 2200 MDT the observed temperature increased. Increased mixing, attributed to the increase in observed wind at this time, is believed responsible for the increase in the observed temperature. Greater mixing transports the warmer air in the inversion down to the surface. Because of the effect of the three-point smoothing employed, the model winds were not increased until after 2300 MDT. Thus the predicted temperature increase by the model was delayed.

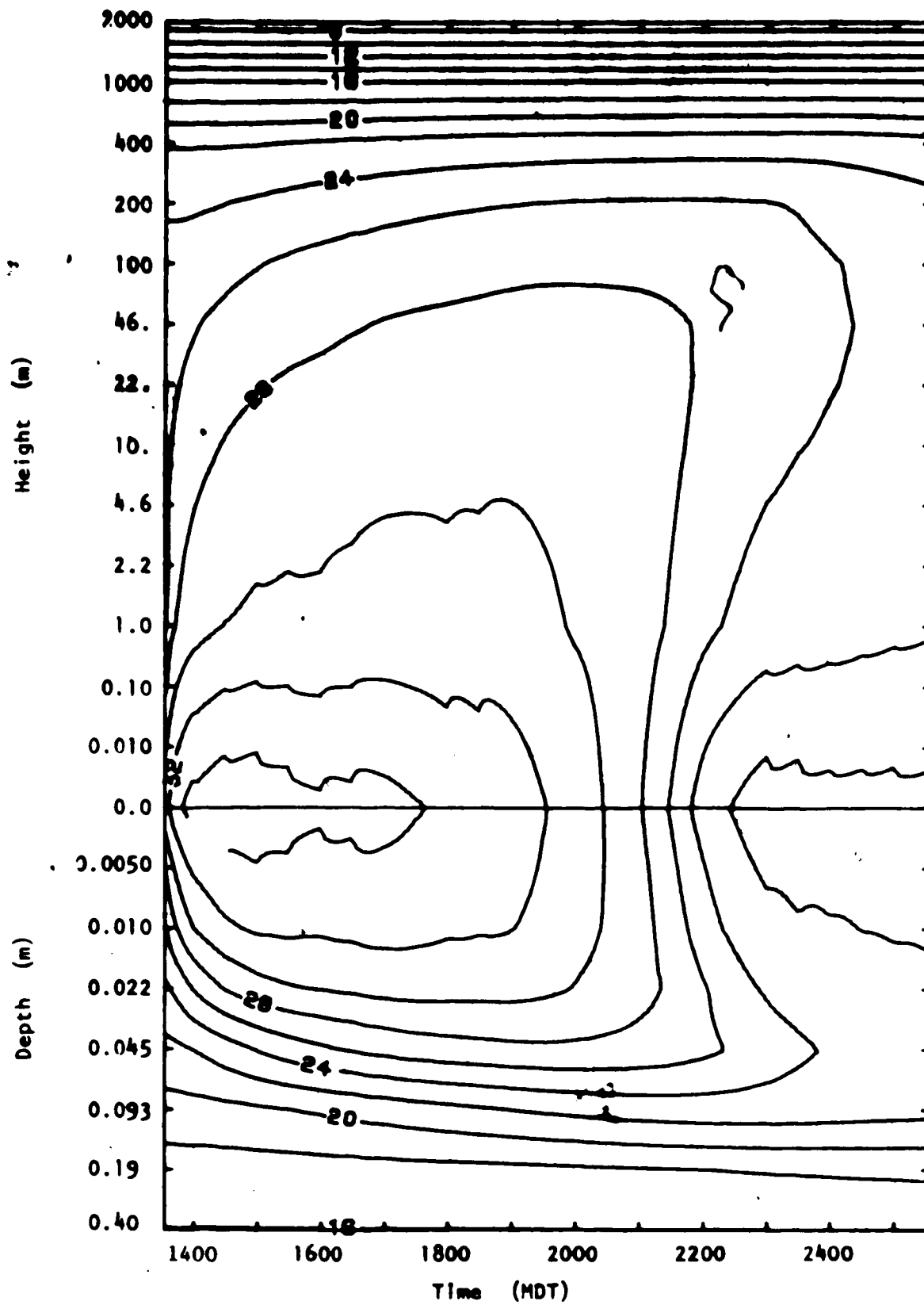


Figure 5.15 The Model-Predicted Temperature Field at the Rim for Experiment 9

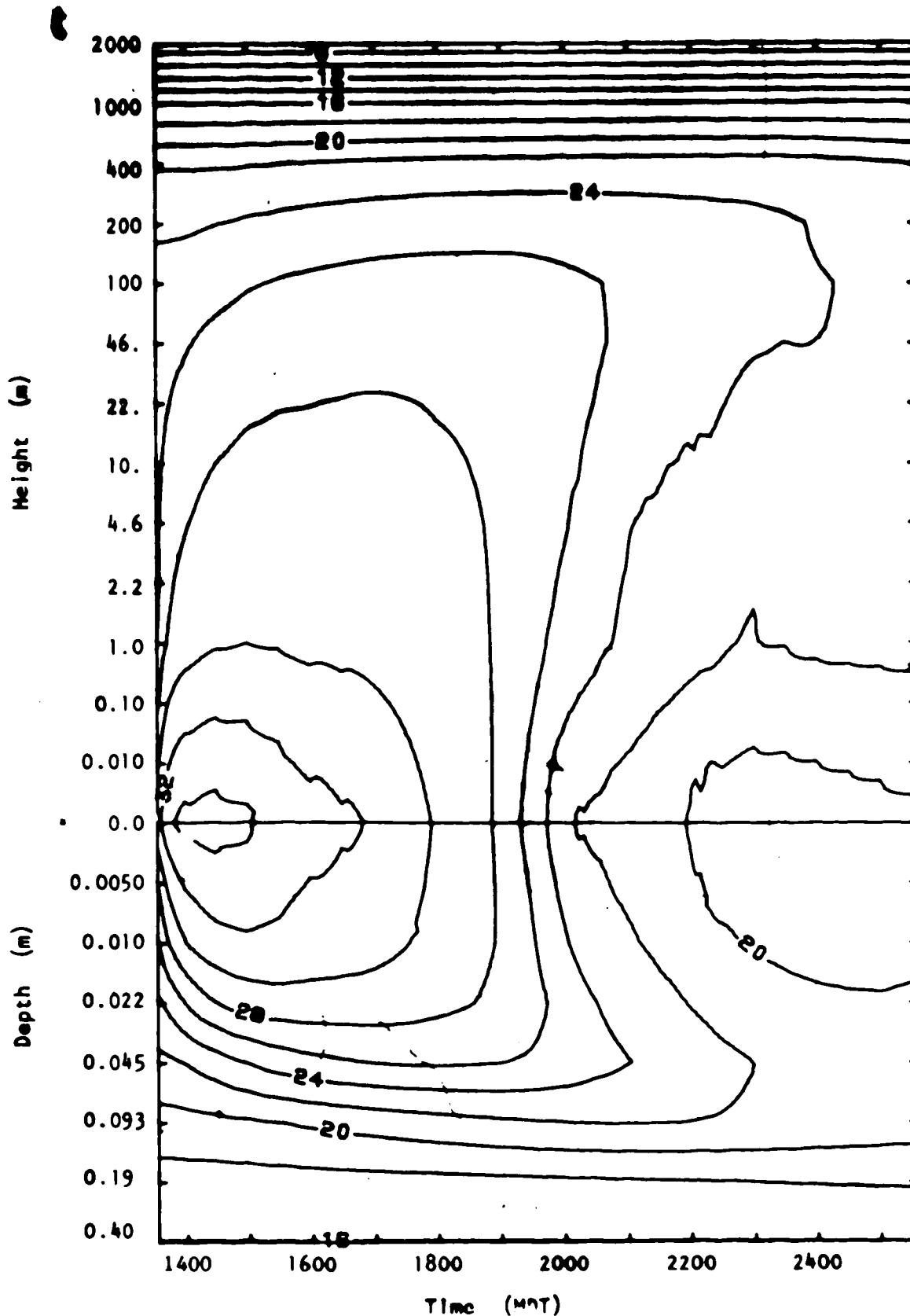


Figure 5.16 The Model-Predicted Temperature Field over the Slope with the Inclusion of the Neutral Surface Layer for Experiment 9

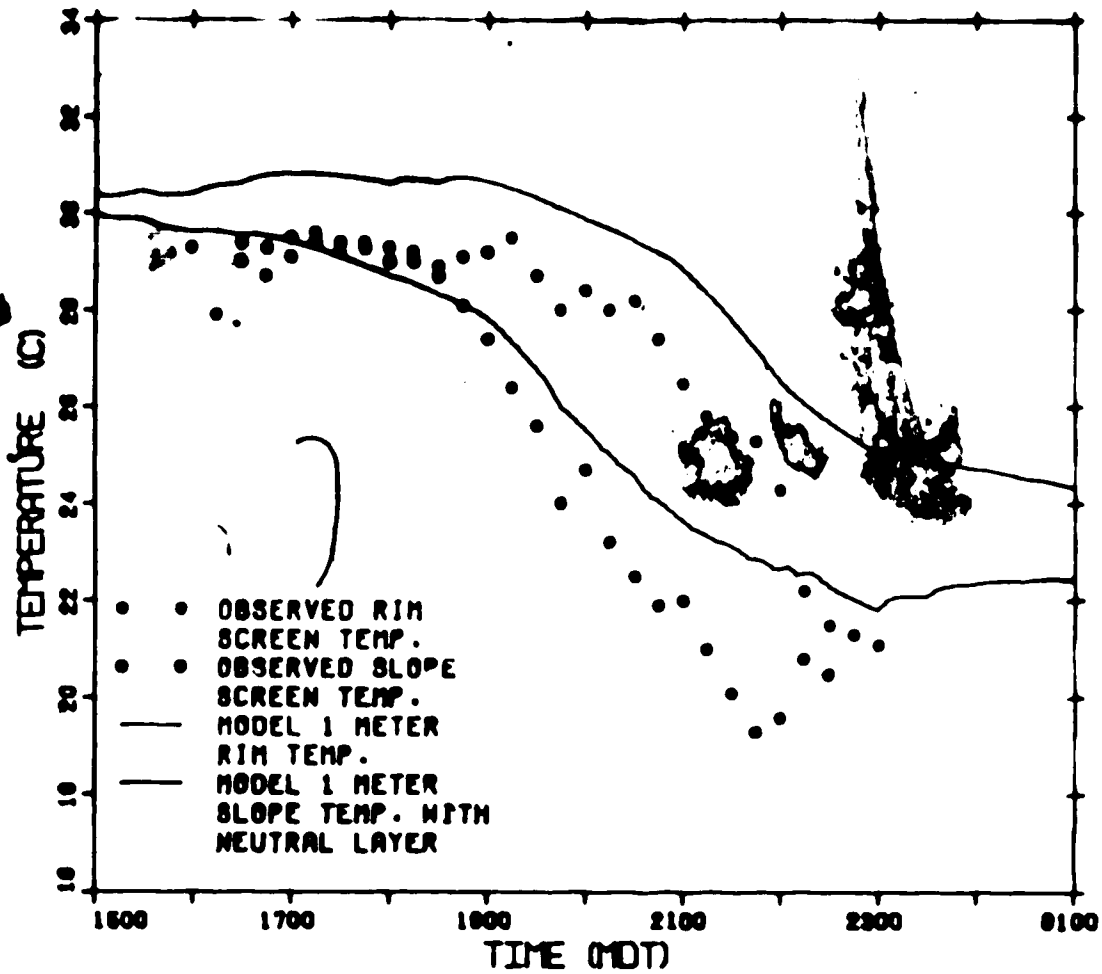


Figure 5.17 Progression of the 1 meter Temperature with time for Experiment 9

5.0 The Results for Experiment 11

5.0.1 General

Experiment 11 was conducted on 28 August 1978. Again, weather conditions on the day were initially favourable. The early afternoon saw scattered cumulus clouds with fairly brisk winds hovering near the 5 m/s mark. By mid-afternoon cumulonimbus clouds had developed in the area and by 1700 MDT there was a line of thundershowers to the north. At approximately 1815 MDT the wind, which had been slowly decreasing, shifted from the northwest to the northeast and picked up to 4.7 m/s in strength. Simultaneously, the temperature dropped nearly 2 degrees in about 10 minutes. Virga was observed in the distance. However, by 1900 MDT, this mesoscale disturbance appeared to have moved completely through the valley, and the usual rate of decrease in both wind speed and temperature resumed. However, at 2300 MDT the wind again picked up before dropping to near calm values for the remainder of the period. Thus conditions for Experiment 11 were not completely ideal, again for three reasons: firstly, the significant convective activity indicated an afternoon latent heat flux density greater than the ideal case assumed by the model; secondly, the mesoscale frontal passage introduced a 2 C° drop which the model can not take into account; and, thirdly, a late evening increase in the wind

resulted in a larger-than-ideal diffusivity for that period.

5.8.2 The Observations

The winds and temperatures from the local airports are given in Table 5.17. Valley winds are displayed in Tables 5.18 and 5.19. Table 5.20 presents the valley temperatures.

5.8.3 The Model Parameters

A set of parameters similar to those of the previous two experiments was used. These are listed in Table 5.21. The start-up profiles for the air and soil are given in Tables 5.22 and 5.23. The 2.64 meter winds required are given in Table 5.24. An n of 0.25 was determined from Table 5.18. Table 5.19 specifies the drainage (slope) winds used by the model. For missing values, the previous interpolation and extrapolation procedures were used.

5.8.4 The Model Predictions

In this section the model predictions for Experiment 11, like Experiment 9, are very briefly presented. Again the main intention is to show the model capability under different situations. The forecast temperature fields between 1235 and 0035 MST for the rim and

Table 5.17 The Temperatures and Winds from the Local Airports on 28 August 1978

Time (GMT)	Airport					
	Municipal		Nanso		International	
	Temp (°C)	Wind (°/ m/s)	Temp (°C)	Wind (°/ m/s)	Temp. (°C)	Wind (°/ m/s)
1800	17.9	310/4.6	18.4	290/6.2	17.5	280/2.6
1900	19.4	280/5.1	19.8	290/5.7 68.7	19.1	280/6.6
2000	19.9	290/5.1	18.2	290/5.7 69.3	19.7	290/4.1
2100	19.7	300/4.6	19.6	290/6.2 610.3	19.6	300/5.1
2200	20.4	290/5.7	20.5	290/5.7 68.7	20.2	290/5.7
2300	20.4	330/4.1	20.6	300/4.1	20.2	320/6.2
0000	20.5	310/4.1	20.4	350/5.7 611.3	20.4	290/4.1
0100	18.1	020/3.6	18.9	330/3.1	19.4	320/3.6
0200	17.0	010/2.1	16.4	310/1.5	16.7	040/1.5
0300	15.2	010/1.0	14.2	280/1.0	13.3	0
0400	15.2	040/3.1	12.1	360/4.1	10.5	0
0500	12.1	070/1.5	11.8	050/1.5	9.9	0
0600	11.8	0	10.6	050/1.0	8.1	0
0700	11.6	0	11.1	0	7.4	190/1.0
0800	10.3	0	9.9	0	7.0	190/1.5
0900	10.3	0	11.3	0	6.9	200/2.1

Table 3.10 The Valley Winds (m/s) on 20 August 1970

Time (HRT)	Mean Wind Station 11			Mean Wind Station 8	
	1.70	Height (m) 2.00 5.00		2.64	Height (m) 2.00
1530-1600					0.07
1600-1630	4				0.08
1630-1700					0.22
1700-1730					0.22
1730-1800	1.20	1.33	1.37	1.26	3.33
1800-1830	1.02	1.00	1.35	1.05	2.50
1830-1900	1.14	1.33	1.50	1.22	3.06
1900-1930	1.07	1.30	1.73	1.21	0.72
1930-2000	0.70	0.93	1.15	0.80	2.90
2000-2030	0.46	0.43	0.50	0.45	1.06
2030-2100	0.57	0.47	0.37	0.53	2.04
2100-2130	0.43	0.41	0.44	0.42	1.77
2130-2200	0.23	0.35	0.45	0.28	0.90
2200-2230	0.31	0.36	0.37	0.33	1.62
2230-2300	0.36	0.39	0.37	0.37	2.55
2300-2330	0.51	0.40	0.50	0.50	2.00
2330-2400	0.35	0.42	0.45	0.38	1.51
0000-0030	0.15	0.08	0.05	0.12	1.92
0030-0100					1.02

*interpolated linearly from 1.70 m and 2.64 m winds.

Table 5.19 The Slope (Drainage) Wind at Station 11
on 28 August 1978

Time (MDT)	Mean Wind (m/s)	Time (GMT)	Mean Wind (m/s)
1830	0.00	2115	0.17
35	-0.07 ¹	20	0.12
40	0.00	25	0.17
1845	0.00	2130	0.15
50	0.12	35	0.21
55	0.00	40	0.19
1900	0.04	2145	0.19
05	-0.04 ¹	50	0.20
10	0.12	55	0.05
1915	0.12	2200	0.06
20	0.02	05	0.30
25	0.12	10	0.23
1930	0.21	2215	0.31
35	0.33	20	0.16
40	0.22	25	0.10
1945	0.32	2230	0.23
50	0.45	35	0.30
55	0.49	40	0.27
2000	0.41	2245	0.41
05	0.52	50	0.40
10	0.48	55	0.42
2015	0.59	2300	0.48
20	0.51	05	0.44
25	0.48	10	0.44
2030	0.44	2315	0.36
35	0.43	20	0.33
40	0.31	25	0.42
2045	0.29	2330	0.33
50	0.33	35	0.28
55	0.36	40	0.23
2100	0.32	2345	0.23
05	0.25	50	0.32
10	0.22	55	0.26

¹minus sign indicates an upslope wind

Table 5.20 The Calibrated Valley Temperatures (°C) on
27 August 1978

Time (MDT)	Station 8			Station 11		
	Height (m)			Height (m)		
	1.20	0.12	1.20	3.72	6.89	14.73
1515	19.8					
30	20.5					
45	20.7					
1600	21.0					
15	20.9					
30	21.1					
45	21.1					
1700	21.2	22.3		20.3	24.4	23.5
15	21.1	20.3	22.1	20.5	20.4	18.8
30	21.1	19.7	21.6	20.6	20.6	20.7
45	21.6	19.8	21.1	20.6	20.7	21.2
1800	21.4	18.7	20.8	20.7	21.0	21.3
15	21.4	17.6	20.0	20.5	21.0	21.3
30	19.3	18.2	18.6	18.7	18.7	19.0
45	18.5	18.2	18.0	18.7	18.6	18.9
1900	18.6	18.4	18.0	18.9	18.9	19.2
15	18.6	17.9	17.9	18.6	18.8	18.8
30	17.7	17.2	17.2	18.3	18.7	19.0
45	17.9	15.1	16.3	17.8	18.4	18.7
2000	17.9	13.0	15.0	17.0	17.1	18.6
15	17.2	12.6	14.1	16.8	18.3	19.1
30	16.8	13.3	13.9	15.6	18.1	18.7
45	16.8	12.2	13.7	15.9	17.0	17.5
2100	16.4	11.7	13.0	14.6	15.6	16.6
15	16.2	11.6	12.6	14.2	15.5	16.9
30	16.0	10.6	12.4	14.0	14.7	16.4
45	15.8	10.8	12.0	13.9	14.8	15.9
2200	15.8	misg	12.3	misg	misg	misg
15	15.1	10.4	11.8	13.4	14.6	15.3
30	14.4	9.0	11.7	12.8	13.6	14.6
45	13.9	10.2	11.3	13.0	14.0	14.6
2300	13.5	8.7	11.2	13.7	14.4	14.5
15	13.2	9.1	10.6	12.5	13.5	14.2
30	13.0	8.7	10.2	12.8	13.4	14.0
45	12.6	8.3	10.1	11.9	12.5	13.5
0000	12.5	8.1	10.0	11.5	11.7	12.7
15	12.4					

Table 5.21 The Model Parameters for Experiment 11

Parameter	Programme Name	Value
Declination	DEC	9° 37.7'
Equation of Time	EOT	1 min 11 sec
Sun's Hour Angle at Model Start-up	HATC	-0° 11.1'
Maximum ϕ_h	PHILIM	1.824
Slope Wind Start Time	TSLP	18.58 hrs MST
Surface Pressure	PB	930 mb
Average Layer Temperature throughout Period	TAV	286.96 °C
Atmospheric Flux Density	FLWA	245 Wm ⁻²

Table 5.22 The Initial Air Temperature Profile
for Experiment 11

Height (m)	Temperature (°K)
2000.	275.49
1497.	278.96
983.	282.76
708.	284.96
1.20	292.85
1.00	293.05
0.46	293.65
0.22	294.35
0.10	295.05
0.05	295.75
0.00	297.41

Table 5.23 The Initial Soil Temperature Profile
for Experiment 11

Depth (cm)	Temperature (°K)
0.00	297.41
0.50	295.31
1.04	293.21
2.15	291.01
4.47	288.71
9.28	286.51
19.30	284.31
40.00	283.21

Table 5.24 The Model Winds (m/s) for Experiment 11

Time (GMT)	Mean Wind (Municipal)	Mean Wind (Observed)	Mean Wind (Filtered ¹)	Friction Velocity (Rim)	Friction Velocity (Slope)
1800	4.63				
1900	5.14		5.06	.363	.207
30			5.14	.368	.210
2000	5.14		5.06	.363	.207
30			4.89	.351	.200
2100	4.63		4.66	.334	.190
30			4.63	.332	.189
2200		4.80	4.53	.325	.185
30			4.45	.319	.182
2300		4.22	3.96	.284	.162
30			3.38	.242	.138
0000		2.58	3.26	.234	.133
30			3.72	.267	.152
0100		4.72	3.85	.276	.157
30			3.19	.229	.131
0200		1.86	2.29	.164	.093
30			1.89	.135	.077
0300		1.77	1.60	.115	.066
30			1.46	.105	.060
0400		1.62	1.72	.123	.070
30			2.32	.166	.095
0500		2.80	2.29	.164	.093
30			2.08	.149	.085
0600		1.92	1.48	.106	.060
30			1.31	.094	.054
0700	1.00 ²		1.01	.072	.041
30			1.00	.072	.041
0800	1.00 ²		1.00	.072	.041
30			1.00	.072	.041
0900	1.00 ²		1.00	.072	.041

¹a three-point Bartlett filter was used.

²calm reading assigned a value of 1 m/s as per section 3.4.

the slope are shown in Figures 5.18 and 5.19. The results again demonstrate that the main features were consistent with the observations. For closer inspection, the evolution of the 1 meter temperatures is given in Figure 5.20. It is seen that when the 2 degree cooling, which occurred with the mesoscale cold front, is removed from the observations, the relationship between the predicted and observed curves was very close to those of Experiments 8 and 9. After 2300 MDT, the predicted rim curve depicts a decrease in the cooling rate, and the predicted slope curve shows a temperature increase. This is consistent with the increased model winds used for this period. Why this warming was not more strongly reflected in the observations (a decrease in the cooling rate only is detected) is not known. Presumably it can be attributed to other processes neglected by the model.

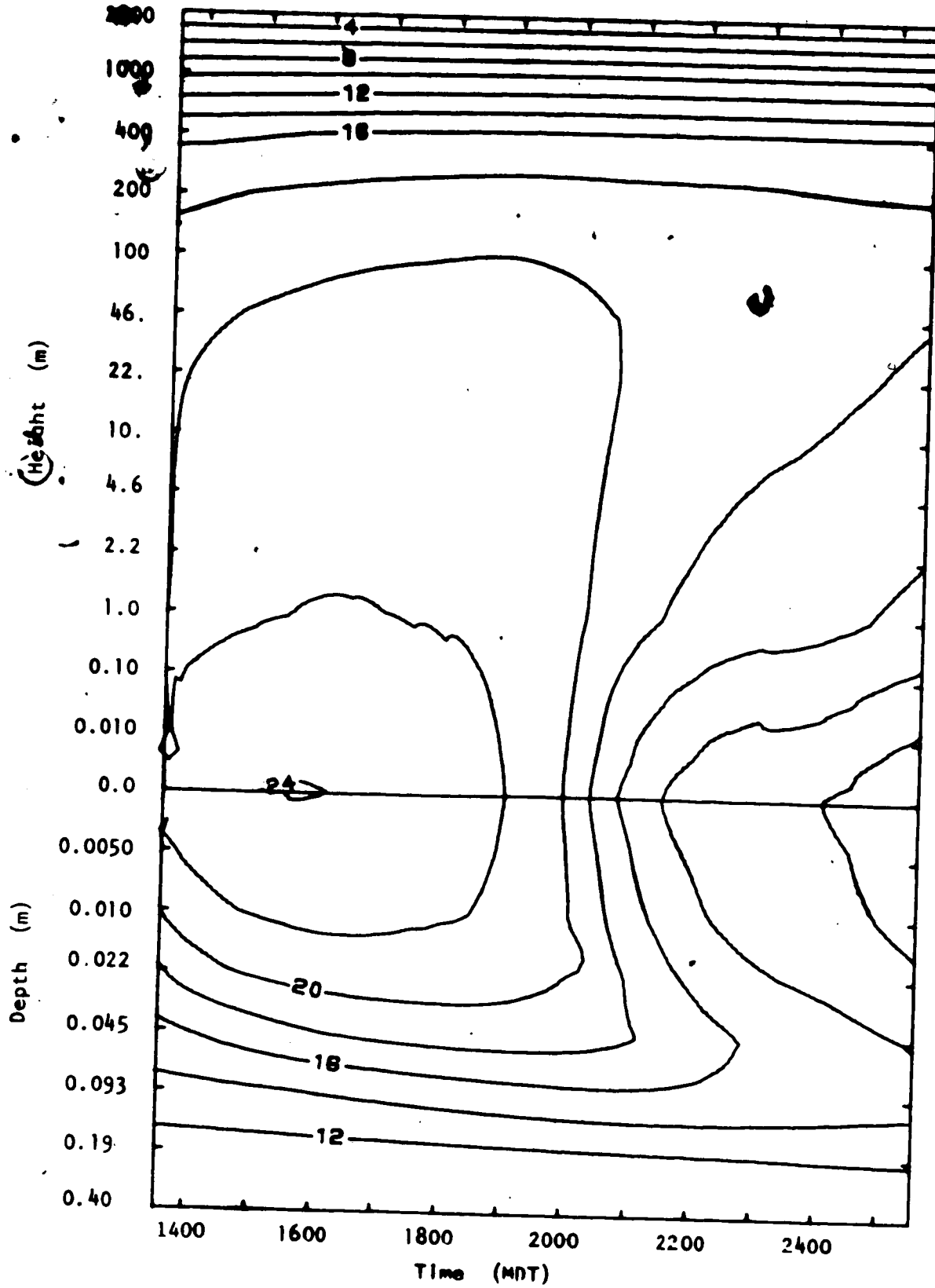


Figure 5.18 The Model-Predicted Temperature Field at the Rim for Experiment 11

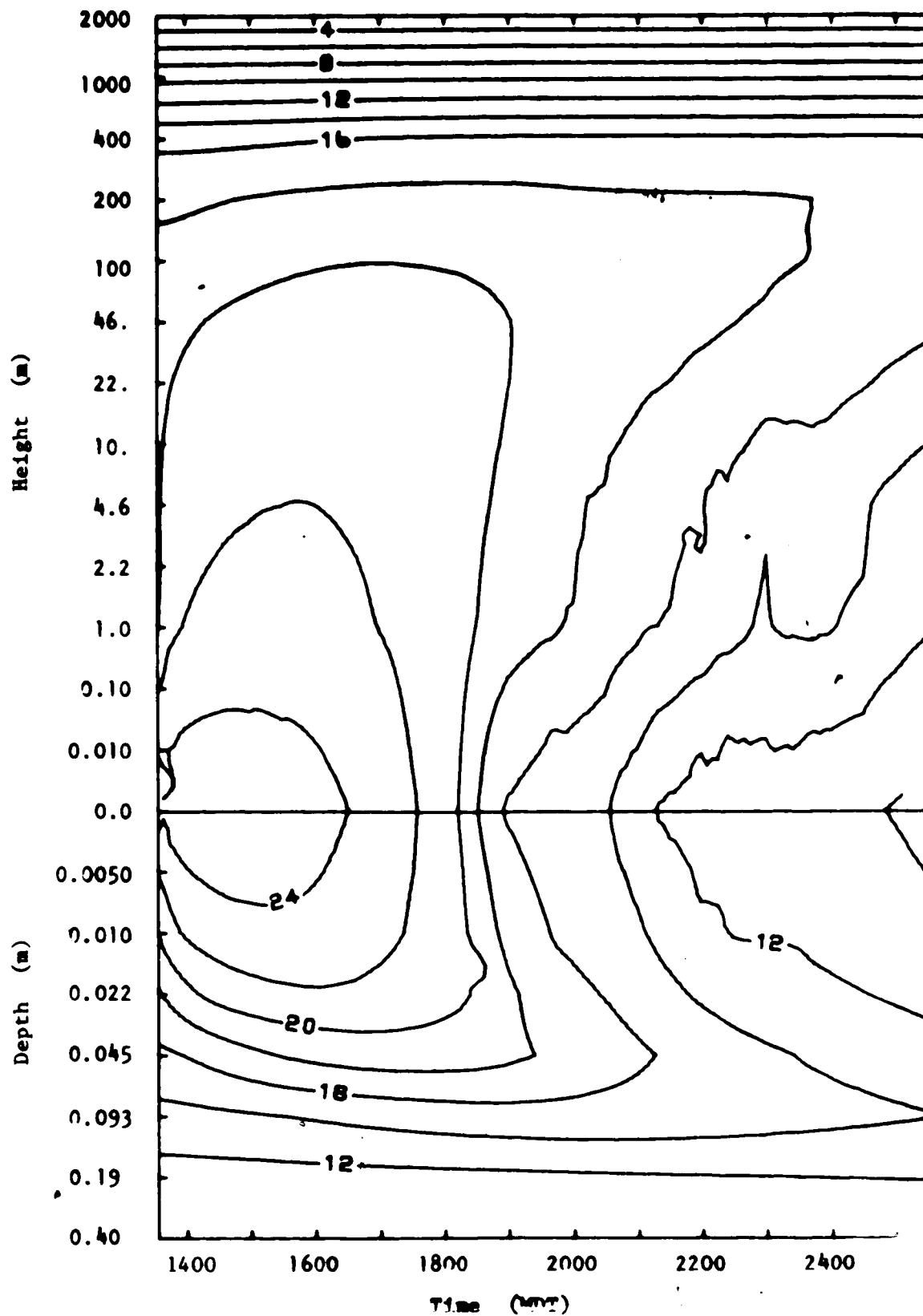


Figure 5.19 The Model-Predicted Temperature Field over the Slope with the Inclusion of the Neutral Layer for Experiment 11

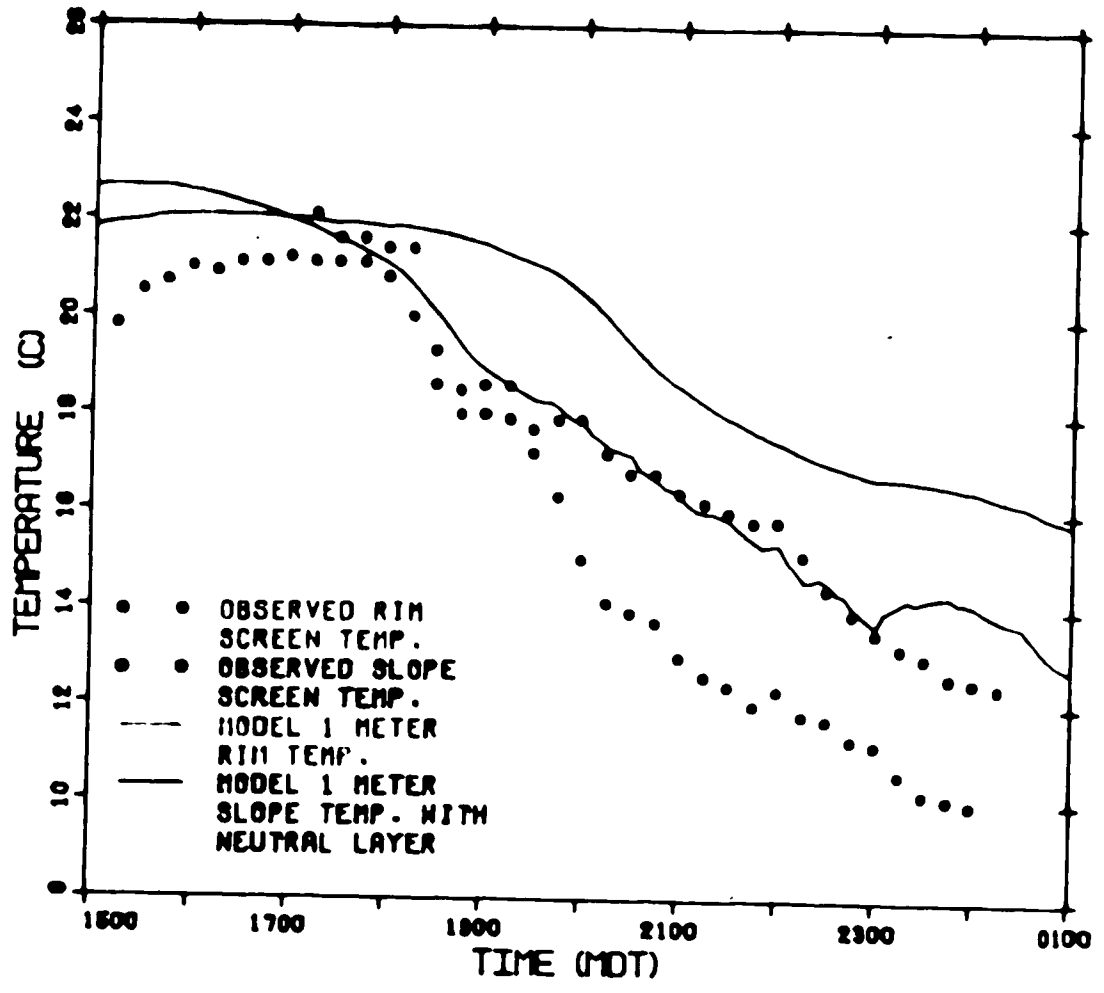


Figure 5.20 Progression of the 1 meter Temperature with Time for Experiment 11

CHAPTER 6

SUMMARY AND CONCLUSIONS

6.1 SUMMARY

Thirteen experiments were carried out in the North Saskatchewan River Valley in Edmonton during 1977 and 1978. The aim of these experiments was to determine the major characteristics of the valley microclimate, and to use this information to create a general simulation model ultimately capable of predicting the pollutant distribution in the valley. The evolution of the valley temperature field is an important component in such a mathematical model. This thesis has concentrated on providing the temperature component by developing a simple radiative-conductive model.

The present radiative-conductive model met with limited success. However, the overall or gross characteristics of the valley temperature field were simulated by the model. Well-mixed afternoon conditions and poorly-mixed evening conditions were replicated. Vertical temperature gradients under both stable and unstable conditions were reproduced.

Stronger inversions and lower temperatures over the north- and east-facing slopes than over the opposing slopes were accounted for. The timing of maximum temperatures and the onset of cooling was good. The performance of the model in predicting a significant difference between an urban and a rural station was disappointing. However, the model did predict slope-rim temperature differences which were close to those observed. In this respect, the inclusion of a neutral layer above the slope was partially successful in accounting for the effect of the slope wind. The viability of a double-structure inversion above the valley in the evening was demonstrated. Generally, the model reproduced all the main micrometeorological features, but did so with limited accuracy.

6.2 Conclusions

The most important conclusion concerns the application of flat-plane profile theory to an inclined surface. It has been demonstrated that, for gentle slopes, the use of the flat-plane theory is quite adequate in the well-mixed unstable regime. In this situation, the slope wind was weak, and the error in neglecting the advective component is small. However, during the evening when the boundary layer becomes stable, and cooler draining air initiates the slope wind, the use of flat-plane theory becomes questionable. Once the slope wind becomes well established, the

logarithmic wind profile of the flat-plane theory is not observed in the lowest levels. In an attempt to correct this discrepancy, a second wind profile was introduced in the domain of the slope wind. This profile was deemed to have properties similar to the flat-plane profile with the only difference being one of scale. Due to the mechanical nature of the motion, the profile was assigned neutral stability characteristics. The results have indicated that this procedure was reasonably successful.

In addition, the importance of advection and drainage flow has been inferred from the results. The predicted late evening slope temperatures were consistently higher than the observed. It is felt that this difference was mainly due to the absence of an advective component in the model, and that the inclusion of an advective term would improve the results.

The model radiative components were generally adequate. On fair-weather days, the atmospheric long-wave flux densities calculated from morning and afternoon radiosonde observations differed by less than 2 per cent. This is less than the accuracy of the computation. Hence the assumption of a constant atmospheric flux density is good. The effects of excluding specific humidity as a predicted variable in the model, and using a rough parameterization for the latent heat flux density are not completely known. Although the flux densities were not unreasonable, this remains an area for future improvement. On ideal cloudless days the solar

radiation was adequate. The time and rate of extinction of solar flux density was important. In this respect, the model was sensitive to the inclination and orientation of the valley slope. Otherwise the model was not sensitive to the slope parameter. It is conjectured that this conclusion would be invalid if an advective term was included. The soil flux density exhibited little sensitivity to the value chosen for the soil diffusivity. This was heartening since the soil parameter was assumed constant with depth and independent of soil moisture.

The model proved sensitive to wind. Whenever an observed wind was input into the model (every 30 minutes), it was reflected in the output. It is suspected that this sensitivity was mostly due to model shock, and that the incorporation of wind as a predicted variable would alleviate the problem.

6.3 SCOPE FOR FUTURE WORK

In any work involving boundary-layer meteorology the inter-relationships between the temperature and wind are complex. Thus the determination of stability functions, such as the Richardson number, should not be based on the explicit separation of these two variables. In this respect, a priority for future work is the incorporation into the model of wind as a prediction element. Moreover, the model could be expanded into two dimensions to include

the effects of advection, and the drainage and pooling of cooler air. Another possibility for future work is to upgrade the radiative components with the inclusion of both cloud and specific humidity. Inclusion of cloud would be important not only in adjusting the short- and long-wave radiation received at the surface but also, in the case of cumulus development, as an indicator for refining the latent heat flux density corrections. Also important are the extensions to a polluted atmosphere in which a radiative-flux divergence term would be necessary; and to winter inversion conditions. The incorporation of wind as a predicted variable is likely to be the most important of all the suggestions. Its inclusion has the potential to improve dramatically the accuracy in the performance of the model.

REFERENCES

- Blackadar, A.K., 1962: The Vertical Distribution of Wind and Turbulent Exchange in a Neutral Atmosphere. J. Geophys. Res., 67, 3095-3102.
- Businger, J.A., 1973: Turbulent Transfer in the Atmospheric Surface Layer. Workshop on Micrometeorology. D.A. Haugen, editor, Amer. Meteor. Soc., 392 pp.
- , J.C. Wyngaard, Y. Izumi, and E.F. Bradley, 1971: Flux Profile Relationships in the Atmospheric Surface Layer. J. Atmos. Sci., 28, 181-189.
- Carl, D.M., T.C. Tarbell, and H.A. Panofsky, 1973: Profiles of Wind and Temperature from Towers over Homogeneous Terrain. J. Atmos. Sci., 30, 788-794.
- Conte, S.D., and C. de Boor, 1972: Elementary Numerical Analysis. 2nd Ed., McGraw-Hill Book Company, Toronto, 396 pp.
- Ekman, V.W., 1905: On the Influence of the Earth's Rotation on Ocean Currents. Arkiv Met. Astron. Fysik, 2(11), 52 pp.
- Elsasser, W.M., 1942: Heat Transfer by Infrared Radiation in the Atmosphere. Harvard Meteor. Studies, No. 6, Cambridge, Harvard Univ. Press, 107 pp.
- Estoque, M.A., 1963: A Numerical Model of the Atmospheric Boundary Layer. J. Geophys. Res., 68, 1103-1113.
- Fisher, E.L., 1961: A Theoretical Study of the Sea Breeze. J. Meteor., 18, 216-233.
- Fleagle, R.G., and J.A. Businger, 1963: An Introduction to Atmospheric Physics. Academic Press, New York, 346 pp.
- Geiger, R., 1966: The Climate Near the Ground. Harvard University Press, Cambridge, 611 pp.
- Golder, D., 1972: Relations Among Stability Parameters in the Surface Layer. Boundary-Layer Meteor., 3, 47-58.
- Hage, K.D., 1972: Nocturnal Temperatures in Edmonton, Alberta. J. App. Met., 11, 123-129.
- , 1979: Air Pollution Study of the North Saskatchewan River Valley in Edmonton, Alberta. Final Report under Research Proposal ES77-6 to the Research Secretariat, Alberta Environment, Edmonton, 90 pp.

- Neer, S.L., 1959: Introduction to Theoretical Meteorology. Holt, Rinehart and Winston, New York, 362 pp.
- Houghton, H.G., 1954: On the Annual Heat Balance of the Northern Hemisphere. J. Meteor., 11, 1-9.
- Jacobs, C.A., and P.S. Brown, Jr., 1973: An Investigation of the Numerical Properties of the Surface Heat Balance Equation. J. App. Met., 12, 1069-1072.
- Kondratyev, K. Ya., 1969: Radiative Heat Exchange in the Atmosphere. Pergamon Press, New York, 411 pp.
- Krishna, K., 1968: A Numerical Study of the Diurnal Variation of Meteorological Parameters in the Planetary Boundary Layer. Mon. Wea. Rev., 96, 269-276.
- Lettau, H.H., and B. Davidson, 1957: Exploring the Atmosphere's First Mile. Vol. 2, Pergamon, New York, 201 pp.
- Lumley, J.L., and H.A. Panofsky, 1964: The Structure of Atmospheric Turbulence. Interscience Publishers, New York, 239 pp.
- Monin, A.S., and A.M. Obukhov, 1954: Basic Laws of Turbulent Mixing in the Atmosphere near the Ground. Tr. Akad. Nauk SSSR Geofiz. Inst., No 24 (151), 163-187.
- Paltridge, G.W., and C.M.R. Platt, 1976: Radiative Processes in Meteorology and Climatology. Elsevier Scientific Publishing Company, New York, 318 pp.
- Panofsky, H.A., A.K. Blackadar, and G.E. McVehil, 1959: The Diabatic Wind Profile. Quart. J. Roy. Meteorol. Soc., 86, 390-398.
- Paterson, R.D., 1978: A Micrometeorological Study of an Urban Valley. Unpublished M.Sc. Thesis, University of Alberta, 91 pp.
- _____, and K.D. Hage, 1979: Micrometeorological Study of an Urban Valley. Boundary-Layer Meteor., 16, (inpress).
- Paulson, C.A., 1970: The Mathematical Representation of Wind Speed and Temperature Profiles in the Unstable Atmospheric Surface Layer. J. App. Met., 9, 857-861.
- Plate, E.J., 1971: Aerodynamic Characteristics of Atmospheric Boundary Layers. U.S. Atomic Energy Commission, 190 pp.

- Sasanori, T., 1970: A Numerical Study of Atmospheric and Soil Boundary Layers. J. Atmos. Sci., 27, 1122-1137.
- Sellers, W.D., 1961: A Simple Derivation of the Diabatic Wind Profile. J. Atmos. Sci., 19, 180-181.
- _____, 1965: Physical Climatology. The University of Chicago Press., Chicago, 272 pp.
- Shir, C.C., 1973: A Preliminary Numerical Study of Atmospheric Turbulent Flows in the Idealized Planetary Boundary Layer. J. Atmos. Sci., 30, 1327-1339.
- Smith, G.D., 1965: Numerical Solution of Partial Differential Equations. Oxford University Press, London, 179 pp.
- Stovel, L.D., 1979: Personal Communication based on uncompleted M.Sc. Thesis, University of Alberta.
- Sutton, O.G., 1953: Micrometeorology. McGraw-Hill Book Company, Inc., Toronto, 333 pp.
- Thorpe, A.J., and T.H. Guymer, 1977: The Nocturnal Jet. Quart. J. Roy. Meteorol. Soc., 103, 633-653.
- Webb, E.K., 1970: Profile Relationships: The Log-linear Range, and Extension to Strong Stability. Quart. J. Roy. Meteorol. Soc., 96, 67-80.
- Zdunkowski, W.G., and D.C. Trask, 1971: Application of a Radiative-conductive Model to the Simulation of Nocturnal Temperature Changes over Different Soil Types. J. Atmos. Sci., 10, 937-948.
- _____, R.M. Welch, and J. Paegle, 1976: One Dimensional Numerical Simulation of the Effects of Air Pollution in the Planetary Boundary. J. Atmos. Sci., 33, 2399-2414.

APPENDIX A

GRAPHICAL INTEGRATION
 OF THE ATMOSPHERIC LONG-WAVE FLUX DENSITY

In section (2.4) the atmospheric long-wave flux density due to water vapour that reached the earth's surface was expressed by

$$F_{LW} = \int_0^{\infty} \sigma T^4 \left(\frac{\partial E}{\partial w} \right) \frac{\partial w}{\partial z} dz \quad (A.1)$$

where E is the emissivity due to water vapour and w is the corrected optical depth. Strictly speaking, this equation is only valid in a plane stratified atmosphere. It is derived (see, for example, Fleagle and Businger, 1963) by summing the monochromatic flux density contributions from all the differential volume elements at an arbitrary level over all levels and emitting wave lengths. Using the hydrostatic equation in conjunction with the definitions of specific humidity and differential optical thickness, this equation may be recast as

$$F_{WV} = \frac{\sigma}{g} \int_0^{P_0} q T^4 \left(\frac{\partial E}{\partial w} \right) dp \quad (A.2)$$

The rate of change of flux emissivity with optical thickness is experimentally known, and the vertical profiles of specific humidity and temperature as functions of pressure can be obtained from an atmospheric sounding. Thus equation

(A.2) may be computed numerically.

Alternatively, the quantity $Q = \frac{\sigma}{g} q T^4 \left(\frac{\partial E}{\partial w} \right)$ may be plotted as a function of the pressure, and the area under the curve, which represents the flux density, determined graphically. The Q-P plot is not unique. By a suitable change of variables, Elsasser (1942) constructed a nomogram, known as the Elsasser diagram, in which the abscissa was a function of temperature, and the ordinate a function of the corrected optical depth. This chart was particularly convenient: the isotherms were straight vertical lines, as were the isopleths of zero and infinite corrected optical thickness. Further the isopleth $w=0$ coincided with the upper edge of the chart, and the isopleth $w=\infty$ with the horizontal axis. Standard curves of constant optical thickness are pre-drawn on this chart. A schematic version of the Elsasser diagram is given in Figure A.1. Properties of this diagram have been detailed by Elsasser. The only property pertinent to present purposes is that the cross-hatched area in Figure A.1 represents the downward atmospheric long-wave flux density due to water vapour. Recall allowance has previously been made (Section 2.4) for the long-wave flux density due to carbon dioxide.

In determining the corrected optical depth, a square root pressure correction was used. Never empirical evidence indicates that a linear correction may be more appropriate. However, Houghton (1954) states that, in the computation of the net flux density, the methods differ by only about 3 per

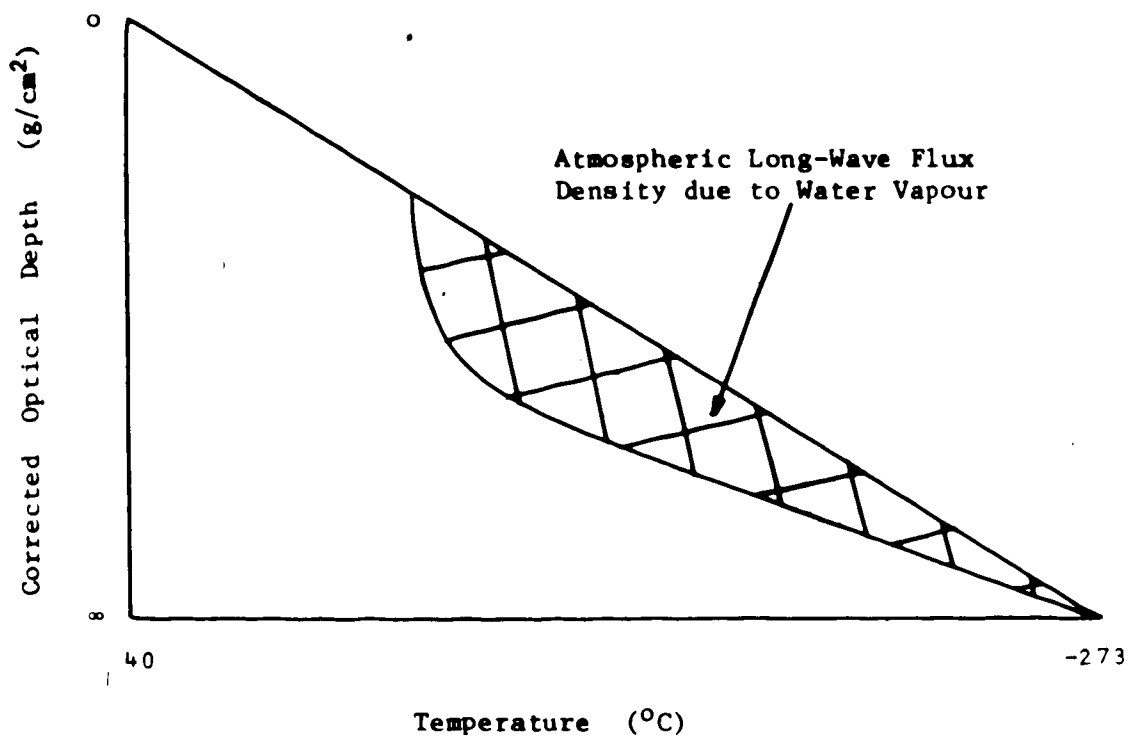


Figure A.1 The Elsasser Diagram

cent. Thus Elsasser's original correction was used.

For model purposes, the atmospheric radiation was assumed constant over the forecast period, and was computed using the radiosonde data taken from Stony Plain. The specific humidity was graphically calculated from the temperature and dew point data using a tephigram.

Tables A.1, A.2, and A.3 list the radiosonde data and the corresponding calculated specific humidity and optical depth for Experiments 8, 9, and 11. Using these tables, the w-T curves were plotted on an Elsasser diagram, and the long-wave flux density determined with a planimeter.

Table A.1 The Atmospheric Sounding for Experiment 8

Pressure (mb)	Temp. (°C)	Dew Point (°C)	Specific Humidity (g/Kg)	Corrected Optical Depth (g/cm ²)
922	24.8	10.8	10.4	0.00
870	18.6	6.6	8.0	0.46
712	4.0	- 0.3	5.5	1.43
655	- 0.5	- 9.5	3.2	1.64
629	- 3.1	-23.1	1.3	1.69
613	- 2.9	-22.9	1.4	1.70
493	-13.5	-32.5	0.70	1.80
479	-13.9	-27.9	0.98	1.81
450	-17.9	-35.9	0.53	1.82
400	-25.5	-34.5	0.59	1.84
313	-39.3	-47.3	0.13	1.86

Table A.2 The Atmospheric Sounding for Experiment 9

Pressure (mb)	Temp. (°C)	Dew Point (°C)	Specific Humidity (g/Kg)	Corrected Optical Depth (g/cm ²)
922	24.6	8.4	9.4	0.00
808	14.0	3.0	6.8	0.88
697	3.4	- 1.6	5.2	1.46
680	2.0	- 9.0	3.3	1.53
577	- 7.1	-18.1	1.9	1.74
462	-16.1	-34.1	0.56	1.85
305	-40.1	-54.1	0.06	1.88

Table A.3 The Atmospheric Sounding for Experiment 11

Pressure (mb)	Temp. (°C)	Dew Point (°C)	Specific Humidity (g/Kg)	Corrected Optical Depth (g/cm ²)
930	19.6	6.6	7.7	0.00
850	11.8	2.8	6.1	0.53
828	9.6	1.6	5.8	0.65
778	5.8	- 5.8	3.8	0.87
700	- 0.1	- 9.1	3.1	1.11
637	- 5.7	-13.7	2.4	1.25
589	- 8.9	-27.8	0.84	1.31
571	- 9.9	-20.8	1.5	1.32
500	-17.1	-32.1	0.62	1.38
400	-28.7	-44.6	0.15	1.41
376	-32.3	-36.1	0.50	1.42
321	-40.1	-44.6	0.15	1.43

APPENDIX B

THE SOLAR FLUX DENSITY

In section (2.4) the expression used to evaluate the solar flux density was given as

$$F_{SW} = S_0(1-\mu) \{ \sin(\delta)\cos(\xi) + \cos(\delta)\sin(\xi)\cos(\text{HAN}-wt-\text{HATO}) \} \quad (\text{B.1})$$

where S_0 = solar constant

μ = albedo-turbidity-diffuse solar radiation factor

δ = declination of sun

ξ = angle between celestial pole and slope normal

HATO = hour angle of sun at $t = 0$

HAN = hour angle of slope normal

w = earth's angular rotation

t = time

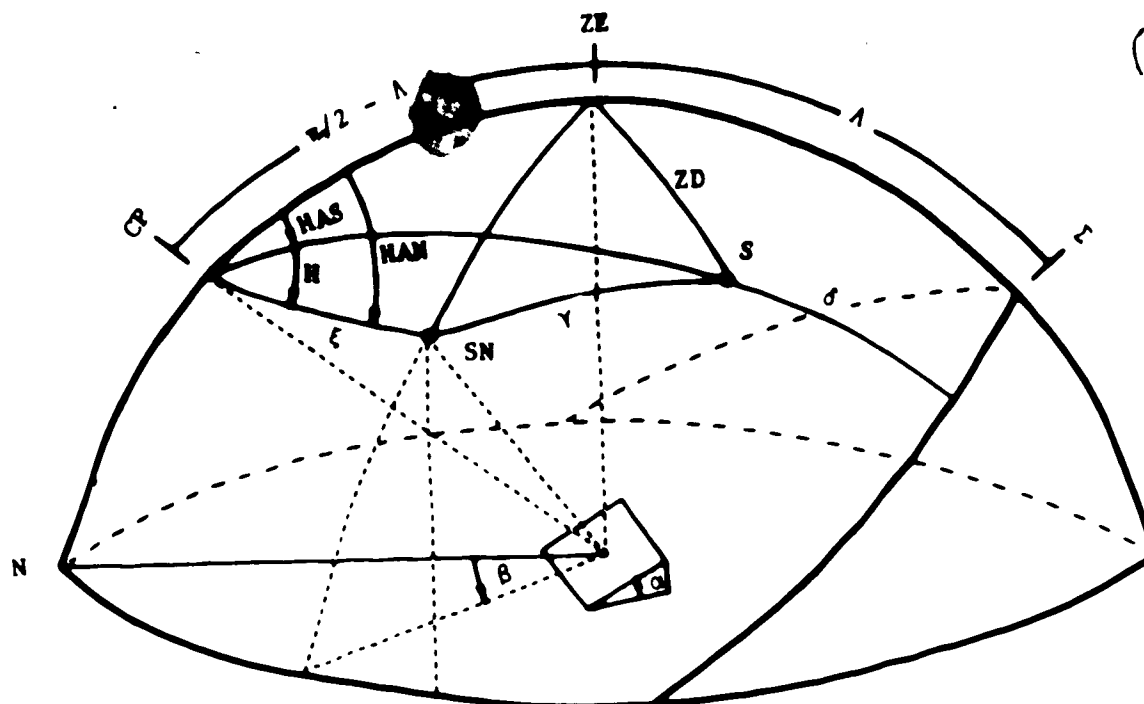
This equation results from the cosine law for radiation, namely

$$F = F_0 \cos(\gamma) \quad (\text{B.2})$$

where F_0 is the radiative flux density through a surface when the flux beam is normal to that surface, and γ is the angle of incidence between the beam and the surface normal. It is clear that F_0 can be identified with $S_0 \cdot (1-\mu)$. Thus it remains to show that the angle of incidence is given by

$$\gamma = \cos^{-1} \{ \sin(\delta)\cos(\xi) + \cos(\delta)\sin(\xi)\cos(\text{HAN}-wt-\text{HATO}) \} \quad (\text{B.3})$$

From the spherical geometry illustrated in Figure B.1, the



CP	=	celestial pole	ZE	=	zenith
H	=	hour angle of slope normal relative to hour angle of sun	α	=	slope inclination
HAN	=	hour angle of slope normal	β	=	slope orientation
HAS	=	hour angle of sun	γ	=	angle of incidence between solar flux beam and slope
N	=	north	δ	=	declination of sun
S	=	sun	λ	=	latitude
SN	=	slope normal	ξ	=	angle between celestial pole and slope normal
ZD	=	zenith distance	ζ	=	south point

Figure B.1 The Celestial Dome

following relationships hold

$$\cos(\gamma) = \sin(\delta)\cos(\xi) + \cos(\delta)\sin(\xi)\cos(H) \quad (B.4)$$

$$H = HAN - HAS \quad (B.5)$$

If the model is started at time $t = 0$, then the hour angle of the sun will be

$$HAS = \omega t + HAT0 \quad (B.6)$$

where HAT0 is the hour angle of the sun at $t = 0$ (initial hour angle). When equations (B.5) and (B.6) are combined with equation (B.4), the expression for the angle of incidence given by equation (B.3) results.

In the model, the zero hour was chosen as 1235 MST. This time is very close to local noon, and hence the initial hour angle is very close to zero. Values for both the sun's declination and initial hour angle were extracted from the 1977 Nautical Almanac¹⁰ and corrected appropriately.

Sunrise or sunset, neglecting both atmospheric refraction and the semi-diameter of the sun, will coincide with a solar flux density of zero. From equation (B.4), this must occur at

$$HAS = \pm \cos^{-1} \left(- \frac{\tan(\delta)}{\tan(\xi)} \right) + HAN \quad (B.7)$$

This expression, in conjunction with equation of time and longitude corrections, was used to determine sunrise and sunset over the slope. Values for the equation of time

¹⁰published by the U.S. Government Printing Office,
 Washington, D.C.

corrections were also taken from the almanac. Between sunset and sunrise, the calculated solar flux density was reset to zero.

APPENDIX C

GAUSSIAN ELIMINATION OF A TRIDIAGONAL MATRIX

This appendix describes the solution by Gaussian elimination of the set of equations

$$A_j Y_{j+1} + B_j Y_j + C_j Y_{j-1} = D_j, \quad j=1, \dots, N \quad (C.1)$$

where Y_1 and Y_N are known.

Since Y_N is known, equation (C.1) can be solved for $j = N-1$ in terms of one unknown Y_{N-2} , i.e.

$$Y_{N-1} = F_{N-1} + G_{N-1} Y_{N-2},$$

$$\text{where } F_{N-1} = \frac{D_{N-1} - A_{N-1} F_N}{B_{N-1} + A_{N-1} G_N}, \quad G_{N-1} = \frac{-C_{N-1}}{B_{N-1} + A_{N-1} G_N},$$

$$F_N = Y_N, \quad \text{and} \quad G_N = 0.$$

Using this expression for F_{N-1} , equation (C.1) for $j=N-2$

becomes

$$Y_{N-2} = F_{N-2} + G_{N-2} Y_{N-3}$$

$$\text{where } F_{N-2} = \frac{D_{N-2} - A_{N-2} F_{N-1}}{B_{N-2} + A_{N-2} G_{N-1}}, \quad G_{N-2} = \frac{-C_{N-2}}{B_{N-2} + A_{N-2} G_{N-1}},$$

This process of determining Y_j in terms of one unknown Y_{j-1} is continued yielding

$$Y_j = F_j + G_j Y_{j-1},$$

$$\text{where } F_j = \frac{D_j - A_j F_{j+1}}{B_j + A_j G_{j+1}}, \quad G_j = \frac{-C_j}{B_j + A_j G_{j+1}}$$

Ultimately $j = 2$ is reached. Since Y_{j-1-1} is known, Y_2 is determined. Back substitution of Y_2 then yields Y_3 . This

process of back substitution is continued until all values of y_j are determined.

APPENDIX D

THE MODEL GRID

The values for the grid points employed in all computer simulations are given in Tables D.1 and D.2.

Table D.1 The Grid Point Values within the Boundary Layer

Grid Point	Height (m)	Grid Point	Height (m)
1	0.0	18	5.000 *10 ⁺²
2	1.000 *10 ⁻²	19	6.000 *10 ⁺²
3	2.154 *10 ⁻²	20	7.000 *10 ⁺²
4	4.642 *10 ⁻²	21	8.000 *10 ⁺²
5	1.000 *10 ⁻¹	22	9.000 *10 ⁺²
6	2.154 *10 ⁻¹	23	1.000 *10 ⁺³
7	4.642 *10 ⁻¹	24	1.100 *10 ⁺³
8	1.000	25	1.200 *10 ⁺³
9	2.154	26	1.300 *10 ⁺³
10	4.642	27	1.400 *10 ⁺³
11	1.000 *10 ⁺¹	28	1.500 *10 ⁺³
12	2.154 *10 ⁺¹	29	1.600 *10 ⁺³
13	4.642 *10 ⁺¹	30	1.700 *10 ⁺³
14	1.000 *10 ⁺²	31	1.800 *10 ⁺³
15	2.000 *10 ⁺²	32	1.900 *10 ⁺³
16	3.000 *10 ⁺²	33	2.000 *10 ⁺³
17	4.000 *10 ⁺²		

Table D.2 The Grid Point Values within the Soil Layer

Grid Point	Depth (m)	Grid Point	Depth (m)
1	0.0	5	-4.472×10^{-2}
2	-5.000×10^{-3}	6	-9.283×10^{-2}
3	-1.038×10^{-2}	7	-1.927×10^{-1}
4	-2.154×10^{-2}	8	-4.000×10^{-1}

APPENDIX E

MODEL PARAMETERS

Table E.1 details the model parameters common to all computer simulations.

Table E.1 Common Model Parameters

Parameter	Programme Name	Value
Latitude	ALAT	53° 33' N
Longitude	ALON	113° 30' W
Slope Elevation	A	16.25°
Slope Orientation	B	103° E
Reference Height	ZNO	0.01 m
Height of Sub-Layer	ZT1	100. m
Height of Boundary Layer	ZT2	2000. m
Number of Points between and including		
a) surface and ZNO	NPGNO	2
b) ZNO and ZT1	NPN011	13
Grid Spacing above Sub-Layer	DZ2	100 m
Depth to Soil Bottom	ZSB	-0.4 m
Soil Reference Depth	ZNOS	-0.005 m
Number of Points between Surface and Soil Bottom	NZSPIS	8
Start-up Time	TO	12 hr 35 min MDT
Termination Time	TF	24 hr 35 min MDT
Time Step	DT	5 min
Solar Constant	SO	1353 W m ⁻²
Carbon-dioxide Correction	CF	.82
Albedo-Turbidity-Diffuse Solar Radiation Factor	ALB	.39
Stephan-Boltzmann Constant	SIGMA	5.67*10 ⁻⁸ W m ⁻² K ⁻⁴
Earth's Angular Rotation	W	7.292*10 ⁻⁵ sec ⁻¹

Table E.1 Continued

Parameter	Programme Name	Value
Eddy Viscosity	KMOL	$2.2 \times 10^{-5} \text{ m}^{-2} \text{ sec}^{-1}$
Soil Diffusivity	KHS	$1.5 \times 10^{-7} \text{ m}^{-2} \text{ sec}^{-1}$
Density * Heat Capacity	LAM	$1.2 \times 10^{+3} \text{ Jm}^{-3} \text{ K}^{-1}$
Soil Conductivity	LAMS	$2.5 \times 10^{-1} \text{ Wm}^{-1} \text{ K}^{-1}$
Error Limit for Surface Temperature Iteration	DER2	.00001 °C
Maximum Number of Iterations for Surface Temperature	NITB	100
Error Limit for Temperature Profiles Iteration	DER4	.00001 °C
Maximum Number of Iterations for Profile Determination	NITC	500
Weights for Implicit Method		
a) for Air	AL, BE	1.5, 0.5
b) for Soil	ALS, BES	
Displacement Time for Friction Velocity Data	TM	.5 hrs
Time Interval between Friction Velocity Data	TL	.5 hrs
Von Karman's constant	VKC	0.4

APPENDIX F**THE COMPUTER PROGRAMME**

The following pages of this appendix list the FORTRAN code for the computer model.

```

      IMPLICIT REAL*8 (A-H,O-Z), INTEGER (I-N)
      LOGICAL*1 P (1) /'*/
      DOUBLE PRECISION KN (10), KNN (50, 10), KH (10), KHH (50, 10),
&      LAM, LAMS, KMOL, KHS
&
      COMMON /A1/I, J
&      /A2/TO, TP, DT, T, TM, TL
&      /A3/ALAT, ALOW
&      /A4/A (10), B (10), IDATE, IDUM1
&      /A5/SST (10), SRT (10), ZET (10), HAN (10), DEC, EOT
&      /A6/NSTNS, NZPTS, NZPTS1, NZPTSA, NPGNO, NPNOT1,
&      NZSPTS, NZSPT1
&      /A7/ZNO, ZT1, ZT2, DZ2, ZNOS, ZSB
&      /A8/Z (50), ZS (10)
&      /A9/THET (2, 50, 10), TS (2, 10, 10)
&      /A10/H22, H12, HX, HS22, HS12, HSX
&      /A11/LAM, LAMS, SIGMA, CP, DER2, NITB, NIT2
&      /A12/KN, KNN /A13/KH, KHH
&      /A14/PLWV (10), PSW, PSH, PSHS, PLH, PLW
&      /A15/DZA (50), DZB (50), DZC (50), C2 (50), C3 (50)
&      /A16/DZAS (10), DZBS (10), DZCS (10), C2S (10), C3S (10)
&      /A17/SO, W, HATO, ALB, DER4, NITD, NIT4
&      /A18/USTAR (10), VKC, KMOL
&      /A19/RI, PHI, BRI, UB
&      /A20/K, IDUM
&      /A21/PHILIM, TSLP, JSLP, IDUM2

```

```

C
C
      D1R (X) = X * .1745329251994329D-01
      RD1 (X) = X / .1745329251994329D-01
      D2R (X) = (AINT (SNGL (X)) + (X - AINT (SNGL (X))) * 100. DO / 60. DO)
&      * .1745329251994329D-01
      D3R (X) = ( AINT (SNGL (X))
&      + ( (X - AINT (SNGL (X))) * 100. DO
&      - (X * 100. DO - AINT (SNGL (X) * 100.)) ) / 60. DO
&      + ( X * 100. DO - AINT (SNGL (X) * 100.) ) / 36. DO )
&      * .1745329251994329D-01
      H2H (X) = AINT (SNGL (X)) + (X - AINT (SNGL (X))) * 100. DO / 60. DO
      H3H (X) = AINT (SNGL (X))
&      + ( (X - AINT (SNGL (X))) * 100. DO
&      - (X * 100. DO - AINT (SNGL (X) * 100.)) ) / 60. DO
&      + ( X * 100. DO - AINT (SNGL (X) * 100.) ) / 36. DO

```

```

C
C
      CALL SUN

```

```

C
C
      DO 100 I=1, NSTNS
      WRITE (7, F) SRT (I), SST (I)
/ 100 CONTINUE

```

```

C
C
      CALL GRD

```

```

C      READ(4,F) HATO, TO, TF, DT,
      8          SO, W, SIGMA, CP, ALB, FLWA,
      8          KMOL, KHS, LAM, LAMS,
      8          DER2, DER4,
      8          NITB, NITD,
      8          AL, BE, ALS, BES,
      8          TM, TL, VKC, PHILIM, TSLP

C
C      T      =0.00
      HATO =DZR(HATO)+D1R(EOT*15.00)
      TO   =H2H(TO)
      TF   =H2H(TF)
      DT   =H2H(DT)
      NSTPS=IFIX(SMGL((TF-TO)/DT+.5))+1

C
C      DO 110 I=1,NSTNS
      110  FLWV(I)=FLWA*DCOS(A(I)/2.00)*DCOS(A(I)/2.00)
      CONTINUE

C
C      DO 120 J=1,NZPTS
      120  WRITE(7,F) Z(J)
      CONTINUE
      DO 130 J=1,NZSPTS
      130  WRITE(7,F) ZS(J)
      CONTINUE

C
C      H22 = Z(3)*Z(3)
      H12 = Z(2)*Z(2)
      HX  = (Z(3)-Z(2))*Z(3)*Z(2)
      HS22= ZS(3)*ZS(3)
      HS12= ZS(2)*ZS(2)
      HSX = (ZS(3)-ZS(2))*ZS(3)*ZS(2)

C
C      CALL FVEL

C
C      DO 140 J=2,NZPTS1
      DZA(J) =Z(J) -Z(J-1)
      DZB(J) =Z(J+1)-Z(J)
      DZC(J) = (DZA(J)+DZB(J))/2.00
      C2(J)  =AL*DT*3600.00/2.00/DZC(J)
      C3(J)  =BE*DT*3600.00/2.00/DZC(J)
      140  CONTINUE

C
C      DO 150 J=2,NZSPT1
      DZAS(J) =ZS(J) -ZS(J-1)
      DZBS(J) =ZS(J+1)-ZS(J)

```

```

DZCS(J) = (DZAS(J)+DZBS(J))/2.D0
C2S(J)  =ALS*DT*3600.D0*KHS/2.D0/DZCS(J)
C3S(J)  =BES*DT*3600.D0*KHS/2.D0/DZCS(J)
150 CONTINUE
C
C
WRITE(7,F) NSTNS,NZPTS,NSTPS,NZSPTS
C
C
CALL SSTS
C
C
DO 200 I=1,NSTNS
C
CALL INIT
C
PSW=SO*( DSIN(DEC)*DCOS(ZET(I))
&        +DCOS(DEC)*DSIN(ZET(I))*DCOS(HAN(I)-HATO) )
&        *(1.D0-ALB)
IF(((T+TO).LT.SST(I)).AND.
&   ((T+TO).GT.SRT(I)),GOTO 210
IF(((T+TO).LT.(SST(I)+24.D0)).AND.
&   ((T+TO).GT.(SRT(I)+24.D0)))GOTO 210
PSW=0.D0
210 CONTINUE
C
CALL DFVTY
C
CALL TSFC
C
TS (2,1,I)=THET(2,1,I)
TS (1,1,I)=THET(2,1,I)
THET(1,1,I)=THET(2,1,I)
KO=1
C
WRITE(7,F) NIT2,I,KO
WRITE(6) (THET(2,J,I),J=1,NZPTS),
&        (TS (2,J,I),J=1,NZSPTS)
FNET=PSW+PLWV(I)-PLW
WRITE(8) PSW,PSH,PSHS,PLH,PLWV(I),PLW,FNET
200 CONTINUE
C
C
DO 900 K=2,NSTPS
C
IF( DMOD(T+TM+TO+1.D-06,TL).LT.1.D-06 )CALL FVEL
T=T+DT
C
C
DC 600 I=1,NSTNS
C
CALL DFVTY
CALL DFVTY2

```

```
C          CALL PROF
C
C          WRITE(7,P) NIT2,NIT0,I,K
C          WRITE(6) (THET(2,J,I),J=1,NZPTS),
C          (TS(2,J,I),J=1,NZSPTS)
C          FNET=PSW+PLWV(I)-PLW
C          WRITE(8) PSW,PSH,PSHS,PLH,PLWV(I),PLW,FNET
C
C          DO 220 J=1,NZPTS
C          THET(1,J,I)=THET(2,J,I)
220      CONTINUE
C          DO 230 J=1,NZSPTS
C          TS(1,J,I)=TS(2,J,I)
230      CONTINUE
C
C          600      CONTINUE
C
C
C          900      CONTINUE
C
C          STOP
C          END
```



```

SST(I) = 50.00
SRT(I) = -50.00
120 CONTINUE
ZET(I) = DIR(90.00) - ALAT
HAN(I) = 0.00
GOTO 290
130 CONTINUE
C
HAN(I) = 0.00
IF( (B(I).EQ.0.00.AND.A(I).LE.(DIR(90.00)-ALAT))
& .OR.(B(I).EQ.DIR(180.00)) ) GOTO 160
IF(B(I).EQ.0.00) GOTO 150
IF( DCOS(ALAT)*DCOS(A(I)).EQ.
& DSIN(ALAT)*DCOS(B(I))*DSIN(A(I)) ) GOTO 140
HAN(I) = DATAN( DSIN(A(I))*DSIN(B(I))
& / ( DCOS(ALAT)*DCOS(A(I))
& -DSIN(ALAT)*DCOS(B(I))*DSIN(A(I)) ) )
IF( (B(I).GT.0.00.AND.HAN(I).GT.0.00)
& .OR.(B(I).LT.0.00.AND.HAN(I).LT.0.00) ) GOTO 160
HAN(I) = DIR(180.00) + HAN(I)
IF(B(I).GT.0.00) GOTO 160
HAN(I) = HAN(I) - DIR(360.00)
GOTO 160
140 HAN(I) = DIR(90.00)
IF(B(I).GT.0.00) GOTO 160
HAN(I) = -HAN(I)
GOTO 160
150 HAN(I) = DIR(180.00)
160 CCNTINUE
IF(HAN(I).EQ.0.00.AND.B(I).LE.DIR(90.00)) GOTO 170
IF(HAN(I).EQ.0.00) GOTO 180
IF(HAN(I).EQ.DIR(180.00)) GOTO 190
ZET(I) = DARSIN(DSIN(A(I))*DSIN(B(I))/DSIN(HAN(I)))
GOTO 290
170 ZET(I) = DIR(90.00) - ALAT - A(I)
GOTO 200
180 ZET(I) = DIR(90.00) - ALAT + A(I)
GOTO 200
190 ZET(I) = A(I) - DIR(90.00) + ALAT
200 CONTINUE
IF(ZET(I).EQ.DIR(180.00).AND.DEC.GE.0.00) GOTO 210
IF(ZET(I).EQ.DIR(180.00)) GOTO 220
IF(ZET(I).EQ.0.00.AND.DEC.GT.0.00) GOTO 220
IF(ZET(I).EQ.0.00) GOTO 210
ARG = 0.00
IF(ZET(I).EQ.DIR(90.00).OR.ZET(I).EQ.DIR(-90.00))
& GOTO 230
ARG = -DTAN(DEC)/DTAN(ZET(I))
IF(ARG.GE.1.00) GOTO 210
IF(ARG.LT.-1.00) GOTO 220
GOTO 230
210 WRITE(5,320)
STOP

```



```

220 WRITE(5,330)
    SST(I) =50.D0
    SRT(I) =-50.D0
    GOTO 260
230 CONTINUE
    H=ACOS(ARG)
    T1=RD1(NAN(I)-H)/15.D0
    T2=RD1(H+NAN(I))/15.D0
    SRT(I)=T1+12.D0+BOT+ALNCOB
    SST(I)=T2+12.D0+BOT+ALNCOB
    IF(SRT(I).GT.0.D0) GOTO 240
    SRT(I) =SRT(I) +24.D0
    SST(I) =SST(I) +24.D0
240 CONTINUE
    IF(SRT(I).LT.SST(1)) GOTO 260
    IF(SST(I).LE.(SRT(1)+24.D0)) GOTO 250
    SST(I) =SST(I) -24.D0
    SRT(I) =SRT(I) -24.D0
    GOTO 260
250 WRITE(5,340) SRT(I),SST(I)
    STOP
260 CONTINUE
    IF(SST(I).LT.SST(1)) GOTO 270
    SST(I) =SST(1)
270 IF(SRT(I).GT.SRT(1)) GOTO 280
    SRT(I) =SRT(1)
280 CONTINUE
290 CONTINUE

```

C
C

```

RETURN
300 FORMAT(//,25H SUN NEVER ABOVE HORIZON,
& 17H EXECUTION HALTED,/)
310 FORMAT(//,25H SUN ALWAYS ABOVE HORIZON,/)
320 FORMAT(//,24H SUN NEVER ABOVE SLOPE,
& 17H EXECUTION HALTED,/)
330 FORMAT(//,23H SUN ALWAYS ABOVE SLOPE,/)
340 FORMAT(//,26H SUN ABOVE SLOPE ONLY WHEN
& 12H BELOW PLANE,2P10.5)
END

```

```

SUBROUTINE SSTS
IMPLICIT REAL*8 (A-H,O-S), INTEGER (I-N)
LOGICAL*1 F(1)/'00'/
COMMON /A2/TO,TF,DT,DUM(3)
      /A5/SST(10),SST(10),DUM2(22)
      /A6/NSTNS,IDUM(7)

```

C
C

```

DO 120 I=1,NSTNS
K2=-99
K3=-99
K4=-99
K5=-99
IF (TO.GT.SST(I)) GOTO 100
I1=IPIX(SNGL( DSIGN(1.D0, SST(I)-TO) ))
K2=IPIX(SNGL( (SST(I)-TO)/DT) )+I1
K3=K2+I1
100 CONTINUE
IF (TF.LT.SST(I)) GOTO 110
I2=IPIX(SNGL( DSIGN(1.D0, SST(I)-TO) ))
K4=IPIX(SNGL( (SST(I)-TO)/DT) )+I2
K5=K4+I2

```

C
C
C
C
C

```

110 WRITE(7,F) I,K2,K3,K4,K5
120 CONTINUE
RETURN
END

```

```

SUBROUTINE GRD
IMPLICIT REAL*8(A-H,O-Z),INTEGER(I-N)
LOGICAL*1 F(1)/'*/
COMMON /A6/NSTNS,NZPTS,NZPTS1,NZPTSA,NPGNO,
&      NPNOT1,NZSPTS,NZSPT1
&      /A7/ZNO,ZT1,ZT2,DZ2,ZNOS,ZSB
&      /A8/Z(50),ZS(10)
&      /A21/DUM(2),JSLP,IDUM2

C
C
      READ(4,F) ZNO,ZT1,ZT2,NPGNO,NPNOT1,DZ2,
&      ZNOS,ZSB,NZSPTS

C
      NZPTSA=NPNOT1+NPGNO-1
      NZPTS =IFIX(SNGL((ZT2-ZT1)/DZ2))+NZPTSA
      NZPTS1=NZPTS-1
      NZSPT1=NZSPTS-1
      JSLP =NPGNO+7

C
C
      Z(1)=0.D0
      D1  =(ZT1/ZNO)**(1.D0/DFLOAT(NPNOT1-1))
      ZLI =DLOG(D1)
      DO 100 J=2,NZPTSA
      Z(J)=ZNO*DEXP(DFLOAT(J-NPGNO)*ZLI)
100    CONTINUE

C
      NZPTSB=NZPTSA+1
      DO 110 J=NZPTSB,NZPTS
      Z(J)=Z(J-1)+DZ2
110    CONTINUE

C
C
      ZS(1)=0.D0
      D2  =(ZSB/ZNOS)**(1.D0/DFLOAT(NZSPTS-2))
      ZLSI =DLOG(D2)
      DO 120 J=2,NZSPTS
      ZS(J)=ZNOS*DEXP(DFLOAT(J-2)*ZLSI)
120    CONTINUE

C
      RETURN
      END

```

```

SUBROUTINE INIT
IMPLICIT REAL*8 (A-H,O-Z), INTEGER (I-N)
LOGICAL*1 F(1) /'*/
DOUBLE PRECISION ZI(50), TH(50), ZIS(10), THS(10)
COMMON /A1/I, J
&      /A6/NSTNS, NZPTS, NZPTS1, NZPTSA, NPGNO,
&      NPNOT1, NZSPTS, NZSPT1
&      /A8/Z(50), ZS(10)
&      /A9/THET(2, 50, 10, 10, 10, 10)

C
C
READ(4, F) FLAG7
IF (FLAG7.NE.1) GOTO 500
READ(2) (THET(1, J, I), J=1, NZPTS), (TS(1, J, I), J=1, NZSPTS)
READ(2) (THET(2, J, I), J=1, NZPTS), (TS(2, J, I), J=1, NZSPTS)
RETURN
500 CONTINUE
J2=NZPTS
READ(4, F) NIDP, (ZI(J), TH(J), J=1, NIDP),
&      NIDPS, (ZIS(J), THS(J), J=1, NIDPS)

C
C
DO 200 JI=2, NIDP
GAM=(TH(JI)-TH(JI-1))/(ZI(JI-1)-ZI(JI))

C
DO 100 J3=1, J2
J4=J3
IF (ZI(JI).LE.Z(J3)) GOTO 110
100 CONTINUE
110 IF (JI.GT.2) GOTO 140
DO 120 J5=J4, J2
J6=J5
IF (ZI(JI-1).EQ.Z(J5)) GOTO 140
IF (ZI(JI-1).LT.Z(J5)) GOTO 130
120 CONTINUE
130 J6=J6-1
140 CONTINUE
DO 150 J7=J4, J6
THET(1, J7, I)=TH(JI)-GAM*(Z(J7)-ZI(JI))
150 CONTINUE
IF (JI.NE.2) GOTO 170
J6A=J6+1
DO 160 J8=J6A, NZPTS
THET(1, J8, I)=TH(JI)-GAM*(Z(J8)-ZI(JI))
160 CONTINUE
170 IF (JI.NE.NIDP) GOTO 190
IF (ZI(JI).EQ.Z(1)) GOTO 200
DO 180 J9=1, J4
THET(1, J9, I)=TH(JI)-GAM*(Z(J9)-ZI(JI))
180 CONTINUE
190 J2=J4
J6=J4-1
200 CONTINUE
C

```

```

C
J2=NZSPTS
DO 400 JI=2,NIDPS
GAMS=(THS(JI)-THS(JI-1))/ZIS(JI-1)-ZIS(JI)
C
DO 300 J3=1,J2
J4=J3
IF(ZIS(JI).GE.ZS(J3))GOTO 310
300 CONTINUE
310 IF(JI.GT.2)GOTO 340
DO 320 J5=J4,J2
J6=J5
IF(ZIS(JI-1).EQ.ZS(J5))GOTO 340
IF(ZIS(JI-1).LT.ZS(J5))GOTO 330
320 CONTINUE
330 J6=J6-1
340 CONTINUE
DO 350 J7=J4,J6
TS(1,J7,I)=THS(JI)-GAMS*(ZS(J7)-ZIS(JI))
350 CONTINUE
IF(JI.NE.2)GOTO 370
J6A=J6+1
DO 360 J8=J6A,NZSPTS
TS(1,J8,I)=THS(JI)-GAMS*(ZS(J8)-ZIS(JI))
360 CONTINUE
370 IF(JI.NE.NIDPS)GOTO 390
IF(ZIS(JI).EQ.ZS(1))GOTO 400
DO 380 J9=1,J4
TS(1,J9,I)=THS(JI)-GAMS*(ZS(J9)-ZIS(JI))
380 CONTINUE
390 J2=J4
J6=J4-1
400 CONTINUE
C
C
C
DO 520 J=1,NZPTS
THET(2,J,I)=THET(1,J,I)
520 CONTINUE
DO 530 J=1,NZSPTS
TS(2,J,I)=TS(1,J,I)
530 CONTINUE
C
RETURN
END

```

SUBROUTINE TSFC

C
C

```

IMPLICIT REAL*8 (A-H,O-Z),INTEGER(I-N)
LOGICAL*1 F(1) /'*/
DOUBLE PRECISION KH(10),KHH(50,10),
& LAM,LAMS,KMOL,KHS
COMMON /A1/I,J
& /A2/TO,DUM4(2),T,DUM5(2)
& /A8/Z(50),ZS(10)
& /A9/THET(2,50,10),TS(2,10,10)
& /A10/H22,H12,HX,HS22,HS12,HSX
& /A11/LAM,LAMS,SIGMA,CP,DER2,NITB,NIT2
& /A13/KH,KHH
& /A14/PLWV(10),PSW,PSH,PSHS,PLH,PLW

```

C
C

```

NIT2=0
FLAG2=0.D0
100 CONTINUE
NIT2=NIT2+1
IF(NIT2.LT.NITB)GOTO 110
T2=TO+T
WRITE(5,180) NIT2,T2,I,ERR2
STOP
110 CONTINUE

```

C
C

```

PSHS=-LAMS*( HS22*TS(2,2,I)-HS12*TS(2,3,I)
& - (HS22-HS12)*TS(2,1,I) )/HSX
PSH=LAM*KH(I)*( H22*THET(2,2,I)-H12*THET(2,3,I)
& - (H22-H12)*THET(2,1,I) )/HX
FLH=PSH
IF(PSH.LT.0.D0)GOTO 115
FLH=-.5D0*PSH.
115 CONTINUE
PLW=PSW+PSH+PSHS+PLWV(I)+PLH
IF(PLW.LT.0.D0)GOTO 120

```

C
C

```

IF(NIT2.GT.20 .AND. DABS(PSH).LT.20.D0 )GOTO 200
FLAG2=1.D0
GT=THET(2,1,I) - (PLW/SIGMA/CF)**.25D0
GTP=1.D0+.25D0*( (LAMS/(-ZS(2)) +2.D0*LAM*KH(I)/Z(2))
& /SIGMA)/(PLW/SIGMA/CF)**(.75D0)
IF(PSH.LT.0.D0)GOTO 117
GTP=1.D0+.25D0*( (LAMS/(-ZS(2)) +.5D0*LAM*KH(I)/Z(2))
& /SIGMA)/(PLW/SIGMA/CF)**(.75D0)
117 CONTINUE
THETP=THET(2,1,I)
ERR2=GT/GTP
THET(2,1,I)=THET(2,1,I)-ERR2
IF(DABS(ERR2).LT.DER2)GOTO 160
GOTO 100

```

```

C
120 CONTINUE
    GT2=THET(2,1,I)
    IF (FLAG2.EQ.1.D0)GOTO 150
C
    THETP=250.D0
130 CONTINUE
    PSHS=LAMS/ZS(2)*(THETP-TS(2,2,I))
    PSH=LAM*KH(I)/Z(2)*(THET(2,2,I)-THETP)
    FLH=PSH
    IF (PSH.LT.0.D0)GOTO 135
    FLH=-.5D0*PSH
135 CONTINUE
    FLW=PSW+PSH+PSHS+FLWV(I)+FLH
    IF (FLW.GT.0.D0)GOTO 140
    IF (THETP.EQ.200.D0)GOTO 170
    THETP=200.D0
    GOTO 130
140 CONTINUE
    GT=THETP-(FLW/SIGMA/CF)**.25D0
C
150 CONTINUE
    ERR2=(GT2-THETP)/(GT2-GT)*GT2
    THET(2,1,I)=GT2-ERR2
    IF (DABS(ERR2).LT.DER2)GOTO 160
    GOTO 100
C
200 CONTINUE
    GT2=THET(2,1,I)-(FLW/SIGMA/CF)**.25D0
    THET1=THET(2,1,I)+ERR2
    ERR2=GT2*(THET(2,1,I)-THET1)/(GT2-GT)
    THET(2,1,I)=THET(2,1,I)-ERR2
    GT=GT2
    IF (DABS(ERR2).LT.DER2)GOTO 160
    GOTO 100
160 CONTINUE
    RETURN
170 CONTINUE
    T2=TQ+T
    WRITE(5,190) FLW,T2,I
    STOP
C
180 FORMAT (3H0**,,/3H **,I15,' * ITR XCD : TSFC ERR ',/,
&          3H **,F15.3,' TIME',/,3H **,I15,' STN',/,
&          3H **,F15.6,' ERR2',/,3H **)
190 FORMAT (3H0**,,/3H **,G15.2,' FLW < 0 : TSFC ERR ',/,
&          3H **,F15.3,' TIME',/,3H **,I15,' STN',/,
&          3H **)
    END

```

```

SUBROUTINE PROF
IMPLICIT REAL*8 (A-H,O-Z), INTEGER (I-N)
DOUBLE PRECISION A (50), B (50), C (50), D (50), F (50), G (50),
& AS (10), BS (10), CS (10),
& DS (10), PS (10), GS (10),
& KH (10), KHH (50, 10)
COMMON /A1/I, J
& /A2/TO, TF, DT, T, TH, TL
& /A5/SST (10), SRT (10), ZET (10), HAN (10), DEC, ROT
& /A6/WSTWS, WZPTS, NZPTS1, NZPTSA, NPGNO,
& NPNOT1, NZSPTS, NZSPT1
& /A8/Z (50), ZS (10)
& /A9/THET (2, 50, 10), TS (2, 10, 10)
& /A10/H22, H12, HI, HS22, HS12, HSX
& /A11/LAM, LAMS, SIGMA, CP, DER2, NITB, NIT2
& /A13/KH, KHH
& /A14/PLWVV (10), PSW, PSH, PSHS, PLH, FLW
& /A15/DZA (50), DZB (50), DZC (50), C2 (50), C3 (50)
& /A16/DZAS (10), DZBS (10), DZCS (10), C2S (10), C3S (10)
& /A17/SO, W, HATO, ALB, DER4, NITD, NIT4

```

C

```

TOLD=0. D0
NIT4=1
DO 100 J=2, NZPTS1
D (J) =C3 (J) * ( (THET (1, J+1, I) -THET (1, J, I))
& /DZB (J) *KHH (J, I)
& - (THET (1, J, I) -THET (1, J-1, I))
& /DZA (J) *KHH (J-1, I) )
& +THET (1, J, I)
A (J) =KHH (J, I) /DZB (J) *C2 (J)
C (J) =KHH (J-1, I) /DZA (J) *C2 (J)
B (J) =A (J) +C (J) +1. D0

```

100

CONTINUE

C

```

DO 110 J=2, NZSPT1
DS (J) =C3S (J) * ( (TS (1, J+1, I) -TS (1, J, I)) /DZBS (J)
& - (TS (1, J, I) -TS (1, J-1, I)) /DZAS (J) )
& +TS (1, J, I)
AS (J) =1. D0/DZBS (J) *C2S (J)
CS (J) =1. D0/DZAS (J) *C2S (J)
BS (J) =AS (J) +CS (J) +1. D0

```

110

CONTINUE

C

```

PSW=SO* ( DSIN (DEC) *DCOS (ZET (I))
& +DCOS (DEC) *DSIN (ZET (I)) *
& DCOS (HAN (I) -W*3600. D0* (T) -HATO) )
& * (1. D0-ALB)
IF ( ((T+TO) .LT. SST (I)) .AND.
& ((T+TO) .GT. SRT (I)) ) GOTO 120
IF ( ((T+TO) .LT. (SST (I) +24. D0)) .AND.
& ((T+TO) .GT. (SRT (I) +24. D0)) ) GOTO 120
PSW=0. D0

```

C

120 CONTINUE


```

C
CALL TSFC
ERR4=THET(2,1,I)-TOLD
IF ( NIT4.LT.10 ) GOTO 122
IF ( NIT4.LT.50 ) GOTO 125
THET(2,1,I)=( THET(2,1,I)+TS(2,1,I) )/2.DO
GOTO 125
122 CONTINUE
THET(2,1,I)=THET(2,1,I)+(THET(2,1,I)-TS(2,1,I))*2.DO
125 CONTINUE
THET(2,1,I)=THET(2,1,I)
IF ( DABS(ERR4).LT.DERR4 ) RETURN

C
NIT4=NIT4+1
IF ( NIT4.LT.NITD ) GOTO 130
T4=TO+T
WRITE(5,180) NIT4,T4,I,ERR4
STOP
130 CONTINUE

C
F(NZPTS) =THET(2,NZPTS,I)
PS(NZSPTS)=TS(2,NZSPTS,I)
G(NZPTS) =0.DO
GS(NZSPTS)=0.DO

C
DO 140 J=2,NZPTS1
JJ =NZPTS-J+1
E = B(JJ)-A(JJ)*G(JJ+1)
F(JJ)=(D(JJ)+A(JJ)*F(JJ+1))/E
G(JJ)=C(JJ)/E
140 CONTINUE

C
DO 150 J=2,NZSPT1
JJ = NZSPTS-J+1
ES = BS(JJ)-AS(JJ)*GS(JJ+1)
PS(JJ)=(DS(JJ)+AS(JJ)*PS(JJ+1))/ES
GS(JJ)=CS(JJ)/ES
150 CONTINUE

C
DO 160 J=2,NZPTS1
THET(2,J,I)=F(J)+G(J)*THET(2,J-1,I)
160 CONTINUE

C
DO 170 J=2,NZSPT1
TS(2,J,I)=PS(J)+GS(J)*TS(2,J-1,I)
170 CONTINUE

C
TOLD=THET(2,1,I)
GOTO 120

C
180 FORSAT(3H0**,,3H **,I15,' # ITR XCD : PROF ERR ',/,
& 3H **,P15.3,' TIME',/,3H **,I15,' STN',/,
& 3H **,P15.6,' ERR4',/,3H **)
END

```

```

SUBROUTINE PVEL
  IMPLICIT REAL*8(A-H,O-Z),INTEGER(I-N)
  LOGICAL*1 P(1)/'.'/
  DOUBLE PRECISION (10),KNN(50,10),KMOL
  COMMON /A3/ALAT,DUM1
  &      /A6/NSTNS,NZPTS,NZPTS1,IDUM3,NPGNO,IDUM4(3)
  &      /A8/Z(50),DUM2(10)
  &      /A12/KN,KNN
  &      /A18/USTAR(10),VKC,KMOL
  &      /A19/DUM3(3),UB

C
C
  READ(3,F) (USTAR(I),I=1,NSTNS),UB
C
C
  DO 120 I=1,NSTNS
  ZT3=.455D0*USTAR(I)/2.D0/7.292D-05/DSIN(ALAT)
C
  KN(I)=USTAR(I)*VKC/2.D0*Z(NPGNO)
  &      *( DEXP(-4.D0*Z(NPGNO)/ZT3)
  &      +1.D0/( 1.D0+16.D0*
  &      (Z(NPGNO)/ZT3)**1.6D0 ) )
  &      +KMOL
C
  DO 110 J=1,NZPTS1
  ZK=(Z(J)+Z(J+1))/2.D0
  KNN(J,I)=USTAR(I)*VKC/2.D0*ZK
  &      *( DEXP(-4.D0*ZK/ZT3)
  &      +1.D0/( 1.D0+16.D0*
  &      (ZK/ZT3)**1.6D0 ) )
  &      +KMOL
110 CONTINUE
C
120 CONTINUE
C
  RETURN
  END

```

```

SUBROUTINE DPTTY
IMPLICIT REAL*8(A-H,O-Z),INTEGER(I-N)
LOGICAL*1 P(1)/'*'/
DOUBLE PRECISION KN(10),KH(10),KMOL
COMMON /A1/I,J
&      /A2/DUM1(6)
&      /A8/Z(50),DUM2(10)
&      /A9/THET(2,50,10),DUM3(2,10,10)
&      /A12/KN,DUM4(50,10)
&      /A13/KH,DUM5(50,10)
&      /A18/USTAR(10),VKC,KMOL
&      /A19/RI,PHI,BRI,UB
&      /A21/DUM6,TSLP,JSLP,IDUM2

```

```

C      THETA V=( THET(1,JSLP-1,I)+THET(1,JSLP+1,I) )/2.DO
DTH      =THET(1,JSLP+1,I)-THET(1,JSLP-1,I)
DZ      =Z(JSLP+1)-Z(JSLP-1)
BRI      =9.806/THETA V*DTH/DZ/UB/UB*Z(JSLP)*Z(JSLP)
J=2

```

```

C      CALL MOPN
C      CALL SLOPE

```

```

C      KH(I)=KN(I)/PHI
C      IF(KH(I).GT.KMOL)GOTO 100
C      KH(I)=KMOL
100     CONTINUE

```

```

C      RETURN
C      END

```

```

SUBROUTINE SLOPE
IMPLICIT REAL*8(A-H,O-Z),INTEGER(I-N)
LOGICAL*1 P(1)/'*'/
COMMON /A1/I,J
&      /A2/TO,DUM4(2),T,DUM5(2)
&      /A18/USTAR(10),DUM(2)
&      /A19/RI,PHI,BRI,UB
&      /A20/K,IDUM
&      /A21/DUM2,PHILIM,TSLP,JSLP,IDUM2

```

```

C      IF(T+TO.LT.TSLP)RETURN
C      IF(I.NE.2)RETURN
C      IF(J.GT.JSLP)RETURN
C      READ(1,P) U
C      CP=U*.4D0/DLOG( (.25D0+.8D0)/-.25D0 )
C      PHI=PHI*USTAR(I)/CP
C      IF(PHI.LT.PHILIM)RETURN
C      PHI=PHILIM

```

```

C      RETURN
C      END

```

```

SUBROUTINE DPVTY2
IMPLICIT REAL*8 (A-H,O-Z), INTEGER (I-N)
LOGICAL*1 P(1) /'*/
DOUBLE PRECISION KN(10), KNN(50,10),
& KH(10), KHH(50,10), KMOL
COMMON /A1/I, J
& /A2/TO, TP, DT, T, TM, TL
& /A6/IDUM2(2), NZPTS1, IDUM1(5)
& /A8/Z(50), ZS(10)
& /A9/THET(2,50,10), TS(2,10,10)
& /A12/KN, KNN
& /A13/KH, KHH
& /A18/USTAR(10), VKC, KMOL
& /A19/RI, PHI, BRI, UB

C
C
FLAG=0. DO
KHH(1,I)=KNN(1,I)/PHI
IF(KHH(1,I).GT.KMOL)GOTO 100
KHH(1,I)=KMOL
100 CONTINUE

C
C
DO 130 J=2, NZPTS1

C
IF( J.LT.10 .OR. I.EQ.1 )GOTO 110
IF( FLAG.EQ.1. DO)GOTO 110
FLAG=1. DO
CALL MCPN
CALL SLOPE
110 CONTINUE

C
KHH(J,I)=KNN(J,I)/PHI
IF(KHH(J,I).GT.KMOL)GOTO 120
KHH(J,I)=KMOL
120 CONTINUE
130 CONTINUE

C
RETURN
END

```

```

SUBROUTINE MOPN
IMPLICIT REAL*8 (A-H,O-Z), INTEGER (I-N)
LOGICAL*1 P(1) /' ' /
COMMON /A1/I,J
      & /A2/TO, DUM4(2), T, DUM5(2)
      & /A8/Z(50), DUM3(10)
      & /A19/RI, PHI, BRI, UB
      & /A21/PHILIM, TSLP, JSJP, IDUM2

C
C
      PHI=.74D0
      IF( (I.GE.2.AND. J.LE. JSJP) .AND. TO>T.GT.TSLP ) RETURN
      IF(BRI.EQ.0.D0) RETURN
      IF(BRI.GT.0.D0) GOTO 150

C
C
      N=0
      GZL=BRI
110  CONTINUE
      X = (1.D0-15.D0*GZL)**.25
      PSI= 2.D0*DLOG( (1.D0 + X)/2.D0 )
      & + DLOG( (1.D0+X*X)/2.D0 )
      & -2.D0*DATAN(X) +3.141592654/2.D0
      RI = ( DLOG(Z(JSJP)/.01D0) -PSI ) *X
      RI =RI*RI*BRI
      FNZL=8.214D0*GZL*GZL*GZL-.5476D0*GZL*GZL-9.D0*RI*RI*GZL
      & +RI*RI
      DRI = ( PSI -X*( 4.D0/(1.D0+X) +1.D0/(1.D0+X*X) ) )
      & *15.D0/4.D0/(X**3.D0)
      FNZLF=-9.D0*RI*DRI*2.D0 +2.D0*RI*DRI
      FNZLP=FNZLP+24.642D0*GZL*GZL-1.0952D0*GZL-9.D0*RI*RI
      IF(FNZLP.EQ.0.D0) GOTO 140
      ERR =FNZL/FNZLP
      ERRL=ERR/GZL
      GZL =GZL-ERR
      N=N+1
      IF(DABS(ERRL).LT..05D0) GOTO 120
      IF(N.GT.100) GOTO 130
      GOTO 110
120  CONTINUE
      PHI=.74D0/( DSQRT(1.D0-9.D0*GZL) )
      RETURN

C
130  WRITE(5,210) N
      STOP
140  CONTINUE
      WRITE(5,220)
      STOP

C
C
150  CONTINUE
      IF(BRI.LT..21D0) GOTO 160
      BRI =.21D0
160  CONTINUE

```

```

A   =22.09D0*BRI-4.7D0
B   = 9.4 D0*DLOG(Z(JSLP)/.01D0)*BRI-.74D0
C   =BRI*DLOG(Z(JSLP)/.01D0)*DLOG(Z(JSLP)/.01D0)
D   =B*B-4.D0*AC
IF(D.LT.0.D0)GOTO 140
GZL =(-B -DSQRT(D) )/(2.D0*A)
PHI =.74D0+4.7D0*GZL
IF(PHI.LT.PHILIM)RETURN
PHI =PHILIM
RETURN

```

```

C
C
210  FORMAT(3H0** ,/,3H **,I15,' @ ITR XCD : MOPN ERR ',/,
&      3H **)
220  FORMAT(3H0** ,/,30H ** DIVISION BY 0 : MOPN ERR ,/,
&      3H **)
C
      END

```

```

IMPLICIT REAL*8(A-H,O-Z), INTEGER(I-N)
LOGICAL*1 P(1) /'0'/
DIMENSION Z(50), T(50), DZ(49), P(50), ZS(8), TS(8)

C
READ(5,F) PB,TAV
READ(5,F) NIDP,(Z(J),T(J),J=1,NIDP)
READ(5,F) NIDPS,(ZS(J),TS(J),J=1,NIDPS)
P(NIDP)=PB
GR      =9.81D0/287.04D0
COR     =T(NIDP)
NIDP1   =NIDP-1

C
DO 100 J=1,NIDP1
DZ(J)=Z(J)-Z(J+1)
100 CONTINUE

C
DO 200 J=1,NIDP1
JJ=NIDP-J
P(JJ)=P(JJ+1)*DEXP(-GR*DZ(JJ)/TAV)
200 CONTINUE

C
DO 300 J=1,NIDP
T(J)=T(J)*((PB/P(J))**.286D0)
300 CONTINUE

C
COR=T(NIDP)-COR
DO 350 J=1,NIDPS
TS(J)=TS(J)+COR
350 CONTINUE

C
WRITE(6,400) NIDP,(Z(J),T(J),J=1,NIDP)
WRITE(6,400) NIDPS,(ZS(J),TS(J),J=1,NIDPS)
400 FORMAT(1H ,I3,(5(2F9.3)))

C
STOP
END

```